

1. Report No. FHWA/TX-81/13+208-1	2. Government Accession No.	3. Recipient's Catalog No.	
4. Title and Subtitle ANALYSES OF POST-TENSIONED GIRDER ANCHORAGE ZONES		5. Report Date June 1981	6. Performing Organization Code
7. Author(s) W. C. Stone and J. E. Breen		8. Performing Organization Report No. Research Report 208-1	
9. Performing Organization Name and Address Center for Transportation Research The University of Texas at Austin Austin, Texas 78712		10. Work Unit No.	11. Contract or Grant No. Research Study 3-5-77-208
12. Sponsoring Agency Name and Address Texas State Department of Highways and Public Transportation; Transportation Planning Division P. O. Box 5051 Austin, Texas 78763		13. Type of Report and Period Covered Interim	
14. Sponsoring Agency Code		15. Supplementary Notes Study conducted in cooperation with the U. S. Department of Transportation Federal Highway Administration. Research Study Title: "Design Criteria for Post-Tensioned Anchorage Zone Bursting Stresses"	
16. Abstract  Several large thin-webbed box girders, with post-tensioned anchorage zones designed in accordance with AASHTO and ACI requirements, have experienced large cracks along the tendon path in the anchorage zones at the design stressing load. Cracking of this nature provides a path for penetration of moisture and salts and thus presents a potential corrosion and frost damage threat. In addition, such cracking negates a major reason for the use of prestressed concrete, the minimization of service load cracking.  This report summarizes an extensive literature review which documents the state-of-the-art in anchorage zone analysis, behavior, and design recommendations. In addition, the report outlines the general utilization of a powerful three-dimensional finite element program--PUZGAP-3D--for analysis of the complex anchorage zone region. The program was used to study both straight and curved tendon paths. Good correlation was found with experimental results up to first cracking which indicated that the program was very useful for exploring the effects of various parameters.			
17. Key Words girder, post-tensioned, anchorage zones, analyses, cracks, tendon, AASHTO, ACI		18. Distribution Statement No restrictions. This document is available to the public through the National Technical Information Service, Springfield, Virginia 22161.	
19. Security Classif. (of this report) Unclassified	20. Security Classif. (of this page) Unclassified	21. No. of Pages 176	22. Price

ANALYSES OF POST-TENSIONED GIRDER  
ANCHORAGE ZONES

by

W. C. Stone and J. E. Breen

Research Report No. 208-1

Research Project No. 3-5-77-208

"Design Criteria for Post-tensioned Anchorage Zone  
Bursting Stresses"

Conducted for

Texas

State Department of Highways and Public Transportation

In Cooperation with the  
U. S. Department of Transportation  
Federal Highway Administration

by

CENTER FOR TRANSPORTATION RESEARCH  
BUREAU OF ENGINEERING RESEARCH  
THE UNIVERSITY OF TEXAS AT AUSTIN

June 1981

The contents of this report reflect the views of the authors, who are responsible for the facts and accuracy of the data presented herein. The contents do not necessarily reflect the views or policies of the Federal Highway Administration. This report does not constitute a standard, specification, or regulation.

## P R E F A C E

This report is the first in a series which summarizes the detailed investigation of the effects and control of tensile stresses in the anchorage zones of post-tensioned girders. This report summarizes the state-of-the-art and presents a three-dimensional finite element analysis procedure which is of great use in understanding the development of these tensile stresses. The second report in this series summarizes an extensive series of model and full-scale physical tests which were performed to document the problem and further explore the effect of variables. The third and final report in the series draws on the analytical and experimental results presented in the first two reports. It uses these results to develop design procedures and suggested AASHTO specification provisions to control the problem. The third report also contains several examples to illustrate the application of the design criteria and procedures.

This work is a part of Research Project 3-5-77-208, entitled "Design Criteria for Post-tensioned Anchorage Zone Bursting Stresses." The studies described were conducted at the Phil M. Ferguson Structural Engineering Laboratory as a part of the overall research program of the Center for Transportation Research, Bureau of Engineering Research of The University of Texas at Austin. The work was sponsored jointly by the Texas Department of Highways and Public Transportation and the Federal Highway Administration under an agreement with The University of Texas at Austin and the Texas Department of Highways and Public Transportation.

Liaison with the Texas Department of Highways and Public Transportation was maintained through the contact representative, Mr. Alan Matejowsky; the Area IV committee chairman, Mr. Robert L. Reed; and the State Bridge Engineer, Mr. Wayne Henneberger; Mr. Randy Losch was the contact representative for the Federal Highway

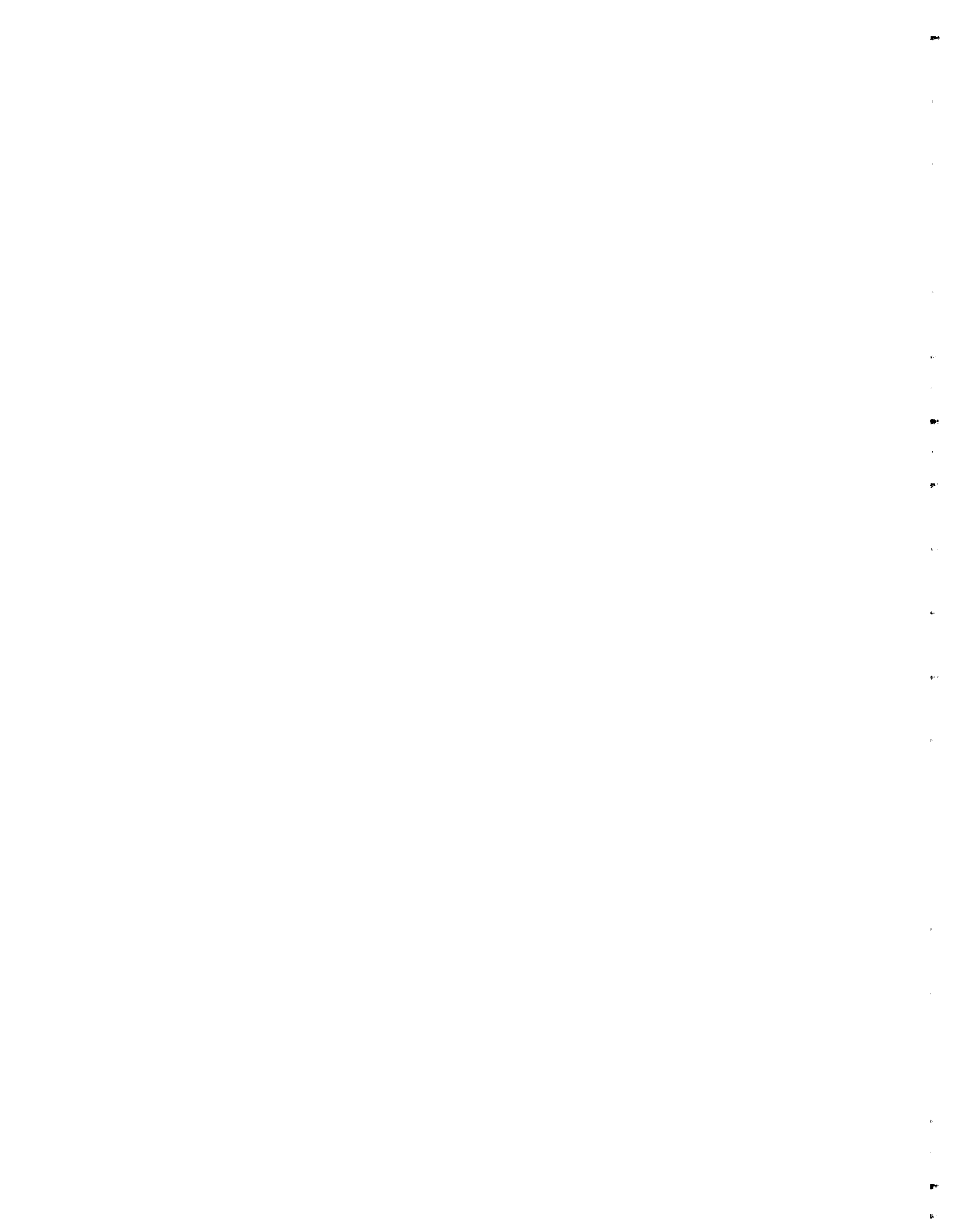
Administration. Special thanks are due to Dr. E. B. Becker and Dr. C. P. Johnson of The University of Texas at Austin, who gave a great deal of assistance and encouragement in developing the program PUZGAP-3D used in the analytical phase.

The overall study was directed by Dr. John E. Breen, The J. J. McKetta Professor of Engineering. The detailed analysis was carried out under the immediate supervision of Dr. William C. Stone, research engineer, Center for Transportation Research.

## S U M M A R Y

Several large thin-webbed box girders, with post-tensioned anchorage zones designed in accordance with AASHTO and ACI requirements have experienced large cracks along the tendon path in the anchorage zones at the design stressing load. Cracking of this nature provides a path for penetration of moisture and salts and thus presents a potential corrosion and frost damage threat. In addition, such cracking negates a major reason for the use of prestressed concrete, the minimization of service load cracking.

This report summarizes an extensive literature review which documents the state-of-the-art in anchorage zone analysis, behavior, and design recommendations. In addition, the report outlines the general utilization of a powerful three-dimensional finite element program--PUZGAP-3D--for analysis of the complex anchorage zone region. The program was used to study both straight and curved tendon paths. Good correlation was found with experimental results up to first cracking which indicated that the program was very useful for exploring the effects of various parameters.



## I M P L E M E N T A T I O N

This report is the first in a series which summarizes a major experimental and analytical project aimed directly at developing specific recommendations for design of post-tensioned girder anchorage zones. The recommendations should be considered by the State Department of Highways and Public Transportation and by AASHTO for inclusion in design specifications and in design manuals of practice. The specific recommendations are included in the third and concluding report of this series.

This report contains background information of interest to those responsible for deciding on specification and codes. In addition, it contains specific information regarding the use of a three-dimensional finite element program for analysis of complex anchorage zones. The analysis is so demanding and complex in input that it is of little practical interest to designers. It is of interest and contains important information for persons wishing to carry out detailed analysis of anchorage zones for the development of criteria, hardware units, or special post-tensioning applications.

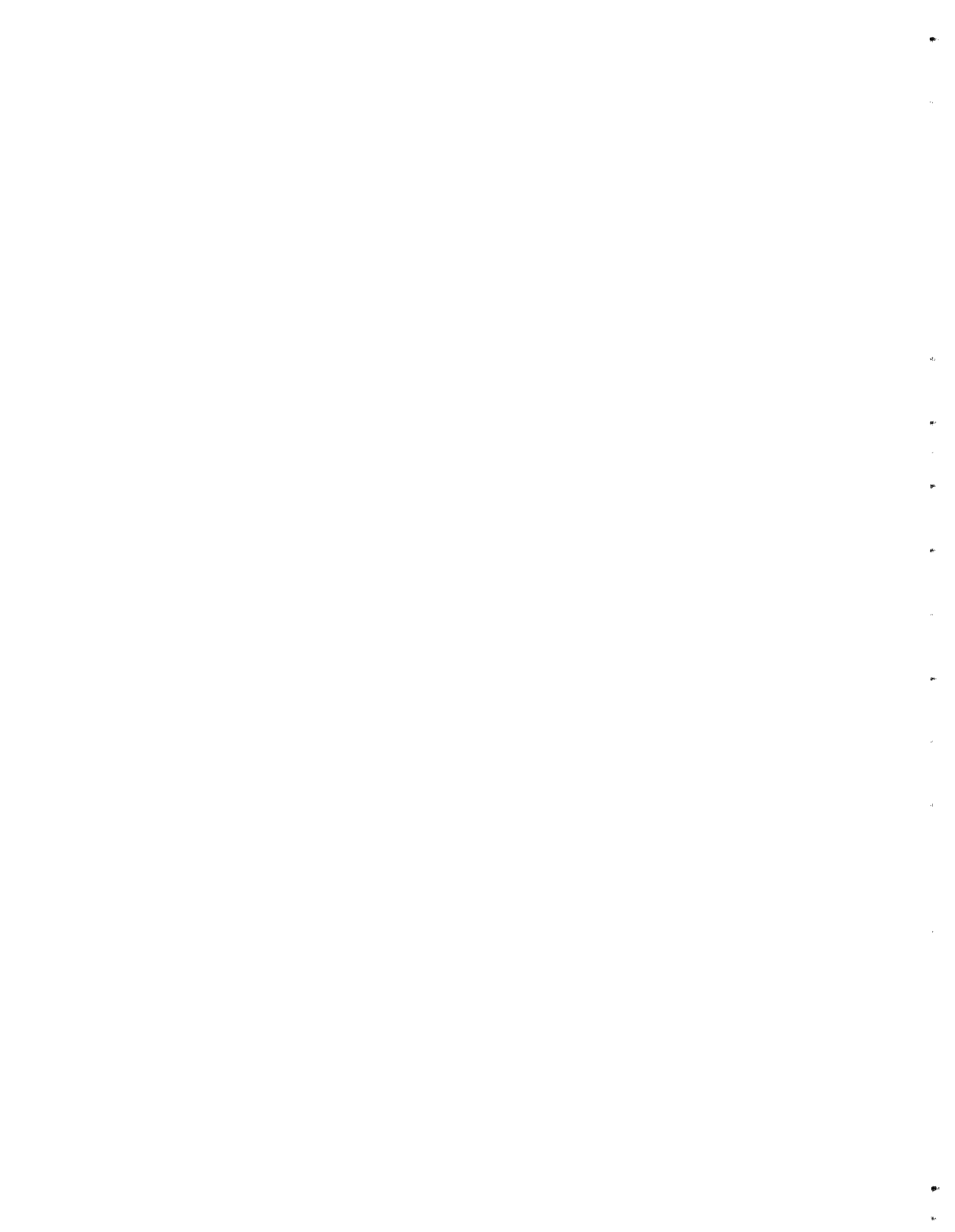


## TABLE OF CONTENTS

Chapter	Page
1 INTRODUCTION . . . . .	1
1.1 Problems in Thin Web Post-Tensioned Structures . . . . .	1
1.2 The Anchorage Zone Stress State . . . . .	4
1.2.1 The Nature of Anchorage Zone Stresses . . . . .	4
1.2.1.1 Bursting Stress . . . . .	5
1.2.1.2 Spalling Stress . . . . .	10
1.2.1.3 Bearing Stress . . . . .	13
1.2.1.4 Additional Considerations . . . . .	13
1.3 Overview of the Project . . . . .	16
1.3.1 Objectives . . . . .	16
2 LITERATURE REVIEW . . . . .	21
2.1 Introduction . . . . .	21
2.2 Previous Research on Anchorage Zones . . . . .	23
2.2.1 Studies Based on Elasticity Solutions . . . . .	23
2.2.1.1 Guyon's Theory . . . . .	24
2.2.1.2 Douglas and Trahair . . . . .	31
2.2.1.3 Iyengar . . . . .	31
2.2.1.4 Gergely, Sozen and Siess . . . . .	31
2.2.2 Other Analytical Solutions . . . . .	31
2.2.2.1 Beam Method . . . . .	31
2.2.2.2 Gergely . . . . .	33
2.2.2.3 Lenschow and Sozen . . . . .	33
2.2.2.4 Yettram and Robbins . . . . .	36
2.2.2.5 Summary of Analytical Studies . . . . .	43
2.2.3 Photoelastic Investigation . . . . .	44
2.2.3.1 Christodoulides . . . . .	44
2.2.3.2 Sargious . . . . .	46
2.2.3.3 Vaughn . . . . .	49
2.2.3.4 Other Photoelastic Studies . . . . .	50
2.2.4 Tests on Concrete Specimens . . . . .	50
2.2.4.1 Zielinski and Rowe . . . . .	50
2.2.4.2 Taylor . . . . .	55
2.2.4.3 Cooper and Gallaway . . . . .	57
2.2.5 Bearing Stresses . . . . .	60
2.3 Present Design Provisions . . . . .	65
2.3.1 Leonhardt . . . . .	65
2.3.2 Guyon . . . . .	67
2.3.3 Rhodes and Turner . . . . .	69

Chapter	Page
2.3.4 ACI . . . . .	77
2.3.5 CEB . . . . .	79
2.3.6 AASHTO . . . . .	81
2.3.7 PTI . . . . .	81
2.4 Summary . . . . .	82
3 ANALYTICAL STUDY USING FINITE ELEMENTS . . . . .	83
3.1 Introduction . . . . .	83
3.1.1 Finite Element Models . . . . .	83
3.1.2 Mesh Generation . . . . .	84
3.1.3 Accuracy . . . . .	85
3.2 Capabilities of TEXTGAP . . . . .	90
3.2.1 General . . . . .	90
3.2.2 TEXTGAP-2D: Two-Dimensional Program . . . . .	91
3.2.3 TEXTGAP-3D: Three-Dimensional Program . . . . .	94
3.2.4 Program PUZGAP-3D . . . . .	98
3.3 Calibration . . . . .	102
3.3.1 Literature Comparisons . . . . .	103
3.3.2 Photoelastic Comparison . . . . .	107
3.3.3 One-fourth Scale Model Tests . . . . .	114
3.3.3.1 Cover Effects . . . . .	116
3.3.3.2 Eccentricity . . . . .	123
3.3.3.3 Inclination . . . . .	123
3.3.4 Calibration: Full-Scale Tests . . . . .	129
3.3.5 Results . . . . .	140
4 CONCLUSIONS . . . . .	153
4.1 General . . . . .	153
BIBLIOGRAPHY . . . . .	157

## L I S T   O F   F I G U R E S

Figure	Page
1.1 Resident engineer pointing to tendon path crack . . .	3
1.2 Radial stresses for semi-infinite half-plane loaded by a point . . . . .	3
1.3 Transverse stresses in a rectangular block loaded by a plate . . . . .	6
1.4 "Rubber analogy" illustrating the nature of bursting and spalling stresses . . . . .	8
1.5 Equilibrium considerations within the lead-in zone .	9
1.6 Bursting stresses in semi-infinite body for various loading areas . . . . .	11
1.7 Bursting stresses for various loaded areas . . . . .	11
1.8 Maximum bursting stress and tensile force from various investigators . . . . .	12
1.9a Combination of end zone, radial and inclined wedge effects . . . . .	14
1.9b Forces due to tendon curvature . . . . .	14
1.10 Models of typical anchors used in post-tensioned construction . . . . .	15
2.1 Bursting and spalling zones from Tesar's photoelastic tests . . . . .	22
2.2 Basic theory--Guyon . . . . .	22
2.3 Isostatic lines of force through the lead-in zone . .	26
2.4 Bursting stresses for various loaded areas . . . . .	26
2.5 Approximate bursting stress distribution for design .	28
2.6 Guyon's symmetrical prism analogy . . . . .	28
2.7 Guyon's successive resultant method for the case of multiple anchorages in a rectangular end block . .	30
2.8 Magnel's beam analysis . . . . .	32
2.9 Gergely's beam analysis . . . . .	32
2.10 Bursting and spalling stresses . . . . .	34
2.11 Exaggerated deformations of end block with fictitious discontinuities . . . . .	34
2.12 The physical analog . . . . .	35

Figure	Page
2.13 Lenschow and Sozen calculations compared to previous work . . . . .	37
2.14 Narrow rectangular prism--FEM results from Yettram and Robbins . . . . .	38
2.15 Wide rectangular prism--FEM results from Yettram and Robbins . . . . .	40
2.16 I-section prism, axial anchor--Yettram and Robbins . . . . .	41
2.17 I-section prism, eccentric anchor--Yettram and Robbins . . . . .	41
2.18 Spalling stress distribution across depth of I-section--Yettram and Robbins . . . . .	42
2.19 Model end block tested by Christodoulides . . . . .	45
2.20 Principal stress trajectories from Christodoulides' photoelastic test of gantry beam . . . . .	45
2.21 Sargious: experimental results for a single applied force on a rectangular end block . . . . .	47
2.22 Sargious: experimental results for three applied forces on a rectangular end block . . . . .	47
2.23 Formation of concrete cone ahead of anchor . . . . .	52
2.24 Zielinski and Rowe: typical dimensions for specimens used in second series . . . . .	54
2.25 Zielinski and Rowe: specimen 1, second test . . . . .	54
2.26 Taylor's test specimens . . . . .	56
2.27 Concrete cones observed by Taylor . . . . .	56
2.28 Strip load dimensions for Eq. 2.4 . . . . .	63
2.29 Variable definitions for Niyogi's Eq. 2.5 . . . . .	63
2.30 Defining eccentric bearing conditions for Niyogi's Eq. 2.6 . . . . .	63
2.31 Detailing of reinforcement as recommended by Leonhardt . . . . .	66
2.32 Anchorage zone reinforcement design as per Guyon . . . . .	68
2.33 Determination of prisms for end blocks--Rhodes and Turner . . . . .	70
2.34 Values of coefficients B, C, and K for Rhodes and Turner equations . . . . .	70

Figure	Page
2.35 Approximate bursting stress distribution-- Rhodes and Turner . . . . .	72
2.36 Placing of reinforcement--Rhodes and Turner . . . . .	72
2.37 Proportioning steel for Rhodes and Turner equations . .	75
3.1 Typical irregular meshes . . . . .	86
3.2 Accuracy improvement with higher order elements . . . .	89
3.3 Two-dimensional modeling capabilities for post- tensioned anchorage zones . . . . .	92
3.4 2D isoparametric elements used to model anchorage zones . . . . .	93
3.5 2D grids used to model box girder web and tendon duct .	95
3.6 TEXGAP-3D general elements--all isoparametric . . . . .	97
3.7 5 x 5 x 10 mesh--3D problem . . . . .	100
3.8 Bursting stress comparison--2D-FEM vs Sargious . . . .	104
3.9 Spalling stress comparison--2D-FEM vs Sargious . . . .	105
3.10 Stress distributions for Sargious' problem--2D-FEM . . . . .	106
3.11 Bursting stress distribution variable check--2D-FEM . .	108
3.12 Spalling stress distribution variable check--2D-FEM . .	109
3.13 Interactive graphics plot of Zielinski and Rowe 6 in. prism . . . . .	110
3.14 Symmetry conditions in post-tensioned structures and equivalent FEM models . . . . .	111
3.15 Calibration with Zielinski and Rowe cube . . . . .	112
3.16 Typical mesh used for modeling Vaughn's Tests . . . . .	113
3.17 Comparison of Vaughn's test #7 with 2D-FEM analysis . .	115
3.18 Typical physical specimens; cover series tests . . . .	117
3.19 Interactive plot of cover series FEM meshes . . . . .	118
3.20 Nodal choice for strain comparison between 3D-FEM and first series model tests . . . . .	119
3.21 Specimen M1-2 versus 3D-FEM transverse bursting stress distribution . . . . .	120

Figure	Page
3.22 Specimen M2-2 versus 3D-FEM transverse bursting stress distribution . . . . .	121
3.23 Specimen M3-2 versus 3D-FEM transverse bursting stress distribution . . . . .	122
3.24 Eccentric tendon model test and FEM mesh . . . . .	124
3.25 Transverse strain along tendon path for eccentric tendon tests . . . . .	125
3.26 Typical inclined tendon model tests . . . . .	126
3.27 Interactive plot of mesh used for curved tendon models . . . . .	127
3.28 Comparison of analytical and experimental bursting strain distribution for inclined tendon model tests . .	130
3.29 Insert gage location for prototype specimens . . . . .	131
3.30 Typical full-scale specimens . . . . .	133
3.31 Typical full-scale specimens . . . . .	134
3.32 Curved tendon mesh for full-scale specimens . . . . .	135
3.33 FS1A 3D-FEM vs experimental bursting strain distribution . . . . .	141
3.34 FS1B 3D-FEM vs experimental bursting strain distribution . . . . .	142
3.35 FS2A 3D-FEM vs experimental bursting strain distribution . . . . .	143
3.36 FS2B 3D-FEM vs experimental bursting strain distribution . . . . .	144
3.37 FS5A 3D-FEM vs experimental bursting strain distribution . . . . .	145
3.38 Statistical comparison of FEM predicted strain vs experimental gage data for various tests . . . . .	146
3.39 FS2A spalling strain distribution: 3D-FEM vs experimental . . . . .	147
3.40 FS2B spalling strain distribution: 3D-FEM vs experimental . . . . .	148
3.41 FS5A spalling strain distribution: 3D-FEM vs experimental . . . . .	149
3.42 FS4A spalling strain distribution: 3D-FEM vs experimental . . . . .	150

# C H A P T E R 1

## INTRODUCTION

### 1.1 Problems in Thin Web Post-Tensioned Structures

Current trends in bridge construction show increased utilization of precast and prestressed concrete. After two decades with major utilization of pretensioned bridge girders, increasing bridge applications are being found for post-tensioning. California and Washington have pioneered in the use of cast-in-place post-tensioned box girder construction. Texas, Colorado, and Indiana have completed major segmentally constructed post-tensioned box girder bridges. A number of states have similar structures under active design or construction, and a variety of applications for lateral and transverse post-tensioning in relatively thin slab and web systems have been proposed.

Pretensioning implies that the strands, or tendons, are stressed before the concrete is cast. Once the concrete has reached the desired strength the load is released from the jacking system and applied to the structure via bond along the tendon. This allows for a gradual transfer of the high prestress loads over some "lead in" length of the girder.

In post-tensioned construction a hollow duct is placed in the structure during the casting phase usually by employing flexible metal tubing. After curing has taken place the tendon is drawn through the duct and stressed. Once the tendon has been stressed the load is locked off and permanently applied to the structure by some sort of anchorage device. Herein lies the fundamental difference between pre- and post-tensioning. The problem of transferring the large prestress force to the structure over a small local anchorage zone becomes a primary concern in the design of a successful post-tensioning system.

In the construction of cast-in-place box girders, it is feasible to use enlarged anchorage zones at the ends of the spans or at interior diaphragms to contain the tensile stresses which generally occur in the vicinity of the point of application of the post-tensioning forces. In construction of post-tensioned "I" beam type girders, it has been the general practice to provide a thickened end block with substantial additional reinforcement to accommodate these anchorage zone stresses. Even in those thickened sections cover over edge tendons is small. However, in two very practical post-tensioning applications, segmentally constructed box girders and relatively thin laterally post-tensioned overhanging deck slabs, it is not economically practical to provide massive thickness to control anchorage zone stresses. In fact, the entire length of the structure becomes the anchorage zone for an appreciable number of tendons and over-conservative anchorage zone design could greatly penalize the economics of this form of construction.

A number of problems have occurred in post-tensioned applications in both the bridge and the building field which indicate that the design procedures and design criteria for post-tensioned anchorage zone tensile stresses need further examination and refinement. Substantial cracking along the tendon path has been experienced in a precast segmental bridge in Texas [1] (see Fig. 1.1) and in a cast-in-place box girder bridge reported by Dilger and Ghali [2]. In both of these bridges the cable profiles had significant curvature, inclination, and eccentricity in and near the anchorage zones. In the case of the Texas bridge, there was some concern over the possible effects of the anchorage hardware geometry. Similar cracking was reported in construction of the Olympic stadium in Montreal and in post-tensioned slab structures and other thin web applications. Significant anchorage zone cracking was experienced in preliminary tests for a major lightweight concrete bridge in California which indicated lightweight concrete may be even more vulnerable.

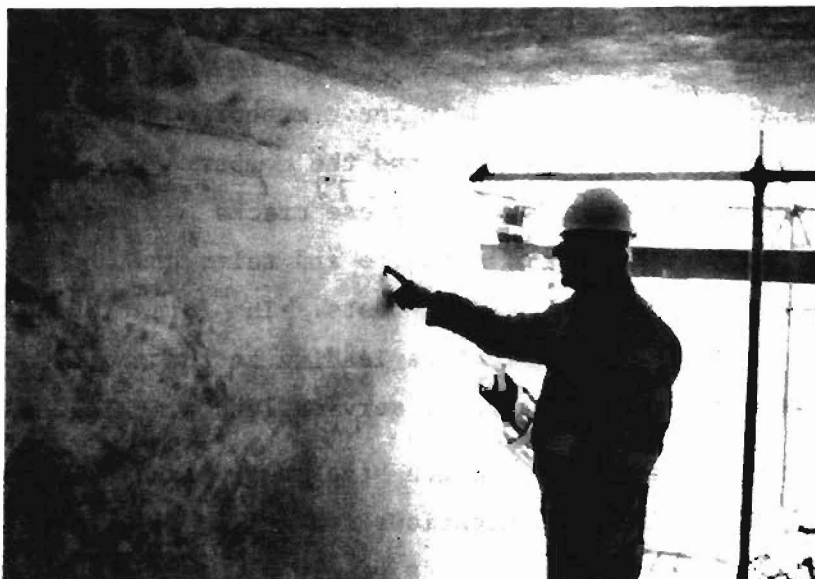


Fig. 1.1 Resident engineer pointing to tendon path crack

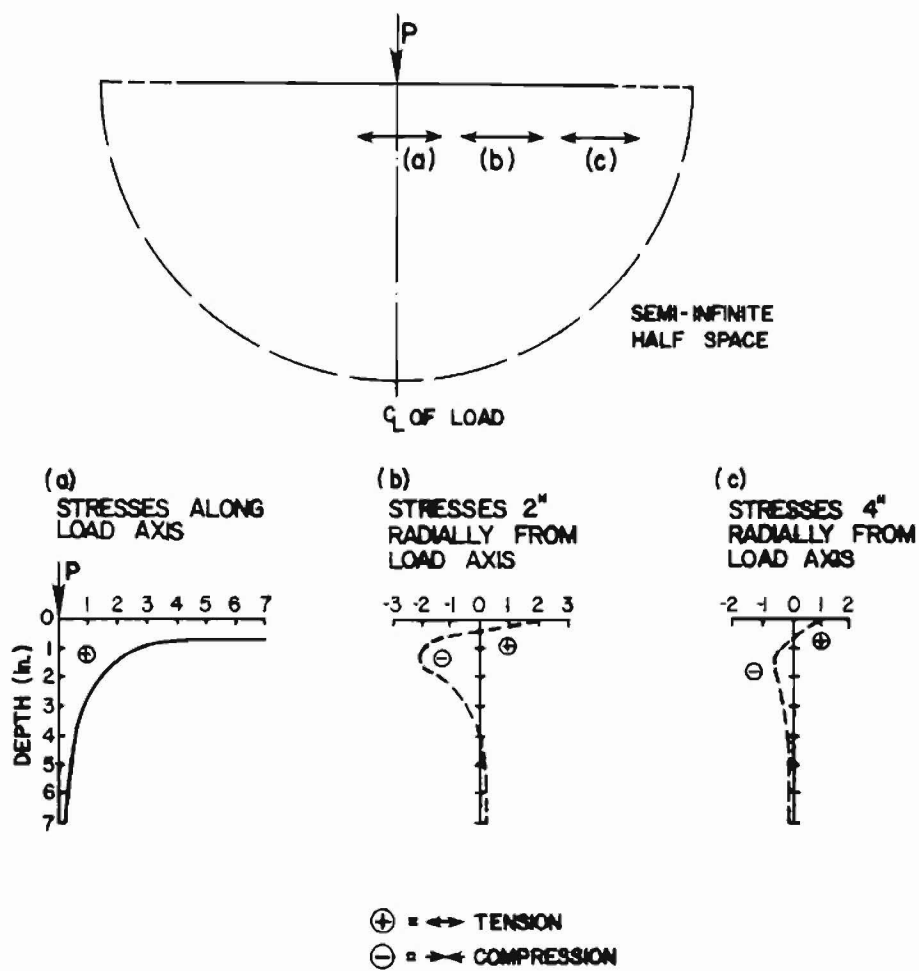


Fig. 1.2 Radial stresses for semi-infinite half-plane loaded by a point

The cracking which occurred in these anchorage regions was controlled by auxiliary reinforcement and the member strength was not appreciably reduced. However harmless these cracks may appear, they provide a path for penetration of moisture and salts and thus present potential corrosion and frost damage threats. The formation of these cracks negates one of the major factors leading to the choice of prestressed concrete, the minimization of service load cracking.

Major and contradictory changes have taken place in the AASHTO, ACI and PCI design specifications for anchorage zones in recent years, based more on the results of field experience and proprietary data than on published analyses or test procedures. Current design recommendations, while vague, seem both conservative and workable for many applications where massive end blocks with large cover can be used with relatively straight or gently curving tendons in cast-in-place post-tensioned construction. However, they do not give sufficient guidance for the wide range of thin web post-tensioned applications currently in use today, or the many new applications being suggested as the industry develops. Thus, this study of the development and control of critical anchorage zone tensile stresses was undertaken. Its goal was to provide more specific guidance to bridge design and construction personnel regarding the behavior of anchorage systems so that they could better assess the performance of a post-tensioning system without having to rely wholly on the recommendations of the hardware supplier.

## 1.2 The Anchorage Zone Stress State

1.2.1 The Nature of Anchorage Zone Stresses. Application of linear, elastic theory shows that if a concentrated normal load acts on a large (semi-infinite) body bounded by a plane, compressive and tensile stresses are set up. The distributions of radial stresses along the line of the load and along lines parallel to the load are shown in Fig. 1.2. Two important tension fields are shown in this

figure: those acting along the line of the load, which, by elasticity theory, become infinite directly beneath the point load (Fig. 1.2a), and those acting on or near the end face at points removed from the load (Figs. 1.2b, c). Figure 1.3 shows the variations in transverse stress for a finite rectangular block loaded by a finite strip loading. The two tensile stress zones are generally called:

- (1) Bursting Stress--located along the line of loading, normal to it, and away from the point of loading.
- (2) Spalling Stress--located along the loading surface, parallel to it and away from the point of loading.

In dealing with a specific post-tensioned anchorage, the load must be applied over a finite area. The compressive stress immediately under the anchor is called:

- (3) Bearing Stress--The load divided by the net bearing area.

The precise role that each of these three stresses plays in the behavior of the anchorage zone has not been fully understood and a positive prediction of cracking loads has proven even more elusive.

1.2.1.1 Bursting Stress. Distress in the anchorage zone is signalled by the sudden formation of a crack along the line of the load. The load at which this occurs depends not only on the size of the loaded area in relation to the geometry of the loaded surface [3], but additionally on the geometry of the surface itself, i.e., the eccentricity, inclination, and curvature of the tendon. In addition, the shape of the anchorage device as well as the action of supplemental reinforcement affect the load at which crack formation occurs.

In Fig. 1.2a, for the semi-infinite body, the tensile stresses increase rapidly near the point of application of the concentrated load. High local transverse tensile stresses occur directly under the concentrated load. On the other hand, in Fig. 1.3, for the finite rectangular body, transverse compressive stresses occur

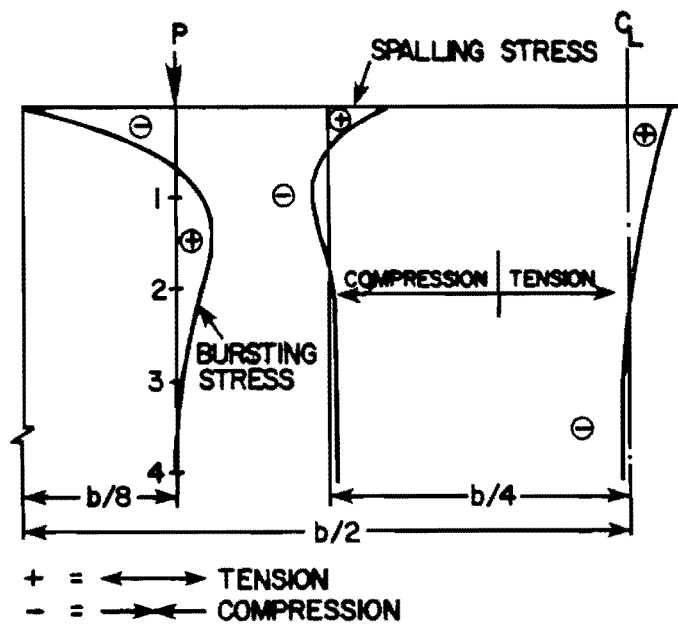
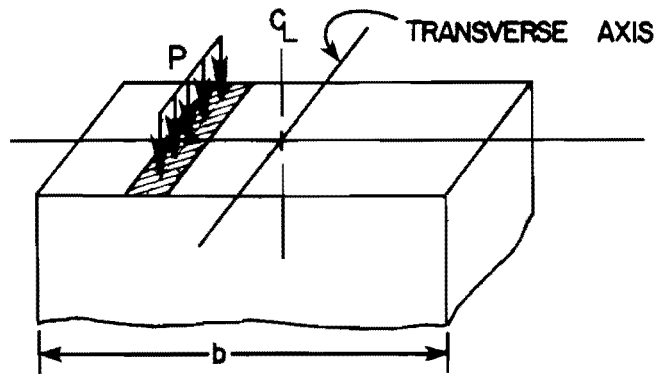


Fig. 1.3 Transverse stresses in a rectangular block loaded by a plate

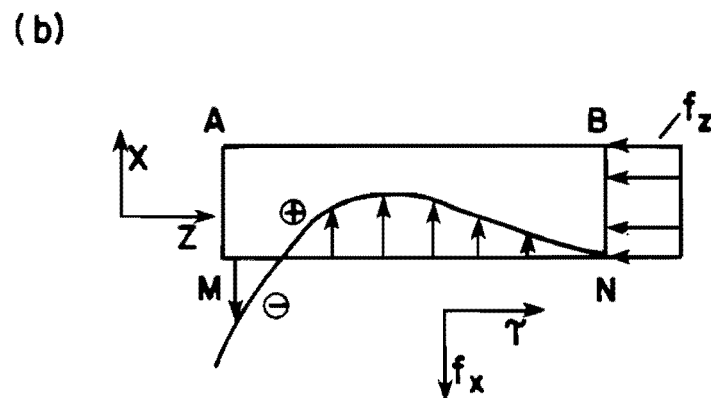
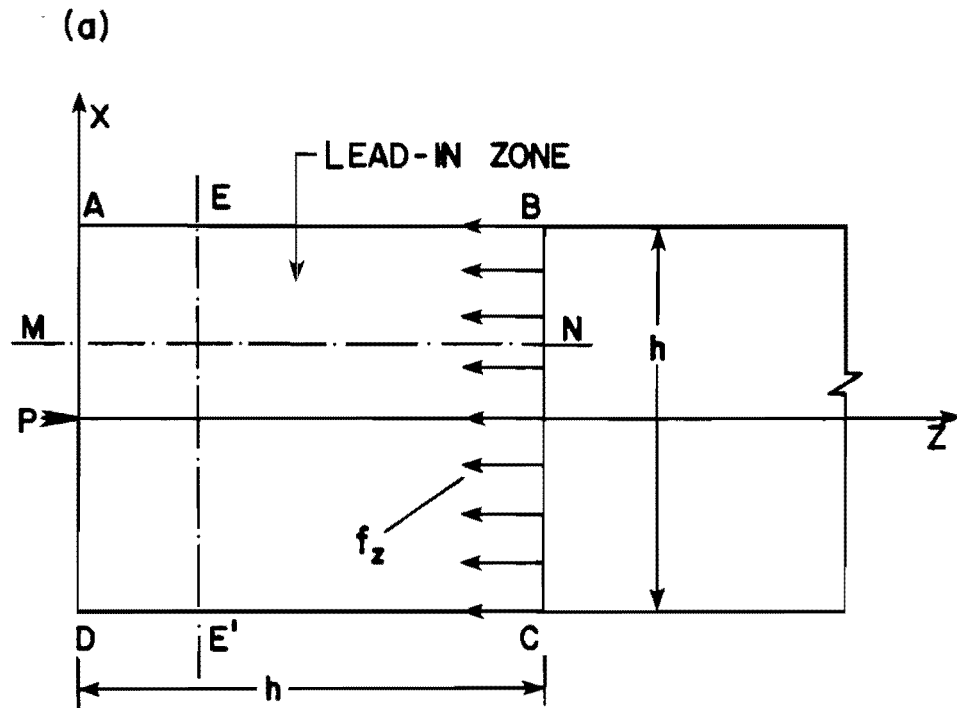
immediately under the load and the transverse tensile stresses occur away from the point of loading. These extreme differences in stress distribution for the two cases demonstrate the need to ensure that the boundary conditions employed in an analytical model correctly represent design conditions.

The presence of tensile stresses in the anchorage zone can be readily visualized by considering two prisms of a low modulus material such as rubber, which are connected at their ends by small rigid plates. When a force is applied to the system through the plates, the final deformed position will be as shown in Fig. 1.4. In a real structure continuity across the tendon load path must be provided by the adjacent concrete. To satisfy compatibility along the vertical load axis a lateral tensile load would have to be applied to each interior edge of the prisms in Fig. 1.4 in order to close the gap. This would represent the bursting force. Similarly, at the upper and lower exterior corners internal tensile loads would have to be applied to return the exterior edges to a straight line configuration. These are the spalling forces and associated stresses.

The above analogy is a physical interpretation of St. Venant's principle applied to a member subjected to a concentrated load  $P$  as in Fig. 1.5(a). A section at a distance approximately equal to the depth of the section from the applied load should exhibit an essentially uniform normal stress distribution. The longitudinal stress distribution within the zone ABCD is not uniform and cannot be analyzed by the usual laws of strength of materials. In fact, the distribution of stresses on Section  $EE'$  is completely discontinuous, with very high stresses at points near the applied load  $P$  and practically zero stress at all other points [4]. This zone of disturbance is called the lead-in zone. Fig. 1.5(b) is a free body of the upper part of the lead-in zone. Equilibrium of horizontal forces requires the shear stress  $\tau$ . Transverse stresses  $f_x$  are required for equilibrium of moments about  $M$ . Finally, the vertical equilibrium of forces



Fig. 1.4 "Rubber analogy" illustrating the nature of bursting and spalling stresses



$f_x$  = BURSTING STRESS DISTRIBUTION

$$\sum F_x = 0 : \sum f_x^{\ominus} + \sum f_x^{\oplus} = 0$$

Fig. 1.5 Equilibrium considerations within the lead-in zone

requires the transverse stress distribution resultant to be equal to zero. Therefore, tensile and compressive transverse stresses must occur within the lead-in zone. However, these equilibrium considerations are not sufficient for the determination of the transverse stress distribution. The various analytical approaches to the solution of the stress distribution in the anchorage zone are discussed in detail in Chapters 2 and 3.

Examination of Boussinesq's solution for the concentrated loading (Fig. 1.2), and for the uniformly loaded circular area with radius  $a'$  (Fig. 1.6) reveals that when  $a'$  becomes zero the two are identical for stresses along the axis of the load. If, as in actual practice, the load acts over a finite area with a reasonably large radius  $a'$ , the stresses are relatively small. These stresses are plotted for a constant load  $P$  in Fig. 1.7 for various values of  $a'/a$ , where  $2a$  denotes the section breadth and  $2a'$  denotes the anchor breadth. Standard design practice in many countries has been to provide massive reinforcement for the total resultant tensile force obtained by integrating the area under curves such as those shown in Figs. 1.7 and 1.8. Experience gained from anchorage zone cracking problems with the Texas bridge at Corpus Christi [1], in which the anchorage zones were reinforced based on a similar set of experimentally derived bursting curves [6] indicated that design based solely upon such consideration of bursting stresses may be unconservative.

1.2.1.2 Spalling Stress. The spalling tensile stresses are maximum at the loaded surface and decrease rapidly away from the surface (see Figs. 1.2 and 1.3). The total spalling tensile force is thus relatively small. In contrast to the attention paid to bursting stresses, the spalling stresses have sometimes been neglected or dismissed because they are so localized. However, the peak spalling stress can be very high, indeed much higher in almost every practical situation examined by the authors than the bursting stresses. This is shown to be of great significance in subsequent reports of this series

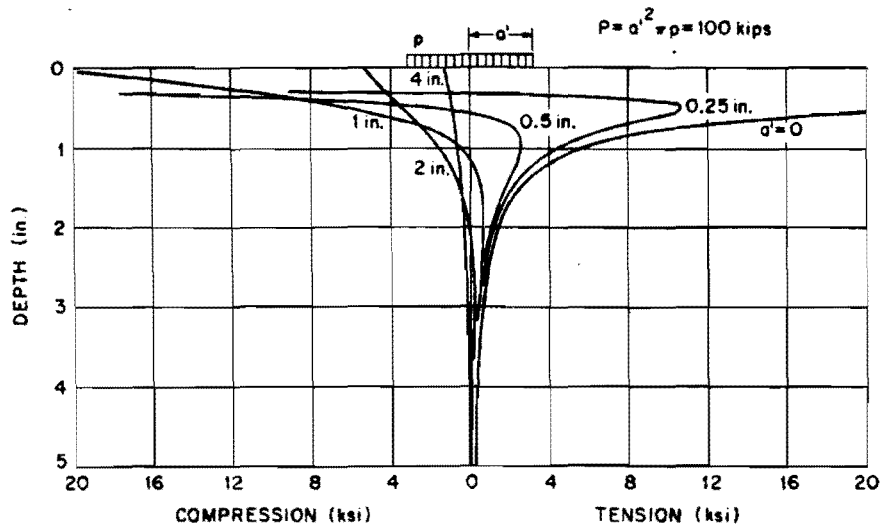


Fig. 1.6 Bursting stresses in semi-infinite body for various loaded areas (Ref. 5)

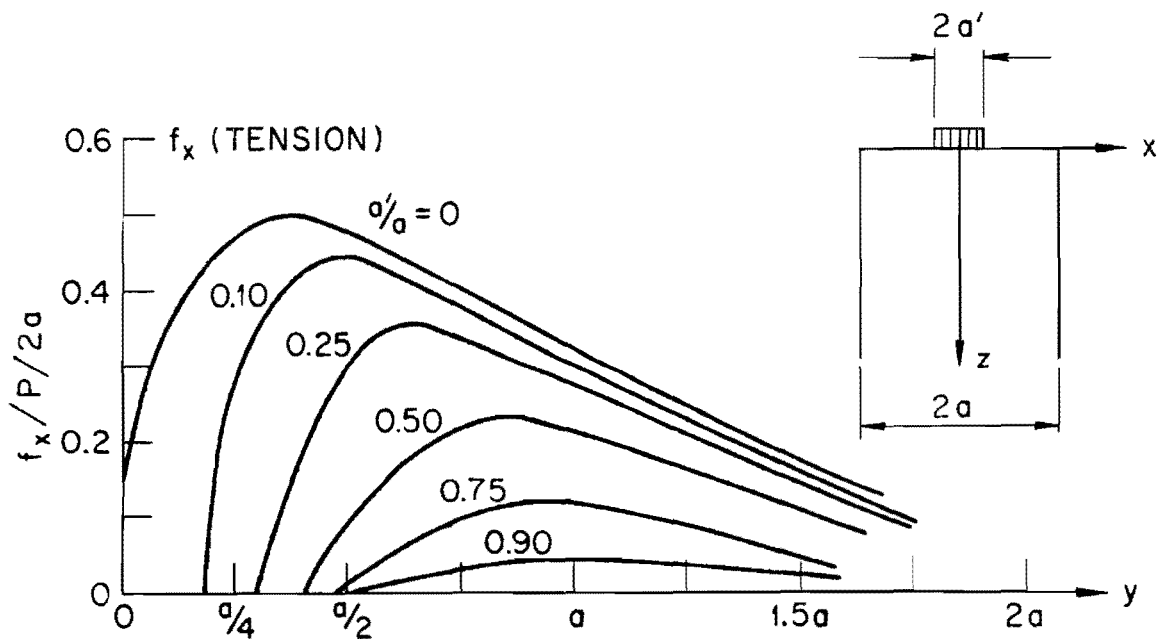
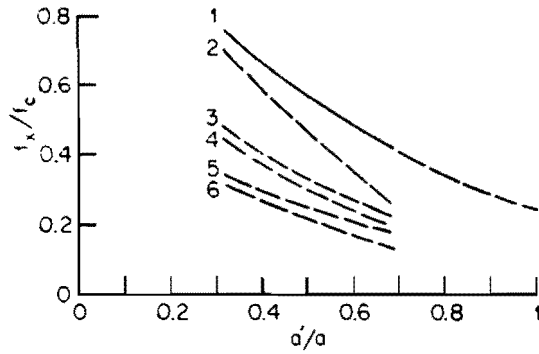
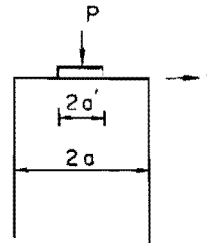


Fig. 1.7 Bursting stresses for various loaded areas (Guyon) (Ref. 5)



- 1 ZIELINSKI-ROWE (EXPERIMENTAL)
- 2 BLEICH-SIEVERS
- 3 BLEICH
- 4 MAGNEL
- 5 MAGNEL MODIFIED
- 6 GUYON
- 7 SARGIOUS (BY WRITER)
- 8 MÖRSCH



$a$  = HALF-WIDTH OF BLOCK  
 $a'$  = HALF-WIDTH OF ANCHORAGE  
 $f_x$  = MAXIMUM TRANSVERSE BURSTING STRESS  
 $f_c$  = AVERAGE STRESS ( $P/2a$ )  
 $T$  = BURSTING TENSILE FORCE  
 $P$  = PRESTRESSING FORCE

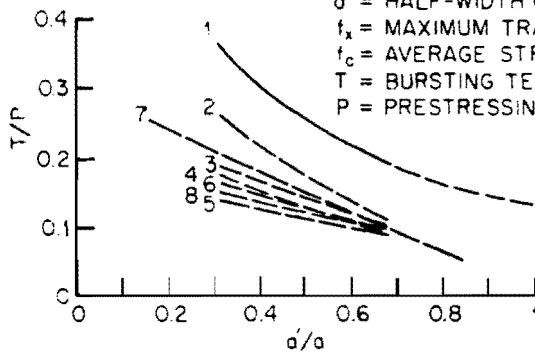


Fig. 1.8 Maximum bursting stress and tensile force from various investigators (from Ref. 5)

where it will be shown that cracking occurred along the tendon path with calculated bursting stresses far below the tensile strength of the concrete. Like bursting stresses, the spalling stress distribution is greatly affected by the geometric variables such as eccentricity, inclination, and proportions of the section. Most of the previous research on post-tensioned anchorage zones has been limited to straight tendon analysis and has been interpreted with emphasis on the role of the bursting stresses. This has been more due to the difficulties in satisfying the proper boundary conditions than lack of interest. The advent of sophisticated finite element programs in the last decade has allowed more realistic modeling for specimens with complex geometries. The results with these analyses indicate a key role of spalling stresses in crack formation.

1.2.1.3 Bearing Stress. The maximum compressive stress developed by a post-tensioning system occurs beneath the anchor. In the case of a flat plate, or bearing type anchor, the average bearing stress is equal to the post-tensioning load divided by the net area of the anchor defined as the projected plate area minus the tendon duct area. Current design specifications in the United States, while specifying the need to examine bursting and spalling stresses, usually phrase their strictest recommendations in terms of allowable bearing stress. Most European specifications permit significantly higher allowable bearing stresses in post-tensioned design [7]. Whether this apparent over-conservatism in the American codes is justified has been a question much pondered but under-researched.

1.2.1.4 Additional Considerations. In addition to the geometric effects such as inclination, eccentricity, width and bearing area, the effects of friction and normal forces along the tendon duct for curved tendons (see Fig. 1.9), the effect of anchor hardware geometry (see Fig. 1.10) and other externally applied loads such as lateral post-tensioning must all be considered to fully grasp the anchorage zone stress state.

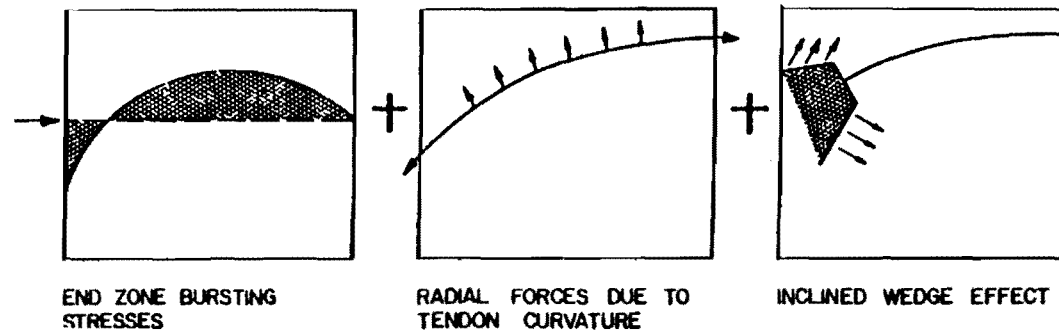


Fig. 1.9a Combination of end zone, radial and inclined wedge effects

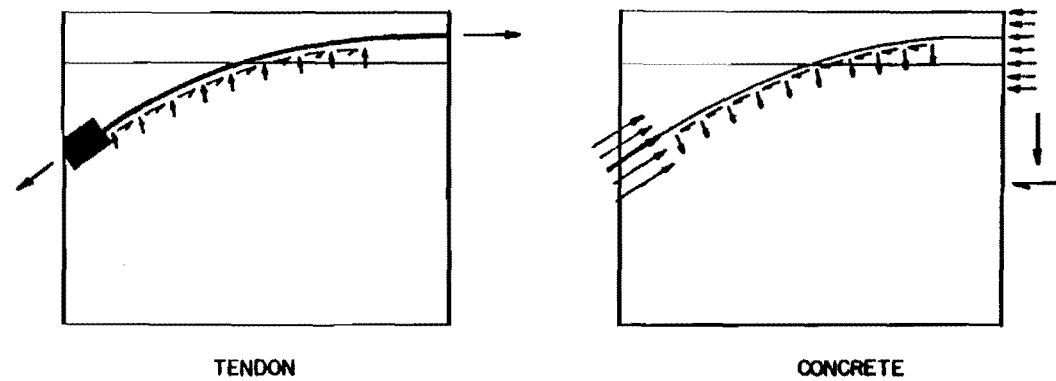
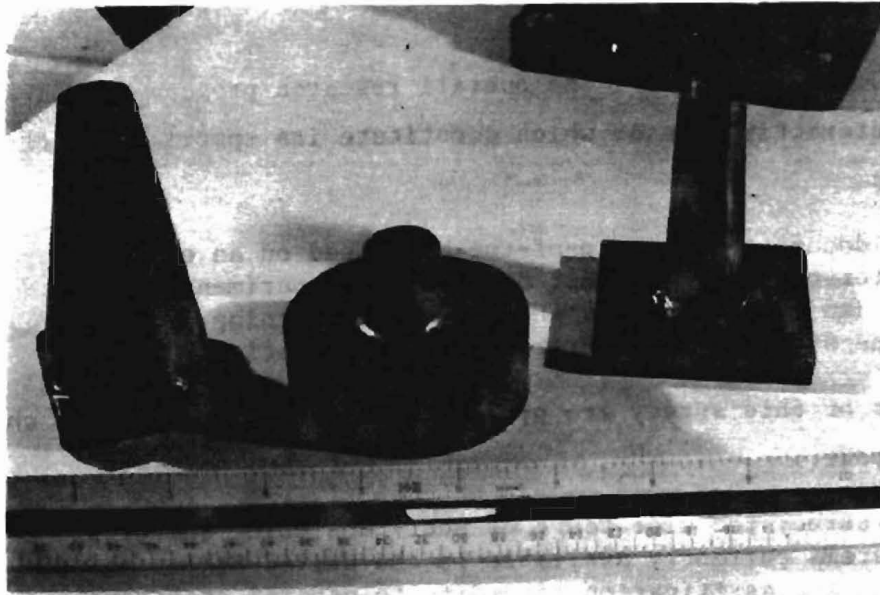


Fig. 1.9b Forces due to tendon curvature



Cone

Bell

Plate

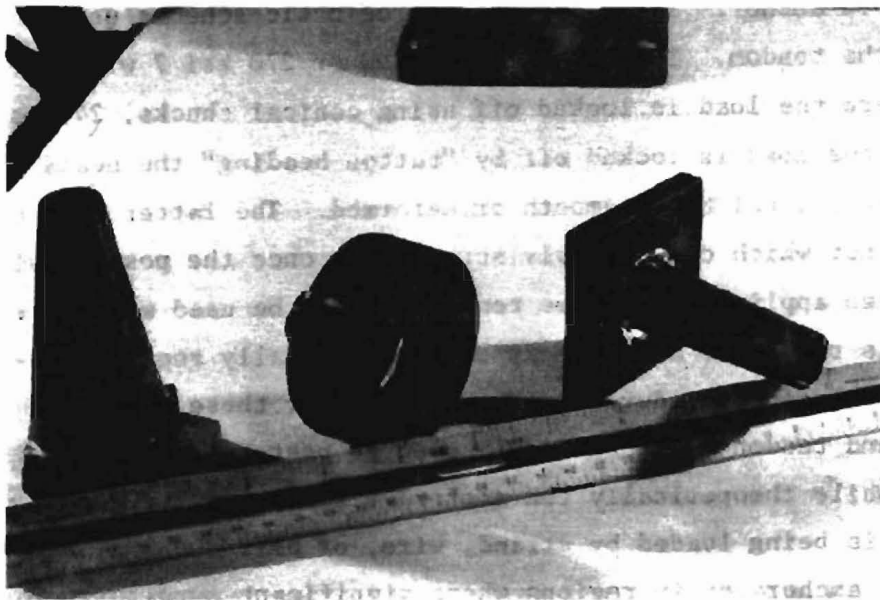


Fig. 1.10 Models of typical anchors used in post-tensioned construction

### 1.3 Overview of the Project

1.3.1 Objectives. The overall research program was broken into six interactive phases which constitute its specific objectives. These were:

- (1) To document the state-of-the-art based on an extensive literature study of all analytical, experimental, and design related papers and reports concerning anchorage zone stresses for post-tensioned applications.

The results of this survey are presented in detail in the next chapter of this report.

- (2) To survey the wide range of post-tensioning anchorage systems currently available in the United States and to make a classification according to general anchorage principles, sizes and shapes.

Figure 1.10 shows the three distinct types of anchorages in use. These are the bearing or plate type anchor, the cone or wedge anchor, and a "bell" shaped anchor. There are also three basic schemes used in making up the tendon. These use either 250 or 270 ksi 7 wire strand tendons where the load is locked off using conical chucks, 240 ksi wire where the load is locked off by "button heading" the heads of the wire, or 160-170 ksi bars, smooth or deformed. The latter uses a heavy duty nut which conveniently screws down once the post-tensioning load has been applied. Bar type tendons cannot be used where a sharp curvature is required, and wire type tendons usually require specialized anchorage procedures in the field. For these reasons the 7 wire strand tendon has been widely used in post-tensioned applications. While theoretically the anchorage zone cannot detect whether it is being loaded by strand, wire, or bar, the overall performance of anchorages in regions where significant curvature of the tendon is required has shown that cracking can occur at locations well removed from the immediate anchorage area. This effect occurs primarily for multiple strand tendons, but can occur for single strand tendons as well, and is discussed at length in subsequent reports.

- (3) To survey present and projected tendon path and anchorage zone characteristics in post-tensioned bridge applications.

A detailed examination of available bridge plans for several segmental projects both in the United States and Europe, indicate three significant factors are present:

- (a) In order to pick up some of the dead load shear, the tendons which are usually carried along the top deck slab are often curved down into the web sections in the segment in which they are anchored. This results in the tendon being sharply inclined at the anchor.

- (b) Since the tendon must be dropped into the web from a horizontal attitude, a significant curvature is developed which gives rise to large normal and friction forces along the duct.

- (c) Often a significant eccentricity of load with respect to web centroid occurs, particularly when multiple anchorages occur in the same web.

These characteristics and their effects on the anchorage zone are illustrated in Fig. 1.9. There is a current trend to anchor out of the web for speed of construction. This technique uses side "blisters" in the interior of the box section to anchor the tendon. Aside from moving the anchorage away from the congestion at the end of the web section, this method often does not eliminate the above factors and in fact may give rise to an additional out-of-plane curvature effect.

- (4) To study systematically by both analytical and experimental procedures, the development of critical tensile stresses in the anchorage zone for typical applications using representative anchorage systems.

In essence this was the core of the project. In this phase the principal variables, inclination, cover (width), eccentricity, bearing areas, and anchorage type were examined using both accurate 1/4-scale models and full-scale prototype specimens in the laboratory. A parallel effort was initiated to predict stress distributions in the

physical specimens through the use of two- or three-dimensional static, linear elastic finite element programs. As primary emphasis was placed on developing a behavioral mode for first cracking, the linear elastic assumption proved to be sufficiently accurate. Once calibrated the computer program could then be used to extrapolate beyond the range of the experimental tests. Ultimate strength trends would be derived from physical specimen test data.

The development and calibration of the analytical programs are detailed in Chapter 3 of this report.

- (5) To evaluate the efficiency of various active and passive reinforcement in anchorage zones, including spirals, conventional reinforcing bars and lateral prestressing.

This objective was an outgrowth of the experimental program but dealt with crack control rather than the behavioral mechanism by which the crack was initiated. If the cracking load could be altered and the ultimate load enhanced by the addition of reinforcement, then major design interest focuses on the most efficient scheme for placement of this reinforcement. Placement was the primary question concerning passive reinforcement. With lateral prestressing, or active reinforcement, a powerful new option was opened. This was due to the fact that the stress field in the anchorage zone could be significantly altered by the addition of a transverse compressive force. Results are discussed in the subsequent reports.

- (6) To develop recommendations for specific design criteria for post-tensioned anchorage zone tensile stresses.

Based upon experimental and analytic data these recommendations can be broken down into two categories:

- (a) If the structure is to be located in a highly corrosive environment where not even minor cracking can be tolerated, what is the maximum permissible stressing load, given the geometry of the anchorage zone?

(b) Given rigid geometric conditions and required load, what is an "acceptable" crack and how can this be controlled through an active or passive reinforcing scheme?

In either case the structure must be capable of performing satisfactorily under service load conditions and with an adequate factor of safety under failure conditions. The design recommendations and examples based on this investigation are contained in the final report.



## C H A P T E R 2

### LITERATURE REVIEW

#### 2.1 Introduction

A pioneering study of post-tensioned anchorage behavior appeared in the early 1950's when Guyon [4] investigated the tensile stresses responsible for cracking problems in early post-tensioning applications in Europe. In his classic 1953 text he states,

The principal effect of localized forces is the production of stresses in planes at right angles to the line of action of such forces and which tend to burst the element transversely to the force.

Hence the origin of the term "Bursting Stress." Using elasticity theory he developed a solution for the case of a load applied normally to the loaded surface. This theoretical solution was reduced to a practical design method known as the symmetrical prism analogy which is still in use in many countries today. This method is discussed in the next section. Guyon used a series of photo-elastic tests performed by Tesar [8] to confirm the symmetrical prism theory. In addition to verifying the presence of the bursting stresses, another tensile stress was brought to light. This stress occurred parallel to the loaded face and had its maximum value at the loaded face, as shown in Fig. 2.1. Since such a tensile stress on the surface of a reinforced concrete beam usually tended to cause the cover concrete to flake or spall off, these surface tensile stresses became known as "Spalling Stresses." The names have remained in the literature ever since.

However, Guyon's work and nearly all the studies which followed, did not adequately consider the effects of loads which were applied inclined to the loaded face or which were applied at high

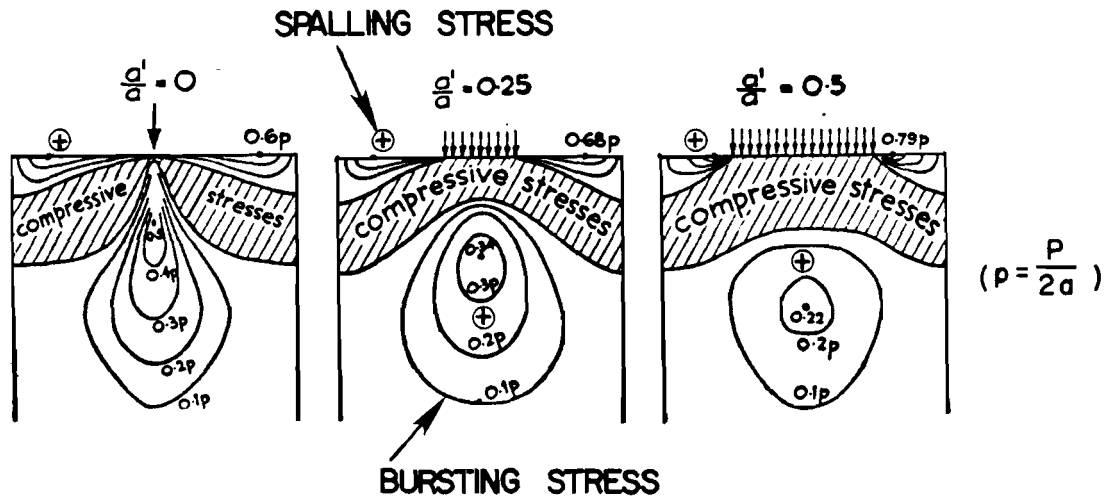


Fig. 2.1 Bursting and spalling zones from Tesar's photoelastic tests (from Ref. 4)

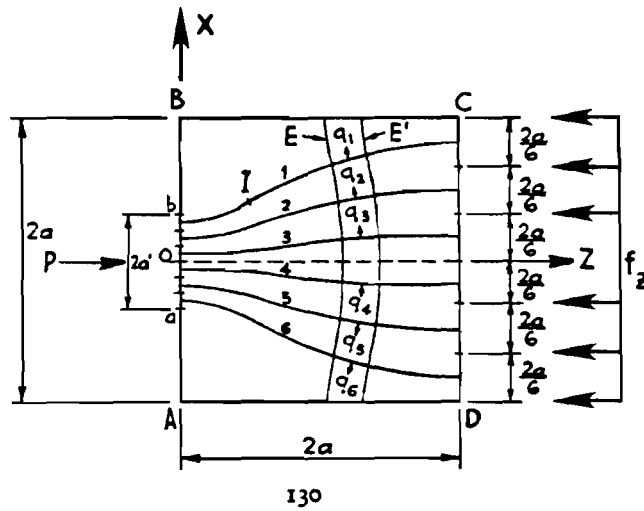


Fig. 2.2 Basic theory--Guyon. Note  $q = f_x$  (load per unit length in x-direction) (from Ref. 4)

eccentricities. Even the Zielinski and Rowe studies [9], widely regarded as the definitive experimental program and upon which many design codes and specifications are based, did not address either of these situations. Primary emphasis was placed on the bursting stress distribution as this was a simple concept to understand and design for. Consequently little experimental or analytical attention was paid to spalling stresses. They were regarded as surface phenomena which posed no threat to structural integrity when sufficient reinforcement was placed close to the loaded face.

This general bias towards criteria based almost completely on bursting stress is cited in a report on post-tensioning anchorage problems in nuclear containment vessels by Gergely in 1969 [3]. He states that, "In contrast with the attention paid to bursting zone conditions, the spalling stresses have sometimes been neglected or dismissed by designers because these stresses are localized." The extent to which this bias affected physical and analytical studies can be seen in the following sections. Indeed, faced with unexplainable cracking in post-tensioned members despite "adequate" bursting reinforcement, it is not surprising to see that the major codes resorted to archaic and overly conservative specifications based upon bearing stress studies from column base plates. It is clear that the problem was far from understood.

## 2.2 Previous Research on Anchorage Zones

2.2.1 Studies Based on Elasticity Solutions. The major initial contribution to elasticity analysis was made by Guyon. It is developed in detail because of its significance. A number of other studies using various solutions based on the classical equations of elasticity were performed in the early to mid-1960's. Most of these generally agreed with the trends first presented by Guyon. They are briefly mentioned for completeness.

2.2.1.1 Guyon's Theory. Guyon [4,5] pioneered a theoretical investigation of the anchorage zone stresses utilizing the two-dimensional theory of elasticity. Some of these results were verified by photoelasticity [8]. Guyon was highly aware of practical implications and developed a series of design aids for single straight concentric tendons, single straight eccentric tendons, and multiple straight eccentric tendons. He also attempted to explain changes in the stress field for slightly inclined tendons by using elasticity theory and by breaking the inclined load into normal and tangential components.

Guyon's approach can be seen for a single axial force applied to a rectangular prism as shown in Fig. 2.2. He reduced the problem to two dimensions assuming the load to be applied across the width of the member. Thus the effect of cover was not considered. Guyon explained the presence of the bursting stress as follows:

The single force  $P$  is uniformly distributed over a height  $2a'$  (the anchor width), symmetrical about the axis of the beam  $OZ$  of Fig. 2.2. The lead-in-zone, of approximate length  $2a$ , carries on the surface  $CD$  a uniform distributed load  $f_z$  (St. Venant) to which  $P$  acts as a reaction; the lead-in-zone may be considered as a beam in equilibrium on the central support  $P$  and submitted to simple bending under the action of the horizontal forces  $f_z$ . We are ignorant, however, of the stress distribution in a beam of such proportions.

The forces can be considered as passing across the block from  $AB$  to  $CD$  along trajectories such as 1,2,3,4,5,6 in Fig. 2.2. These trajectories are the isostatics issuing from the loaded area  $ab$ . At their origin in  $ab$  they are parallel to the force  $P$ . Between these two sections then, they must adopt an S-form with a point of inflection at  $I$ . Having divided  $ab$  and  $CD$  into  $n$  equal parts, each isostatic can be supposed to carry a force of  $P/n$  from the center of one division in  $ab$  to the center of the corresponding division in  $CD$ . The material in the interior of the zone may thus be considered as made up of a series of curved fibers, each carrying a fraction of the compressive force. Now these fibers cannot support compression without exerting a transverse force normal to the fiber caused by their curvature. This force acts inwards or outwards according to the direction of convexity of the curve. The transverse stresses are at a maximum on the axis  $OZ$ . The shearing stress  $\tau$ , by symmetry, is zero on this axis. On the axis

OZ therefore, the only stress is  $q$ , the transverse stress (where  $q = f_x$  for convenience). Its value varies from AB to CD at which point it becomes zero, or at least negligible.

An idea of the variation of  $q$  (or  $f_x$ ) along OZ may be gained by replacing the isostatics on each side of OZ by an "average" isostatic carrying  $P/2$  to the center of the upper or lower half of CD in Fig. 2.3. Then if  $R$  is the radius of curvature at any point along the line of this isostatic, the transverse force per unit of length of OZ is  $P/2R$  and this transverse force per unit length equals  $q$ , the bursting force.  $R$  is negative in the neighborhood of AB and  $q$  is thus compressive. At the inflection point I,  $R$  becomes infinite and  $q$  is zero. Between I and CD,  $R$  is positive and  $q$  becomes tensile, increasing until it reaches a maximum at approximately  $4a'$  from the loaded face and then tending to zero as CD is approached since  $R$  again becomes infinite. The position of the point of inflection, the maximum compressive stress near ab, and the value and position of the maximum tensile stress all depend on the ratio of the anchor width  $2a'$  to the section height  $2a$ . The variation of  $q$  (or  $f_x$ ) along the axis for various values of  $a'/a$  is shown in Fig. 2.4, where  $f_x$  is normalized by the value  $P/2a$ .

Guyon was also aware of the presence of tensile stresses along the loaded face. From Fig. 2.1 it is apparent that in addition to the tension produced deep in the block along the line of action of the force, there are appreciable tensions near the surface adjacent to the anchor, the spalling stresses. Based upon the photoelastic work by Tesar [8] Guyon calculated the resulting spalling tension for various values of  $a'/a$  follows:

$a'/a =$	0	0.10	0.25	0.5
Total Surface Tension	0.04 P	0.03 P	0.025 P	0.02 P

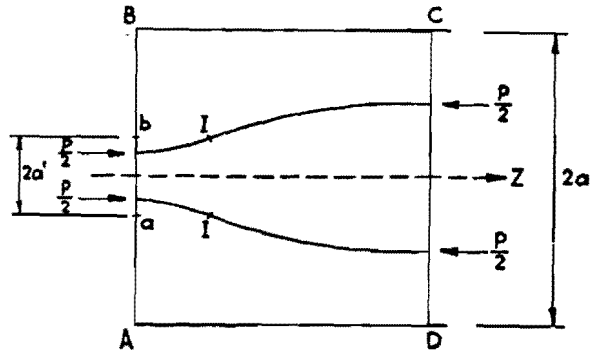


Fig. 2.3 Isostatic lines of force through the lead-in zone (from Ref. 4)

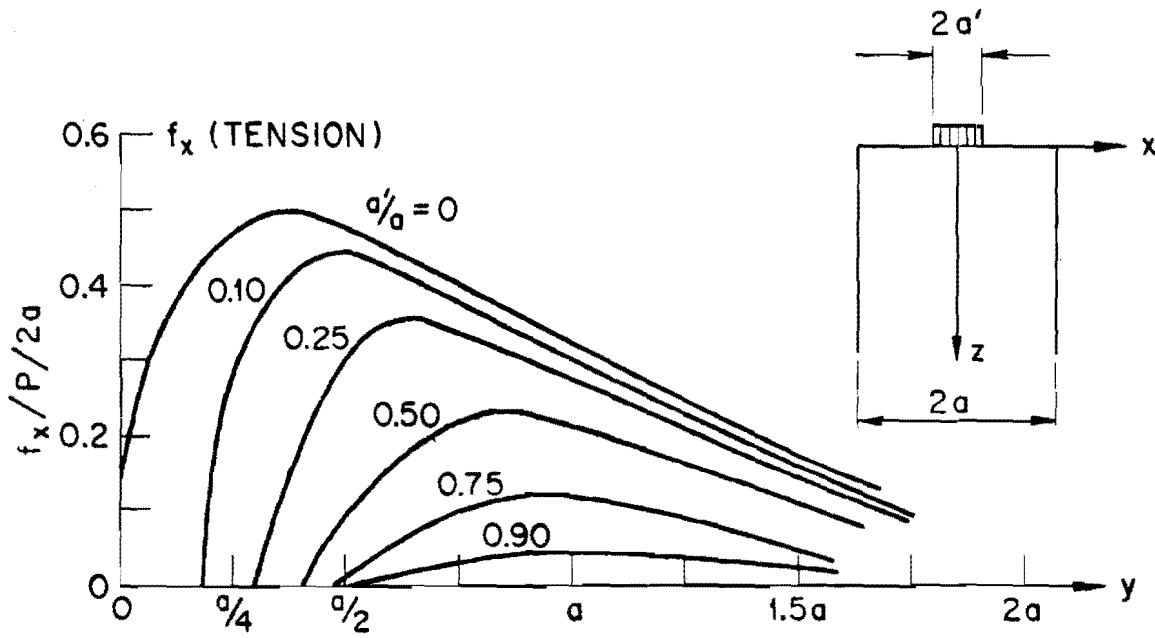


Fig. 2.4 Bursting stresses for various loaded areas (from Ref. 4)

The sizing of reinforcement was thus a very simplified calculation. He recommended that this reinforcement should,

be placed as near the bearing surface as possible. This surface binding, which should be composed of steel of small diameter, need not be extensive since though the stresses are high on or near the surface, the depth of material on which they act is small. The resultant tension tending to crack the surface is thus not large.

Proportioning of reinforcement for bursting stresses was handled in a similar manner. Given Fig. 2.4, an idealized triangular approximation such as shown in Fig. 2.5 could be arrived at. These criteria [4] for determining spalling and bursting reinforcement became widely accepted in European practice.

The preceding discussion has been limited to axial, symmetric loading. For the case of nonuniform precompression produced by an eccentric force, Guyon proposed the "symmetrical prism" method. In this method the prestress load  $P$  is assumed to be applied over an imaginary symmetrical prism represented in Fig. 2.6, by the shaded areas of depth  $2a_1$ . The stresses are then determined by using the results of the single concentric force case. Upon comparing analytical results for a specific problem, Guyon found errors of 22 percent and 7 percent respectively for maximum stresses and total bursting force. Since the errors indicated stresses computed by the symmetrical prism method to be larger than a more exact solution, he concluded that, for design purposes, the approach would be reasonable.

From Fig. 2.6 it can be seen that for larger and larger eccentricities the ratio of  $a'/a_1$  used for calculation of bursting stress slowly trends toward the value of unity. Thus, Fig. 2.4 shows that the bursting stress would decrease toward zero. As the bursting stress decreases, so should the required reinforcement. This is a key point in assessment of the test results of specimens with eccentricities reported in the second report of this current investigation. If the cracking load were dependent upon bursting stress, Guyon's theory indicates cracking loads should be higher for larger eccentricity. In

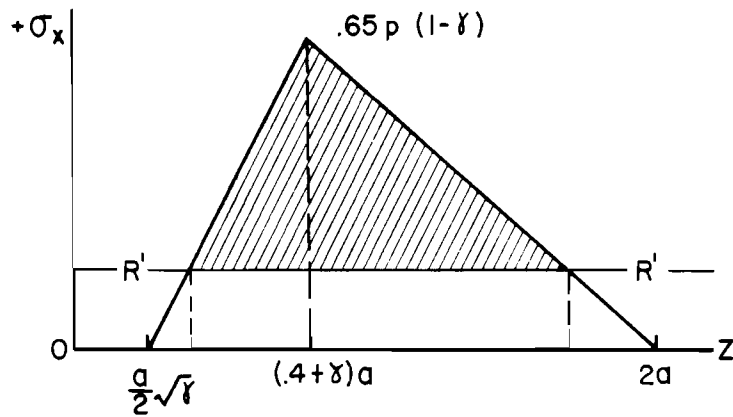


Fig. 2.5 Approximate tensile bursting stress distribution for design (from Ref. 4) (shaded area indicates region where bursting reinforcement must be supplied.  $R'$  is the tensile strength of the concrete and  $\gamma = a'/a$ )

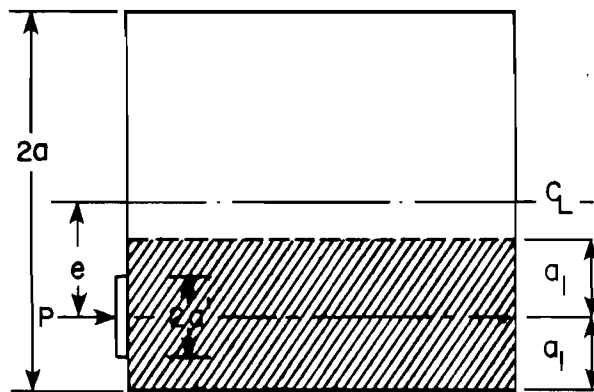


Fig. 2.6 Guyon's symmetrical prism analogy (shaded area indicates appropriate prism to be used for calculating bursting stresses for eccentric loading)

fact the opposite was seen to be the case. The cracking load  $P$  drops for increasing eccentricity. This paradox, and others which will be pointed out later, leads to the conclusion that a different indicator than bursting stresses is needed for design.

For the more complex case of several eccentric forces, another approximate method was proposed by Guyon. This is termed the "successive resultants" method, as illustrated in Fig. 2.7. It is assumed that maximum stresses occur on the axes of the individual forces, on the axes of the resultants of the groups of two forces, and on the axis of the resultant of the entire set of forces. In Fig. 2.7, the prism depth  $2a_r$  for the total resultant  $R$  is defined as shown using the symmetrical prism analogy. Similarly, for the partial resultants I and II, prisms of depth  $2a_I$  and  $2a_{II}$  are defined. Finally, the individual prisms for each of the forces  $P_{1-4}$  can be defined. The tensile stresses and forces in each individual prism may be found from the ratios  $a'/a_r$ ,  $a'/a_I$ ,  $a'/a_{II}$ , etc., where  $2a'$  is the width of the anchor. According to Guyon this approximate method will lead to some excess of reinforcement over that actually required.

Lastly, Guyon briefly examined the case of a slightly inclined tendon (lv:20h) by breaking the inclined force into a normal and tangential force applied to a rectangular prism, and using a standard elasticity approach. He concluded that the bursting tensile distribution is "scarcely changed" from that of a normally applied force and recommended the use of an appropriate "symmetrical prism." In passing he noted that, "spalling tensions (for inclined loads) on the contrary are appreciably modified." His solution neglected the fact that in actual practice a block-out is usually required to achieve tendon inclination at the face. The above-mentioned phenomena are echoed in the work of Christodoulides and Sargious (Sec. 2.2.2) for slightly inclined tendons.

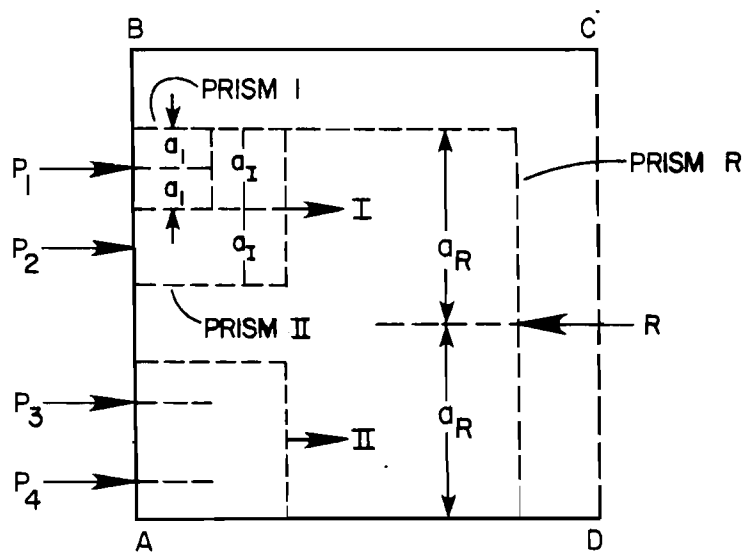


Fig. 2.7 Guyon's successive resultant method for the case of multiple anchorages in a rectangular end block

2.2.1.2 Douglas and Trahair. Using a three-dimensional axisymmetric analysis Douglas and Trahair studied the stress distribution in an axially loaded, hollow cylinder [11], and found good agreement with Guyon's theory except they did not detect spalling stresses because only large ratios of loaded area to cross section area were investigated.

2.2.1.3 Iyengar. Iyengar presented a theoretical solution [12] for the two-dimensional problem and compared these with the results of other elasticity solutions by Guyon [4], Bleich [13], and Sievers [14]. His transverse stress distribution results agreed with those of Guyon. However, he concluded that Guyon's longitudinal and shear stress distributions were inappropriate. With Prabhakava [15], he developed a three-dimensional solution for a rectangular end block with a single straight tendon and found that the symmetrical prism method could effectively be used for design purposes.

2.2.1.4 Gergely, Sozen and Siess. Gergely, Sozen and Siess [16] reported a finite difference solution for a few cases with rectangular sections and straight tendons and found results which agreed closely with Guyon's solution.

## 2.2.2 Other Analytical Solutions

2.2.2.1 Beam Method. In this method, approximate solutions for transverse tensile stress are obtained using a simple equilibrium analysis. For example, in Magnel's solution [17] a prism is isolated as shown in Fig. 2.8. The reference plane is one boundary and the prism is assumed to be acted upon by a concentrated prestressing force on one side and by a linear distribution of stress on the other side. The transverse stress distribution on the reference plane is assumed to be a cubic parabola. This type of approach was first applied by Morsch [18] and subsequently extended to different loading configurations by Sievers [14] and Schlee [19].

CUBIC PARABOLA ASSUMED FOR TRANSVERSE STRESS DISTRIBUTION

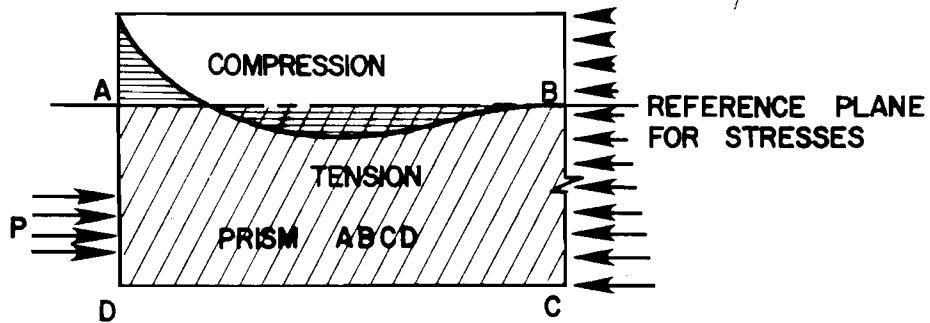
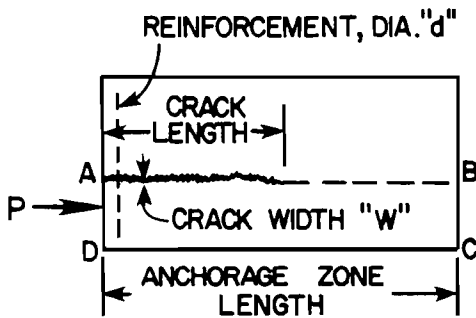
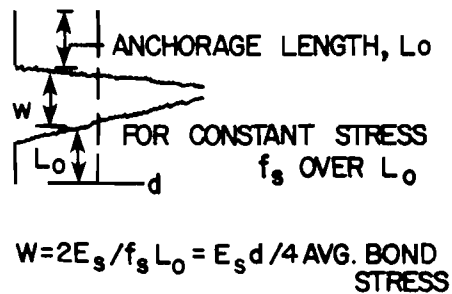


Fig. 2.8 Magnel's beam analysis

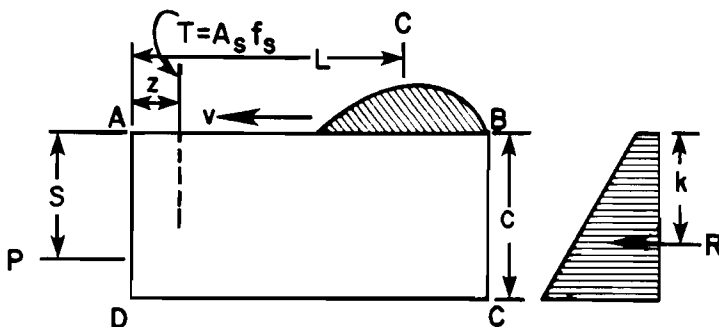
(a) END BLOCK



(c) CALCULATION OF CRACK WIDTH



(b) FREE BODY DIAGRAM OF SECTION BELOW CRACK



(d) EQUILIBRIUM CONDITIONS

FOR EQUILIBRIUM OF BODY ABCD:

$$P_s - Rk = T(L - z)$$

FOR DESIGN:

$$T = (P_s - Rk) \text{MAX. VALUE} / h - z$$

Fig. 2.9 Gergely's beam analysis

2.2.2.2 Gergely. Similar types of analysis were used by Gergely [20] and Lenschow and Sozen [21]. Gergely's approach is illustrated in Fig. 2.9. He argued that in many cases cracking could not be prevented and that a better approach was to limit crack widths to acceptable values. Equilibrium conditions were examined for a series of free bodies such as ABCD. For each free body a potential crack line, AB, served as one boundary and the end of the anchorage zone, BC, as another boundary. For equilibrium there had to be a moment  $M$  and a shear  $V$  along AB. The most likely position for cracking was determined by finding the height BC for which the moment  $M$  was a maximum. Reinforcement requirements were determined by calculating the force  $T$  for this moment and limiting the maximum reinforcement stress so that the crack width would not exceed an acceptable value. Conservative approximations suggested for design were that the compressive force  $C$  in the concrete be assumed to act at the end of the crack and the bond-slip relationship for the reinforcement be assumed to be rigid plastic with a limiting value of  $4\sqrt{f'_c}$  (see Fig. 2.9b).

2.2.2.3 Lenschow and Sozen. Lenschow and Sozen [21] developed a physical analog for anchorage zone cracking based upon elemental beam equilibrium. As an example, consider a prismatic beam subjected to a concentrated force as shown in Fig. 2.10. It is desired to find the transverse tensile stresses along a section to be called the "reference plane," parallel to the longitudinal axis. Instead of the classical elasticity methods of solution, the beam in Fig. 2.10 can be represented by the multiple beams in Fig. 2.11. The loading in Fig. 2.12a is symmetrical about the beam centroid as are the cuts introduced, one of these being at the reference plane. Fictitious springs, representing the concrete, resist the deflection of the outer parts of the beam. The loading in Fig. 2.12b is adjusted so that the two parts of the cut beam have the same curvature; the fictitious springs are not required. The loading conditions in Fig. 2.12b are prescribed so that they may be superimposed to yield the

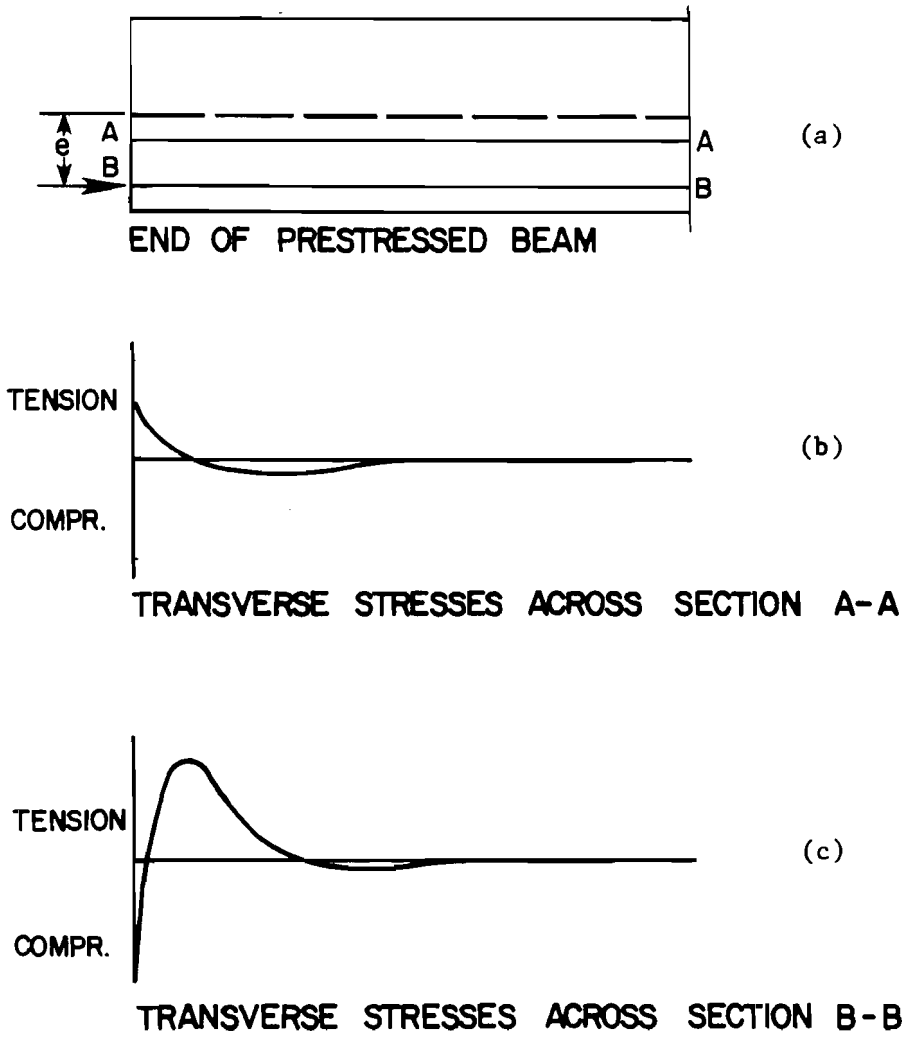


Fig. 2.10 Bursting and spalling stresses

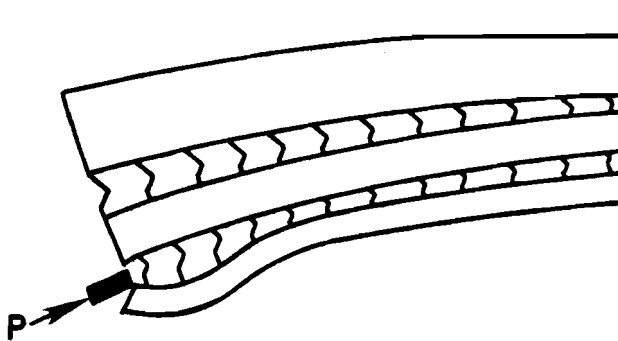


Fig. 2.11 Exaggerated deformations of end block with fictitious discontinuities

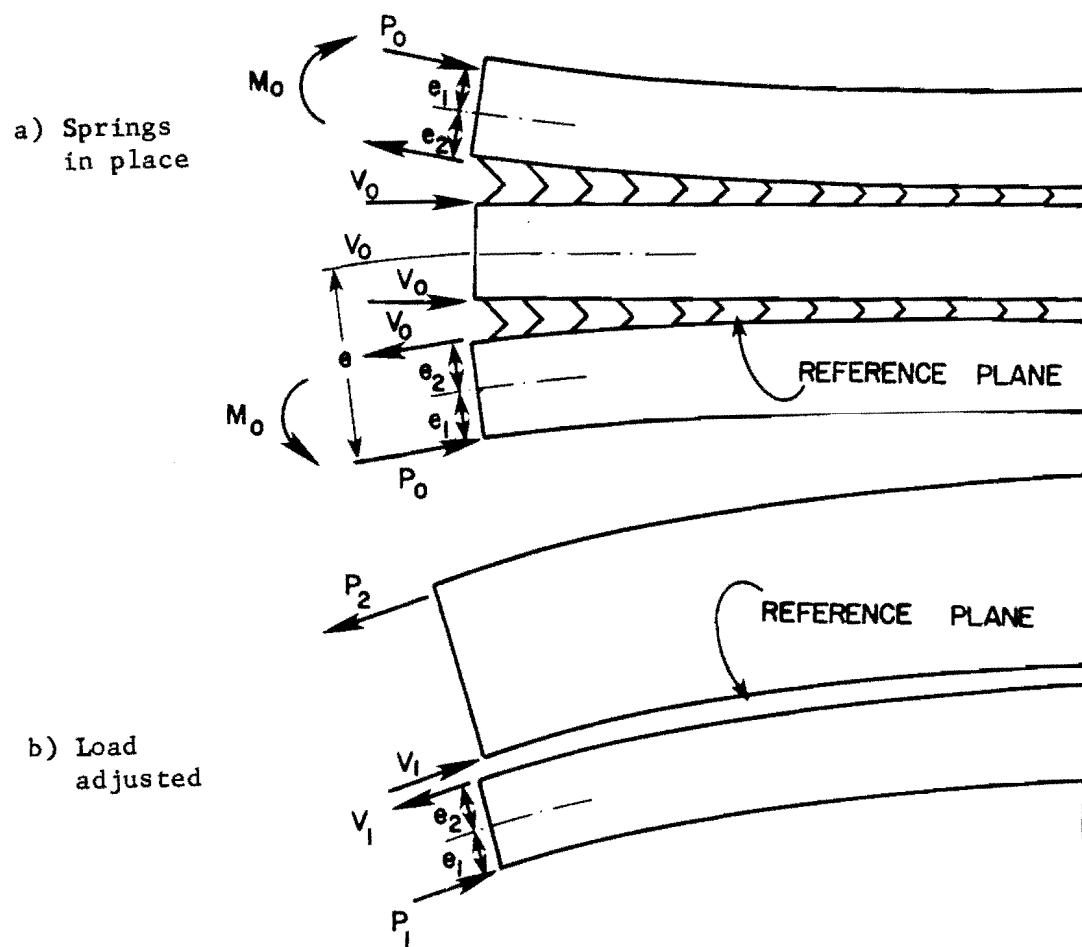


Fig. 2.12 The physical analog (from Ref. 21)

actual loading of Fig. 2.10. The solution then utilizes equilibrium equations and compatibility of curvatures based on an elastically supported beam analysis to determine the transverse stresses on the reference plane.

The results of the analysis compare quite favorably with those of Guyon and others as shown in Fig. 2.13. Good agreement is reported for both concentric and eccentric loads applied normal to a rectangular section. While the method has promise, the difficulty in defining the value of the spring stiffness for a given problem is a clear drawback. In order to obtain a comprehensive spalling stress profile a large series of calculations must be done since the reference plane only considers a line of stress parallel to the load. The method's advantage lies in the relatively direct proportioning of the reinforcement once the stress distribution across a critical plane is obtained. With proper boundary conditions, cracks in the beam can be modeled.

2.2.2.4 Yettram and Robbins. In 1970 Yettram and Robbins [22] reported a series of three-dimensional finite element analyses of post-tensioned anchorage zones using 8 node brick elements. Prior to this present study their work seems to be the only finite element study done specifically to investigate bursting and spalling distributions. The results agreed quite well with those of Guyon. Several meaningful conclusions were drawn, indicating finite element techniques had great potential for predicting anchorage zone stresses up to cracking.

The basic accuracy of the symmetrical prism analogy was examined for single eccentric anchorages as shown in Fig. 2.14a and for two symmetrically placed anchorages as shown in Fig. 2.14b. The individual prism of Fig. 2.14c would be assumed applicable in both cases. The bursting stresses  $\sigma_x$  are compared on the critical plane  $x = a_1$  ( $x = \pm a_1$  for case b). The individual prism (case c) results are reasonable approximations of both the magnitude and the distribution of the bursting stresses. They are higher and thus more

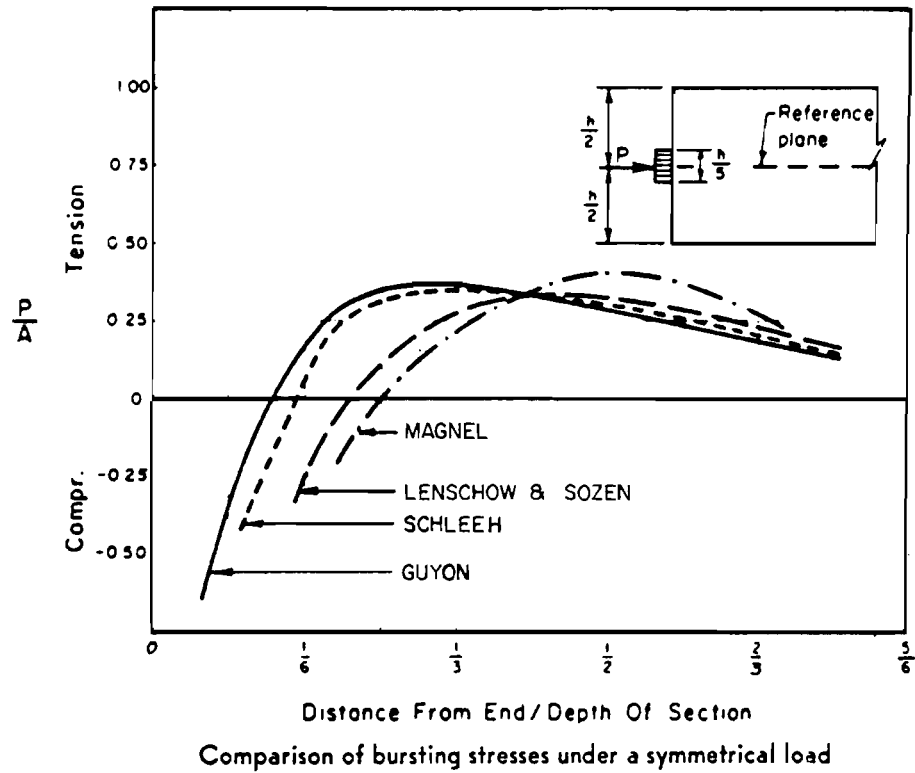
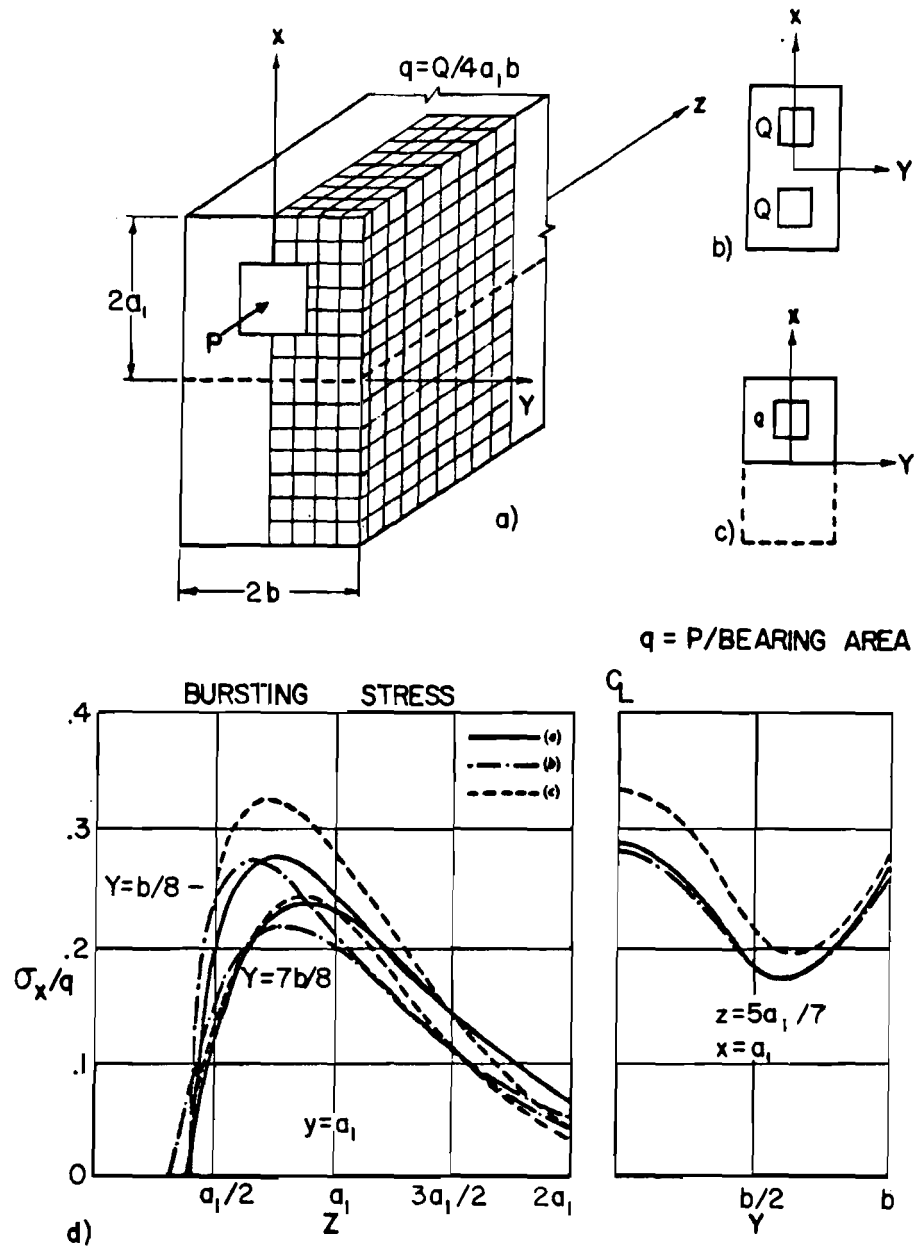


Fig. 2.13 Lenschow and Sozen calculations compared to previous work (from Ref. 21)



Narrow rectangular prism with (a) single eccentric anchorage and (b) symmetrically placed double anchorage across depth

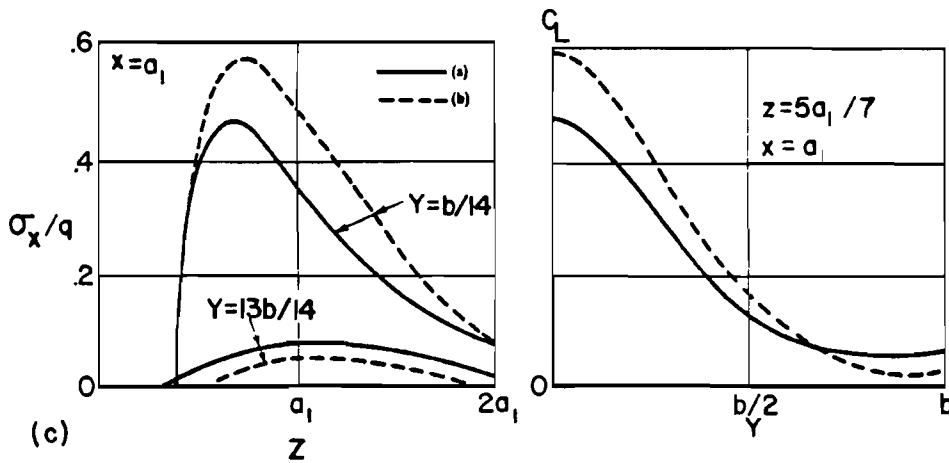
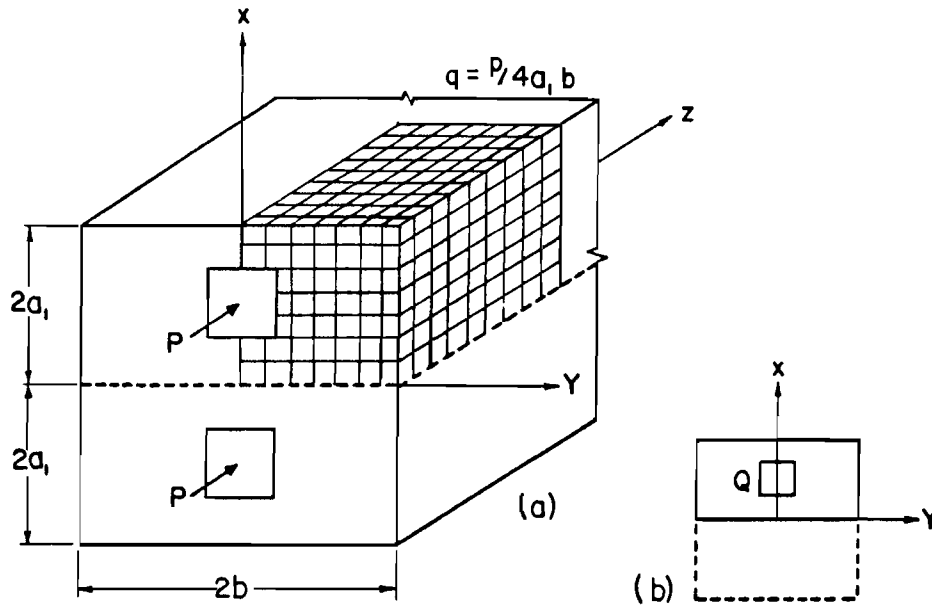
Fig. 2.14 Narrow rectangular prism--FEM results from Yettram & Robbins (Ref. 22)

conservative than the stresses for the complete prisms throughout the region of greatest interest. This same agreement is seen in Fig. 2.15 for a wider prism. Both Figs. 2.14 and 2.15 show that the maximum bursting stress occurs in the center and the stress drops toward the side face of the member. The drop in the wide member is substantial. Many physical studies have based their measurements of bursting stress on mechanical extensometer readings taken on the outer surface. Thus for most cases this value will not reflect the true maximum transverse tensile stress which occurs along the centerline of the load.

Application of the symmetrical prism method to anchorage zones of I, T, or box beams often results in individual prisms of nonrectangular section. The bursting stresses in such a prism are generally evaluated by considering an equivalent prism of rectangular section (i.e., two-dimensional). In order to evaluate the accuracy of this approximation, rectangular sections were compared with I sections for varying eccentricity of load.

In Fig. 2.16a the prism is subjected to a single axial force through an anchorage of the same width as the web. The stress distribution in the web, except in the immediate vicinity of the flanges, is therefore two-dimensional. In Fig. 2.16c, the distributions of bursting stress on two longitudinal sections in the web of the prism are compared to corresponding distributions in the equivalent "two-dimensional" prism of Fig. 2.16b.

Fig. 2.18c indicates that the use of an equivalent flangeless prism gives a reasonable approximation for the maximum bursting stresses along the line of action of the post-tensioning force ( $x = 0$ ). However, on the section ( $x = 5a/12$ ) immediately below the flange, the stresses for the rectangular section are less than half those of the I section. The I section stresses near the flange are only 25 percent less than those on the critical section. Clearly the flanges have the effect of increasing the depth of the web over which the bursting stresses should be considered as acting.



Wide rectangular prism with symmetrically placed double anchorage across depth

Fig. 2.15 Wide rectangular prism--FEM results from Yettram & Robbins (Ref. 22)

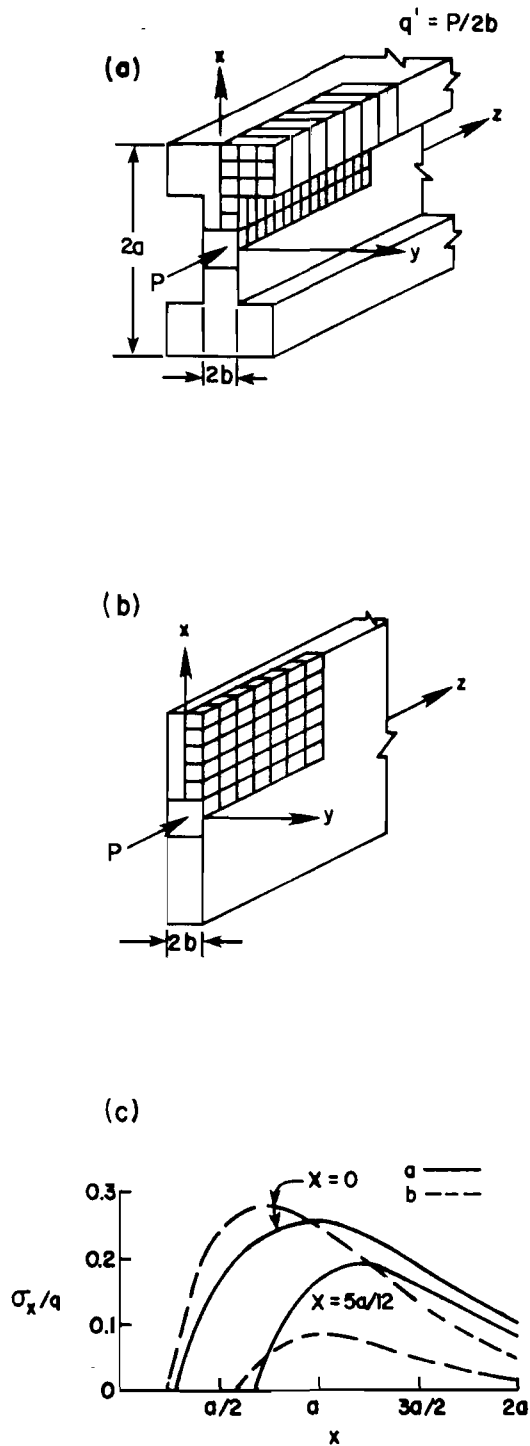


Fig. 2.16 I-section prism, axial anchor--Yettram & Robbins (Ref. 22)

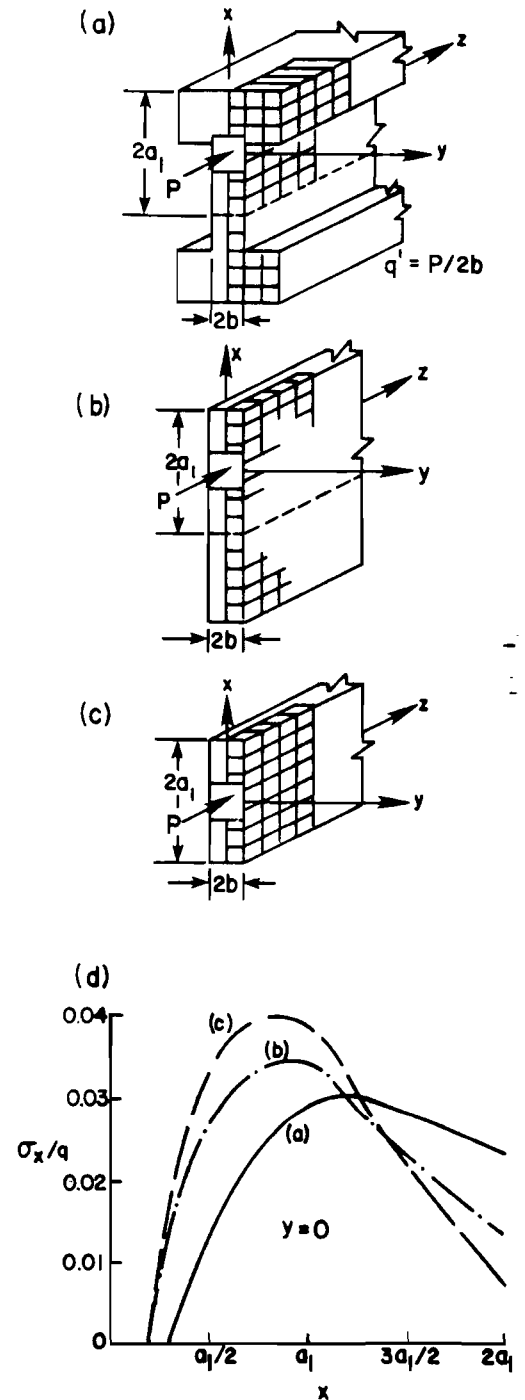


Fig. 2.17 I-section prism, eccentric anchor--Yettram & Robbins (Ref. 22)

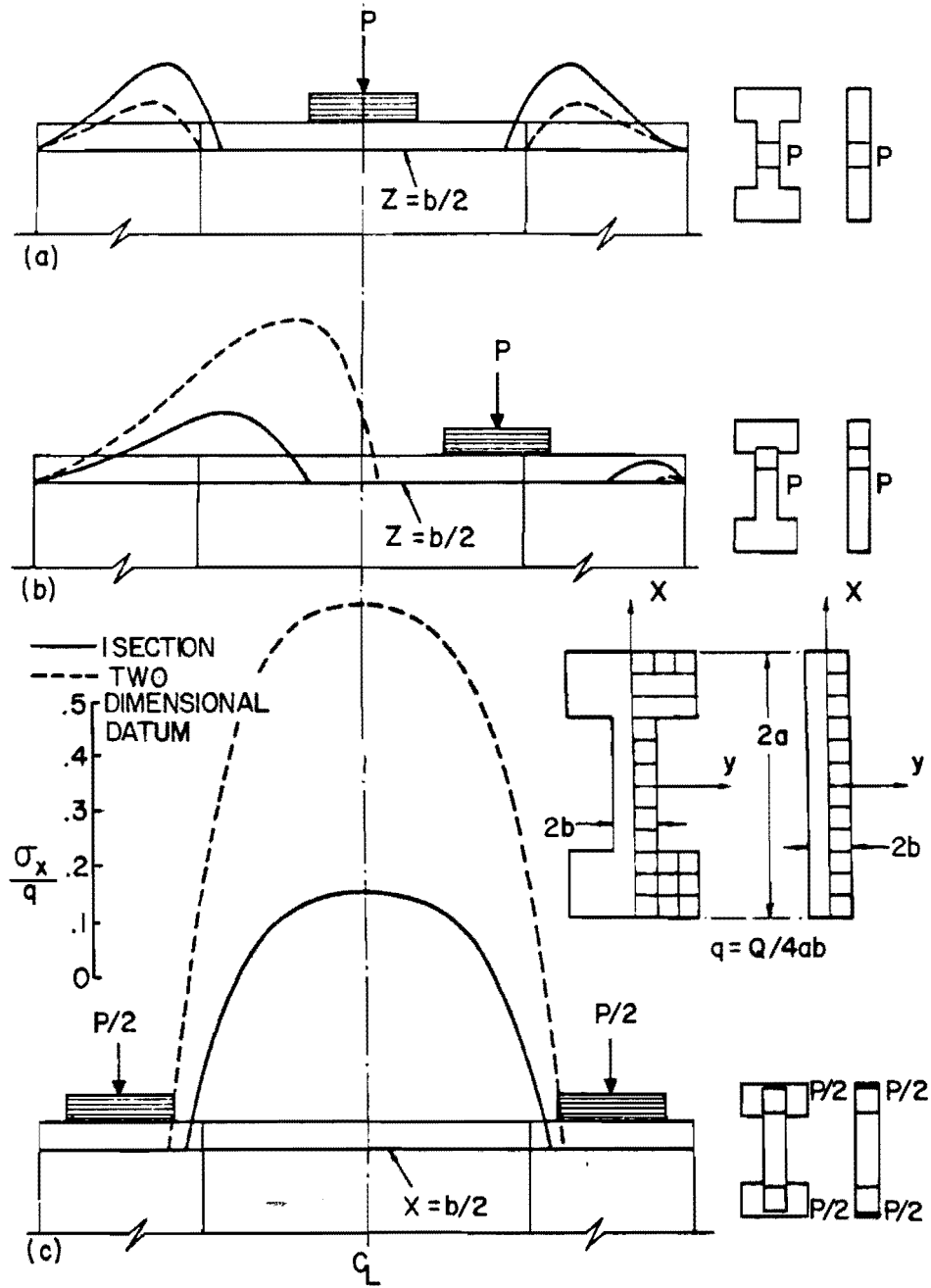


Fig. 2.18 Spalling stress distribution across depth of I-section--Yettram and Robbins (Ref. 22)

In a comparison example, the I beam of Fig. 2.17a is subjected to a single eccentric force. In this example the bursting stress distribution along the line of action of the force is compared to that of two equivalent rectangular sections. The first (Fig. 2.17b) corresponds to the full height of the I section, and the second (Fig. 2.17c), corresponds to the equivalent symmetrical prism. In Fig. 2.17 the discrepancy between curves b and c represents the order of accuracy normally associated with the symmetrical prism method. Both rectangular prisms give larger values for the maximum bursting stress than that predicted for the I section, the difference being about 30 percent for the symmetrical prism c.

Close comparison of Figs. 2.16c and 2.17d shows an interesting trend not pointed out in the Yettram and Robbins report. The maximum bursting stress for the eccentric loading was only one-seventh the value for the equivalent axial loading, for both flanged and rectangular sections. This would lead to the same erroneous conclusion as pointed out in Section 2.2.1 that less reinforcement would be required in the anchorage zone of eccentrically loaded sections.

While no in-depth analysis of spalling stresses was attempted, a few examples were given. Figure 2.18 shows that for all sections (I or rectangular), the spalling stress increases with increasing eccentricity. For rectangular sections, this increase is dramatic. These trends for bursting and spalling stresses should be recognized when dealing with eccentric loads: for increasing eccentricity the spalling stress increases sharply, the bursting stress decreases.

2.2.2.5 Summary of Analytical Studies. In a review of analytical studies, Hawkins [23] found the following areas in agreement:

- (1) There are at least two distinct zones of transverse tensile stresses. These are the spalling and bursting zones.

- (2) Principal tensile stresses may occur along an axis other than the transverse axis. However, for practical purposes it is sufficient to consider transverse tensile stresses only.
- (3) For a single concentrated load the spalling stresses increase rapidly as the eccentricity of the load increases.
- (4) The maximum bursting stresses decrease as the eccentricity of the load increases.
- (5) The maximum bursting stresses decrease with an increase in the ratio of the loaded area to the block cross section area.
- (6) St. Venant's Principle is verified by most of the investigators.

In general, all theoretical solutions presented were analytical models for:

- (1) Homogeneous, isotropic and linearly elastic anchorage zones.
- (2) End blocks which were subjected to loads applied by non-curved tendons. A few studies made on slightly inclined forces in draped tendons divided the load into normal and tangential components.
- (3) Two-dimensional or axi-symmetric three-dimensional problems.

2.2.3 Photoelastic Investigation. Besides the previously mentioned work of Tesar [8], whose photoelastic tests were used to verify Guyon's studies, three other photoelastic studies dealing with post-tensioned anchorage zones warrant mentioning.

2.2.3.1 Christodoulides. Christodoulides [24] carried out tests on the end of post-tensioned section gantry beam (Figs. 2.19 and 2.20) with a rectangular end block. He replicated the physical test using a one twenty-fifth scale model cast using Araldite B photoelastic resin. The ducts in this three-dimensional model were formed by 1/16 in. diameter holes drilled through the plastic. In order to obtain stresses on the plane along the axis of loading the photoelastic technique of stress freezing was used.

The results of the photoelastic tests showed that the maximum tensile stresses occurred between and near the anchorages in

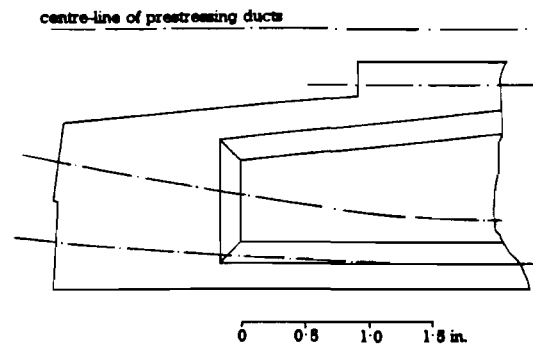


Fig. 2.19 Model end block tested by Christodoulides (from Ref. 24)

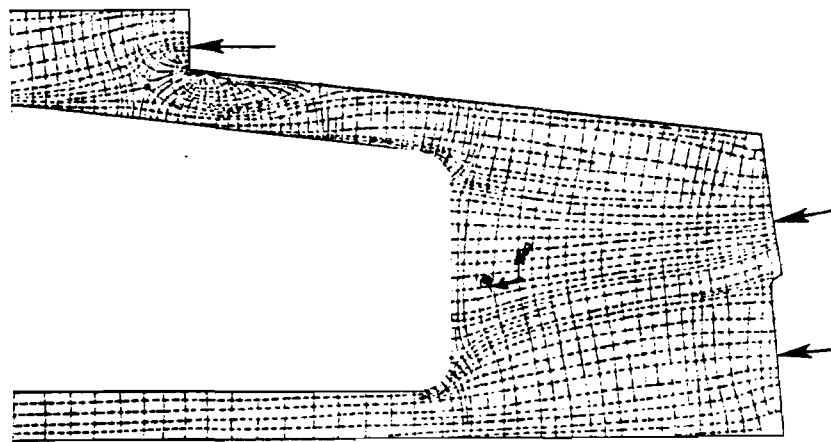


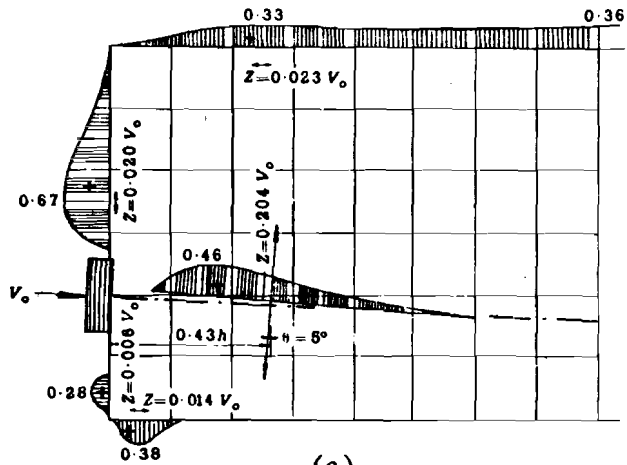
Fig. 2.20 Principal stress trajectories from Christodoulides' photoelastic test of gantry beam (from Ref. 24)

the central plane and had a value approximately twice the average compression as calculated on a section taken halfway between the anchorages and the beginning of the web of the I section. The agreement between the results for stresses obtained photoelastically and on the actual beam was within 20 percent. Christodoulides stated that the maximum stresses were considerably greater than those calculated using Guyon's approach.

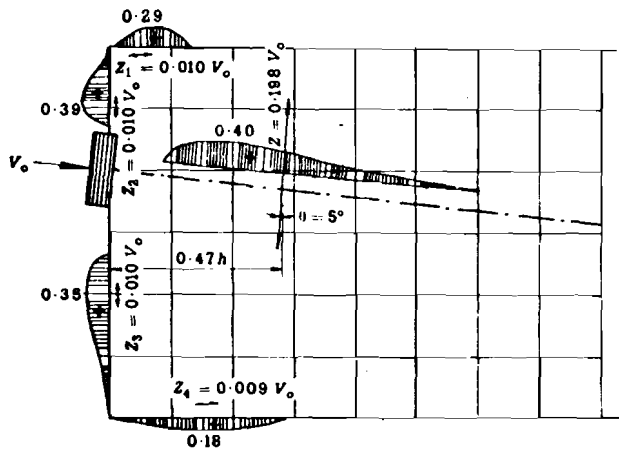
In earlier two-dimensional photoelastic tests, the presence of the tendon duct was ignored and two eccentric loads were applied. The results had compared favorably with analysis values of Guyon and Iyengar. However, the basic assumptions of the two-dimensional analyses were the same. Christodoulides made the following important statement regarding the reproduction of post-tensioned anchorage zone stresses through photoelastic techniques:

It must be remembered that the actual distribution of stress in the end blocks of post-tensioned beams is a three-dimensional one, i.e., the stresses vary along the width of the beam as well as the depth and length. Also the cable ducts cast in the concrete will affect the distribution of stress.

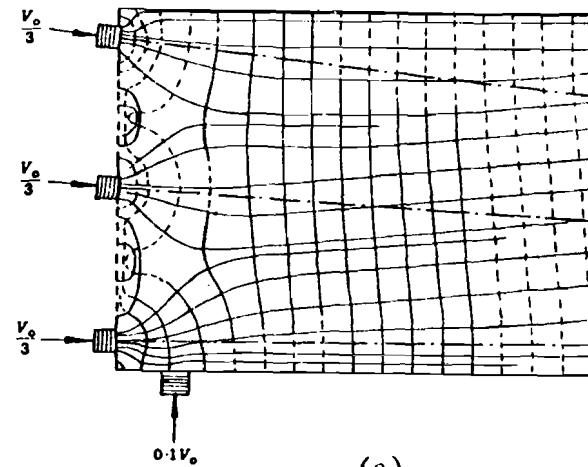
2.2.3.2 Sargious. Working under Leonhardt in the mid-1960's, Sargious [25] carried out a series of two-dimensional photoelastic tests on model end blocks to investigate the effect of the beam support reaction on the stress distribution of post-tensioned anchorages. The models were of rectangular and T sections with single eccentric forces or three nonlinearly distributed forces. In each case one test was carried out with a zero support reaction. From the isoclinics and isochromatics, the principal stress trajectories were derived. Typical results are shown in Fig. 2.21 for a force applied at either the upper or the lower kern limits of the rectangular section for zero support reaction. Figure 2.22 shows the stress trajectories and the tensile stress distribution in a rectangular end block having three applied forces in which the support reaction was



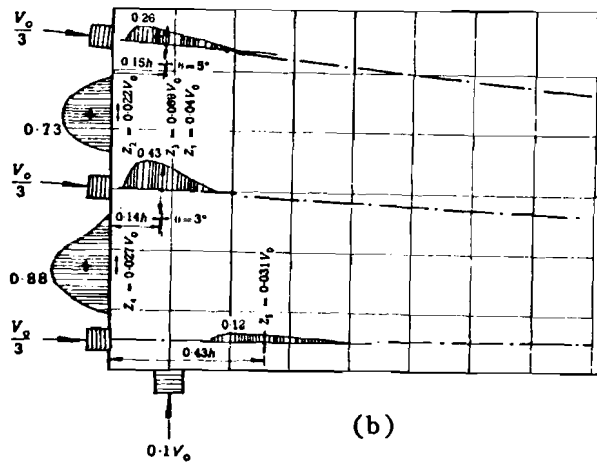
(a)



(b)



(a)



(b)

Fig. 2.21 Sargios: experimental results for a single eccentric applied force on a rectangular end block (Ref. 26)

Fig. 2.22 Sargios: experimental results for three applied forces on a rectangular end block (Ref. 26)

10 percent of the applied forces. In Fig. 2.22 the maximum transverse stress is 0.46 of the uniform compressive stress. The stress distribution in this figure does not conform to the successive resultant theory of Guyon. In addition to the transverse bursting stresses, there were considerable spalling tensile stresses between the forces close to the loaded face. The maximum value was 0.94 times the uniform compressive stress, or more than double the maximum bursting stress.

Sargious did not find any significant difference between the transverse stress distribution in a rectangular or a T end block when loaded by a single eccentric force and hence concluded that the effect of the flange could be ignored in such cases. However, in his cases the eccentricity was not great. As Yettram and Robbins pointed out in the later finite element study, eccentric load stress distributions are definitely affected, usually decreased, when the load is applied in near proximity to the flange. The effect of the support reaction decreased the value of the maximum transverse stresses and affected the position of the maximum stress. This will be reflected later in this series when discussing the design of specimens with lateral post-tensioning. In general, lateral compressive loads tend to reduce the transverse tensile stresses. The question of how much and where becomes the key issue in reinforcement optimization.

To confirm the photoelastic tests, Sargious carried out a single test on a reinforced concrete end block, of rectangular section, subjected to a single symmetrical load. It was stated that the spalling tensile stresses were higher by 30 percent than those obtained in the corresponding photoelastic test, but that the transverse bursting stresses were in good agreement.

Sargious' work was limited to relatively small angles of inclination (up to 6.3 degrees from the horizontal axis) and his results were later used by Leonhardt [26] in developing a series of design recommendations. These are discussed in a following section.

2.2.3.3 Vaughn. In 1976, as part of an exploratory series of tests to investigate the possibility of using two-dimensional photoelastic techniques to model multiple tendons, eccentricity, and inclination for post-tensioned thin sections, Vaughn [27] performed a series of nine tests at The University of Texas at Austin. He used three different anchorage geometries--conical, bearing, and inset bearing. Anchors were fashioned from lead cast in precisely machined brass molds. The web section was machined from 3/8 in. plates of PSM-S photoelastic resin. Vaughn attempted to model the tendon duct by splitting the specimen into two separate two-dimensional pieces along the duct line or in some multiple tendon cases, with three separate pieces. This technique is questionable for modeling physical concrete specimens, since for the bursting stress phenomena to exist there must be continuity across the tendon duct. While simple plate loading on a two-dimensional sheet may be less accurate than a three-dimensional model where the tendon duct is accounted for, it is unquestionably more accurate in predicting bursting stresses than where no continuity is developed. Despite this drawback, the tests did reveal some interesting results.

(1) Conical Anchors produced principal tensile stresses on the order of 150 percent of those for flat, bearing-type anchors, and produced maximum shearing stresses on the order of 250 percent larger.

(2) Eccentricity: Spalling stresses increased dramatically for increasing eccentricity.

(3) Multiple Anchorages: Large spalling stresses were set up between the anchors along the loaded face. These were considerably higher than for a single anchor. Uniform longitudinal stress was achieved at a shorter distance from the loaded face than for single anchors.

(4) Inclination: Spalling stress was markedly increased for increasing angles of inclination. Very high stresses were noted at the anchorage blockouts due to the reentrant corner used to achieve proper geometry. Normal and friction forces along the duct could not be modeled.

(5) Influence of Tendon Duct: In regions of high tendon curvature, often encountered in segmental bridge construction, considerable forces were exerted normal and tangential to the duct, particularly at points where the duct had a small radius of curvature. This is an important point because it indicated the possible creation of cracks extending outward from the tendon duct which were initiated by tendon pressure against the walls of the duct. This situation would be accentuated in real life tendons which contain as many as twenty-five or more individual strands, because of the tendency for the bundle to flatten out when the load is applied.

2.2.3.4 Other Photoelastic Studies. Two-dimensional tests for beams with short end blocks have been made by Rydzewski and Whitbread [28]. They observed that in addition to the bursting stresses under the load point, significant spalling stresses occurred along the loading face. Mahajan [29] tested eccentrically loaded specimens whereas other investigators had used primarily axial, symmetric loading. Values of bursting stress for various ratios of loaded width to total width were investigated by Hiltcher and Florin [30]. For this two-dimensional problem they found close agreement between the magnitude and distribution of their measured stresses and those calculated by Guyon's analysis.

One of the major disadvantages of photoelastic investigations is that they must be classified with analytical methods since they yield elastic stresses. Photoelastic investigations can be used to check an elastic analysis (as will be shown in Chapter 3), but they cannot fulfill the same function as tests on concrete specimens.

#### 2.2.4 Tests on Concrete Specimens

2.2.4.1 Zielinski and Rowe. One of the most extensive investigations reported using concrete specimens to determine the behavior of post-tensioned anchorage zones was carried out by Zielinski and Rowe in the mid-1960's [9,10]. The first phase of the study dealt with single, axial symmetric loadings. The following variables were considered:

- (1) The anchorage system, including position (external or embedded), type (square or circular) and method of transmission of the force (conical action or bearing plate).
- (2) The ratio of the loaded area to cross-sectional area of the specimen.
- (3) The duct for the post-tensioning cable.
- (4) The type, position, and amount of reinforcement.

Four types of relatively small concrete prisms (6 in. x 6 in. x 16 in., 6-11/16 in. x 6-11/16 in. x 16 in., 8 in. x 8 in. x 12-1/2 in. and 8 in. x 8 in. x 16 in.) were tested. Typical specimens are shown in Fig. 2.23. The results were obtained in terms of surface strain measurements and both cracking and ultimate loads. The following conclusions were reached:

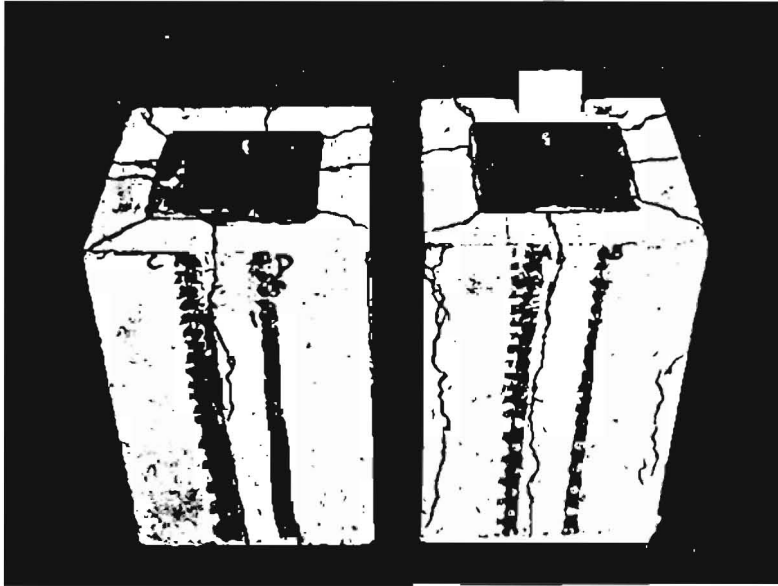
(1) The anchorage system geometry investigated did not appreciably affect either the distribution of transverse stresses or the ultimate load capacity. In other words, they concluded that conical anchorages performed as well as bearing type anchorages. (This has been the subject of some debate since that time and stiff conical anchors are often considered suspect.)

(2) For the specific case of a single symmetric load, the ratio of the loaded area to the cross section area was the most important factor in the transverse stress distribution. The smaller the ratio, the higher the stress.

(3) The position of the maximum bursting stress was not substantially affected by the above ratio.

(4) The maximum bursting stress occurred on the axis of the load and was greater than that predicted by Guyon using the symmetrical prism analogy.

(5) Spiral reinforcement was more efficient in containing transverse bursting stresses than the use of orthogonal mats.



(a) Crack pattern on end-blocks with embedded C.C.L. spiral anchorages



(b) Crack pattern on 6 in. cubes with same value of  $a_1/a$  as C.C.L. prisms

Fig. 2.23 Formation of concrete cone ahead of anchor (from Ref. 9)

(6) Increasing the percentage of transverse reinforcement raised the ultimate load capacity, but this effect was limited in that a bearing type failure could occur in the case of an over-reinforced section.

(7) The size of the duct did not seem to be a major factor influencing the bursting stress distribution.

Zielinski and Rowe did not note an important possible mechanism of failure. In Fig. 2.23 an extremely significant point can be noted. In almost all cases where a bearing type anchorage was used, a pyramidal "cone" of crushed concrete formed beneath the plate at a load stage close to the sighting of the visible longitudinal "bursting" crack. The sides of the cones had a dusty coating of powdered concrete typically found in a shear type failure. Nearly identical "cones" were reported by Taylor [31] and were observed, without exception, in all specimens of the current Texas study tested by the authors which had bearing type anchors. The significant role of this cone of concrete in the failure process is discussed in the second report of this series.

In a second series of their tests, the effects of multiple anchorages were studied. Eleven tests on I-section specimens and nine tests on rectangular specimens were carried out. Figures 2.24 and 2.25 show typical details of these specimens. The following conclusions were drawn:

(1) The cross-sectional geometry of the end block can significantly affect the transverse stress distribution.

(2) The multiple anchorage end block can be analyzed satisfactorily by using Guyon's successive resultants method for the determination of bursting stresses.

(3) Tensile spalling zones exist between the applied loads (multiple anchorages) on the loaded face of the end block. These are a function of the distance between the loads. The test

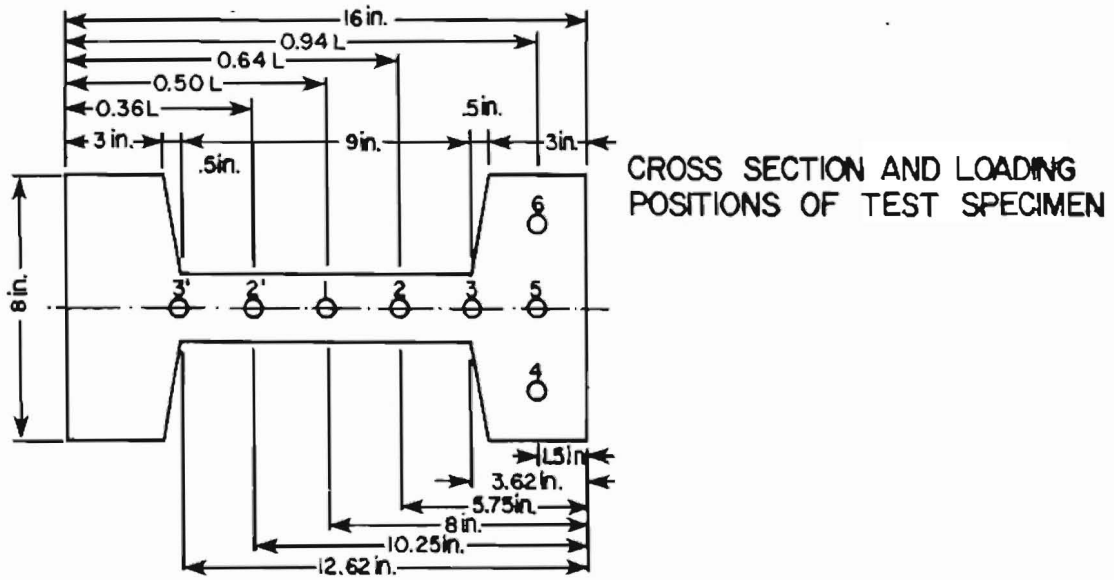


Fig. 2.24 Zielinski and Rowe: typical dimensions for specimens used in second series (from Ref. 9)



CRACK PATTERN

Fig. 2.25 Zielinski and Rowe: specimen 1, second set (from Ref. 9)

results were insufficient to make a precise statement as to their variation with the distance between the anchors.

(4) The spalling stresses increase as the ratio of the loaded area to the cross section area decreases.

(5) In end blocks, by virtue of the complex stress state that exists, the stress-strain relation of the concrete in tension is modified. The strain capacity prior to cracking is much greater than in normal flexural tension.

2.2.4.2 Taylor. As part of a study of prestressed concrete pressure vessels, Taylor [31] performed a series of seven tests, as shown in Fig. 2.26, in a preliminary effort to formulate a failure criterion for plain concrete. Several important conclusions were drawn:

(1) The maximum transverse stress in a single axi-symmetrically loaded end block was found to be greater than those predicted by the classical theories, but lower than those obtained by Zielinski and Rowe.

(2) The mode of failure of a single anchorage appeared to be by wedging action of a cone of stiffer concrete under the bearing plate, formed by shear forces due to the incompatible stiffnesses of the anchorage unit and the concrete.

(3) Uniform tensile stress applied to the anchorage zone reduced the load-carrying capacity of the anchorage unit and caused a reduction in the maximum tensile strain at cracking.

(4) Uniform (transverse) compressive stress applied to the anchorage zone increased the carrying capacity of the anchorage unit and the maximum tensile strain at cracking was increased.

Taylor further stated that:

### DETAILS OF TEST SPECIMENS

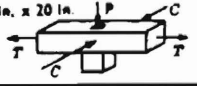
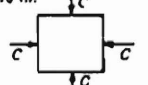
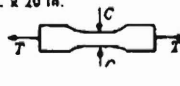
Test series	Spec. no.	Size of specimen	Purpose of test
2.1	PV 2 PV 3 PV 4	3 in. x 3 in. x 15 in. 	Axisymmetrical loading strain distributions
2.2	PV 5-10 inc. PV 26-31 inc. PV 46-57 inc.	4 in. x 4 in. x 20 in. 	Effect of uniform tension on the anchorage zone
2.3	PV 11-16 inc.	4 in. x 4 in. x 20 in. 	Effect of biaxial compression-tension on the anchorage zone $P$ (const.) = 10 000 lb (4536 kg)
2.4	PV 17-25 inc.	3 in. x 3 in. x 15 in. 	Effect of uniform compression on the anchorage zone (1)
2.5	PV 34-35 inc.	4 in. x 10 in. x 10 in. 	Effect of uniform compression on the anchorage zone (2)
2.6	PV 58-63 inc.	4 in. x 10 in. x 10 in. 	Biaxial compressive strength of plain concrete
2.7	PV 64-69 inc.	4 in. x 4 in. x 20 in. 	Biaxial compressive tensile strength of plain concrete

Fig. 2.26 Taylor's test specimens (from Ref. 31)

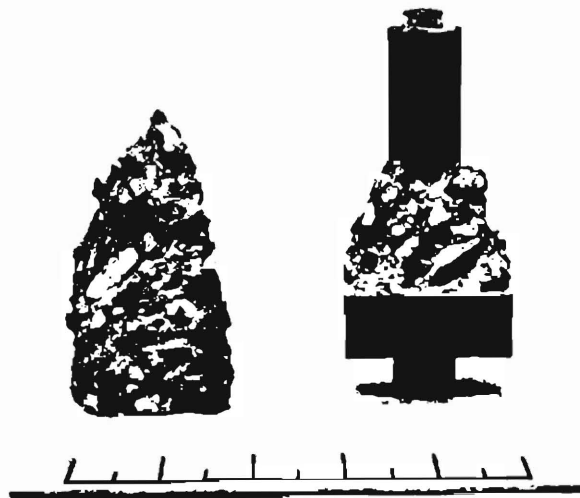


Fig. 2.27 Concrete cones observed by Taylor (from Ref. 31)

The results of the tests carried out on square prisms show that whereas at first sight, all the prisms tested appeared to have failed by single tensile cracks (bursting cracks), closer examination of the failed specimens showed that there was a cone [Fig. 2.27] of concrete under the bearing plate, the surfaces of the cone exhibiting the extensive shattering of aggregate and powdering of mortar associated with a shear type failure. It would appear that due to the different stiffness characteristics of the steel plate and the concrete, the bearing plate restrains the lateral expansion of the concrete, inducing complex triaxial compressive stresses. The concrete below the plate is thus relatively stronger than the surrounding concrete, and it would appear that failure is initiated along the boundary of a cone (pyramid for square anchors) at points of maximum shear stress. Once the shear resistance along the surface of the cone has been overcome, together with any additional resistance provided by compressive bursting (or lateral prestress) acting normal to the shear planes, it would appear that the cone is forced into the end block creating a wedging action and setting up high tensile stresses perpendicular to the load. The propagation of tensile cracks in a complex compression-tension stress field caused by the wedging action of the cone apparently governs failure of the end block.

In this one statement, Taylor made what could be considered as the most important contribution up to that point in time concerning the behavior of post-tensioned anchorage zones. This is not to say that his statement solved the problem. In fact, it is curious that Taylor went on to make his design recommendations based upon experimentally obtained bursting stress distributions, just as had all previous investigators. Most elusive, of course, was the explanation for the initiation of the shear failure and subsequent cone formation. This topic will be discussed in detail in the second report in this series.

2.2.4.3 Cooper and Gallaway. The problem of post-tensioned anchorage zone tensile stresses is complicated by the increasing use of thin sections with inclined, curved tendons which result in significant radial and friction forces along the tendon duct.

An extensive research program in this area has been carried out at The University of Texas at Austin since 1968 in connection with the construction of the first segment precast post-tensioned

box girder bridge in the United States at Corpus Christi, Texas. During construction of the actual bridge, cracks were found along the tendon paths near the anchors in numerous segments. As a consequence, construction was slowed and another model study initiated in February 1973. A detailed investigation revealed that three basic differences existed between the prototype details and those used earlier to build a 1/6-scale model span which had not experienced any cracking. These were described by Breen, Cooper and Gallaway [1] as follows:

(1) In some prototype units, web and top slab reinforcing bars were cut for placement of post-tensioning hardware, but the sections which had been removed were never replaced or only partially replaced.

(2) The prototype used a cone-type anchor whereas the model used a bearing-type anchor.

(3) The spiral reinforcement along the tendon in the anchorage zone used in the model was relatively much longer and heavier than the spiral reinforcement used in the prototype.

Based upon this information a precise model replica of one of the cracked sections was constructed and loaded in an effort to reproduce the situation which led to cracking. The results of the model tests revealed the same cracking pattern as the prototype units. However, ultimate strength tests of the models showed no significant reduction in strength due to the cracking. The construction of the bridge was therefore continued and completed in June 1973.

In order to isolate the causes for the formation of the tendon path cracks and to recommend measures to prevent their occurrence, a further exploratory investigation was undertaken by Breen, Cooper and Gallaway [1]. Fifteen microconcrete I section specimens were designed as one-sixth models corresponding to the web section of the prototype bridge. Variables explored anchorage geometry, concrete strength, local reinforcement pattern, the effects of longer spiral reinforcement, transverse post-tensioning, tendon curvature, and percentage of

web steel. The following quantitative conclusions were reached from the model study:

(1) The behavior of the I-section model is representative of the prototype web.

(2) There is no significant reduction in the ultimate shear strength of a well-reinforced member due to the presence of tendon path "bursting cracks." However, they represent a possible path for moisture and salt penetration and thus present potential corrosion and frost damage threats.

(3) The formation of cracks along the tendon appears to be accelerated by conical anchorages, inadequate anchorage zone reinforcement, and radial forces due to tendon curvature.

(4) The cracking load is only slightly affected by the concrete compressive strength.

(5) Specimens using bearing type anchorages performed much better than specimens with cone-type anchors.

(6) The cracking load is not affected by increasing the percentage of web reinforcement, although crack widths can be effectively controlled by the presence of reinforcement.

(7) Substantially longer spiral reinforcement is effective in delaying first cracking.

(8) The cracking load is not substantially affected by increasing the bearing area of the anchor.

(9) Transverse post-tensioning seems to be a very effective means of controlling (preventing) tendon path cracks.

Due to the limited number of tests and the fact that full-scale prototype specimens were not available, the above conclusions were only qualitative. They do, however, reinforce many of the behavioral patterns for post-tensioned anchorage zones indicated by previous

research and bring up one extremely important point: nominal bearing stress apparently has little or no influence on the mechanism of crack formation.

2.2.5 Bearing Stresses. Most design specifications limit allowable bearing stresses to substantially lower values than would appear necessary. The origin of the so-called "cube root" and "square root" formulas used in most specifications dates back to the late 1940's and early 1950's when active research was underway to determine the proper size of column base plates. Three important studies dealing with this topic indicate how the current specifications evolved and provide an appropriate background for Sec. 2.3 dealing with current code provisions.

Based upon a number of tests of cylinders loaded through rigid bearing plates, in 1948 Billig [32] developed the following formula for permissible bearing stresses:

$$f_{cp} = 0.6f'_{ci} \sqrt[3]{A_c/A_b} \leq f'_{ci} \quad (2.1)$$

where

- $f_{cp}$  = permissible compressive stresses
- $f'_{ci}$  = cylinder strength at age of loading
- $A_c$  = area of entire concrete section
- $A_b$  = bearing area

In 1952 Komendant [33] published the same formula with the exception that the cube root was replaced by the square root. This was based on a substantial number of tests using, again, cylinders loaded through rigid bearing plates.

Four substantial studies performed under the direction of Middendorf [34] were carried out in 1960. Using both rectangular blocks as well as cylinders ranging from 6 in. to 16 in. in diameter Middendorf reaffirmed the recommendations of Komendant, i.e., to switch to the following formula currently used in the ACI and PTI codes.

$$f_{cp} = 0.6f'_{ci}\sqrt{A_c/A_b} \quad (2.2)$$

He further recommended that the restriction  $f_{cp} \leq f'_{ci}$  be dropped and the value be increased to a multiple of  $f'_{ci}$ , probably  $3f'_{ci}$ .

He further concluded:

- (1) The formula has no apparent limit based on 28-day strengths.
- (2) Tilting of up to 5 degrees (limit of their tests) of the bearing plate does not affect the bearing ability.
- (3) The conclusions are applicable to concrete with  $f'_c$  ranging from 4000 to 6000 psi.
- (4) The results are consistent in concrete from three days of age upward.
- (5) The results are directly applicable to lightweight as well as normal concrete.

In 1968, Hawkins [35] performed another series of tests designed to develop a more accurate formula for the bearing strength of concrete loaded by rigid plates. His test results showed:

- (1) No visible cracking or spalling of plain concrete until immediately before failure.
- (2) First warnings were usually vertical cracks on the sides of the block closest to the loaded area.

(3) Failure revealed a wedge of concrete beneath the bearing plate.

Based upon this data Hawkins proposed the following formula:

$$q/f'_c = 1 + \frac{K}{\sqrt{f'_c}} (\sqrt{R} - 1) \text{ for } R < 40 \quad (2.3)$$

where

$q$  = ultimate bearing strength (psi)

$f'_c$  = cylinder compressive strength

$K$  = constant =  $A \cot^2 \alpha \approx 50$  for most cases

$\alpha = 45^\circ - \phi/2$      $\phi$  = internal angle of friction (33-35°)

$A = f_{\text{tensile}} / \sqrt{f'_c}$

$R$  = effective unloaded area/loaded area where the effective unloaded area is geometrically similar and concentric with the loaded area.

In 1970, based upon further tests, Hawkins [36] recommended the following formula for strip loading of concrete through rigid plates.

$$q = C \sqrt{f'_c} \sqrt[3]{D/W} \quad (2.4)$$

where  $C = 18.5$

$D$  = distance from the block edge to the centerline of the plate

$W$  = width of the plate

(see Fig. 2.28)

In closing this section, the recent work of Niyogi [37] deserves mention. The first paper contains a general discussion of the bearing strength of concrete and discusses the problems associated with the calculation of the allowable stresses and the probable mechanics of failure. The primary parameters were the geometry of

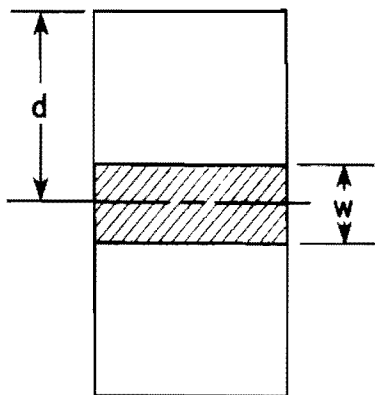


Fig. 2.28 Strip load dimensions for Eq. 2.4

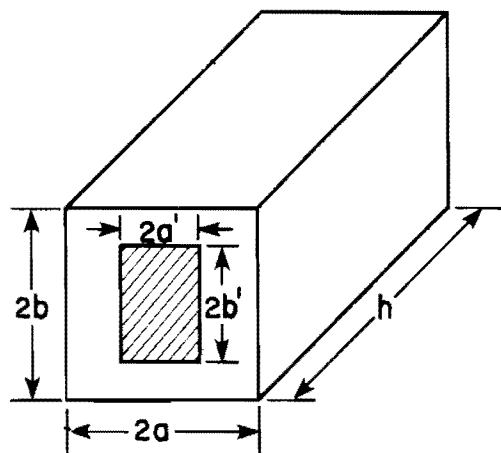


Fig. 2.29 Variable definitions for Niyogi's Eq. 2.5

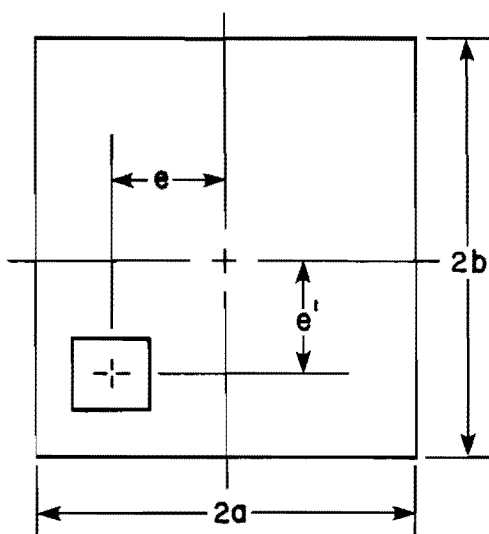


Fig. 2.30 Defining eccentric bearing conditions for Niyogi's Eq. 2.6

the bearing plate to the loaded surface and the plate geometry. Square, rectangular and strip loadings were considered. He postulated the following formula for allowable bearing stress:

$q$  = ultimate bearing strength

$$\frac{q}{f'_c} = 0.42 \left( \frac{a}{a'} + \frac{a}{b'} \right) - 0.29 \left[ \left( \frac{a}{a'} - \frac{a}{b'} \right)^2 + 5.06 \right]^{1/2} \quad (2.5)$$

See Fig. 2.28 for geometry definitions.

According to Niyogi, the bearing strength decreased for increasing height, with all other conditions the same. Also, eccentricity of the load tended to decrease the ultimate bearing strength such that:

$q_e$  = eccentric load bearing stress

$$\frac{q_e}{q} = 2.36 \left[ 0.83 - \left( \frac{e}{2a} - \frac{e'}{2a} \right)^2 \right]^{1/2} - 0.94 \left( \frac{e}{2a} + \frac{e'}{2a} \right) - 1.15 \quad (2.6)$$

See Fig. 2.30 for variable definitions.

In a second series of tests performed in 1975, the same method of testing was used except that reinforcement was the prime variable. Both spiral and grid reinforcement were examined. The findings indicated:

- (1) Large diameter spirals appeared to be the most effective against cracking.
- (2) Large bearing plate performance was enhanced to a lesser extent by the provisions of reinforcement than smaller plates.
- (3) Visible cracking loads were increased by the addition of reinforcement.
- (4) Grid steel increased bearing strength, though not as efficiently as spiral reinforcement.

(5) Spiral reinforcement increased bearing strength due to lateral confinement of the concrete cover. For spirals, the following relation was found to hold:

$$\frac{q_{\text{spiral}}}{q_{\text{plain concrete}}} = 1 + k \cdot p \quad k = 55 \text{ for spiral} \quad (2.7)$$

$p = \text{volumetric percent of lateral steel}$

(6) For small bearing plates, and large diameter spirals, the bearing strength increased for greater steel percentages.

### 2.3 Present Design Provisions

2.3.1 Leonhardt. Based upon the work of previous investigators, notably Sargious and Guyon, Leonhardt [26] developed recommendations for the design of tensile reinforcement in the anchorage zone. For the two-dimensional problem, where the concentrically applied force is assumed to be spread over the entire width of the member, Leonhardt suggested the following expression for the total splitting force attributed to the bursting stresses:

$$Z = 0.3F(1 - a/h) \quad (2.8)$$

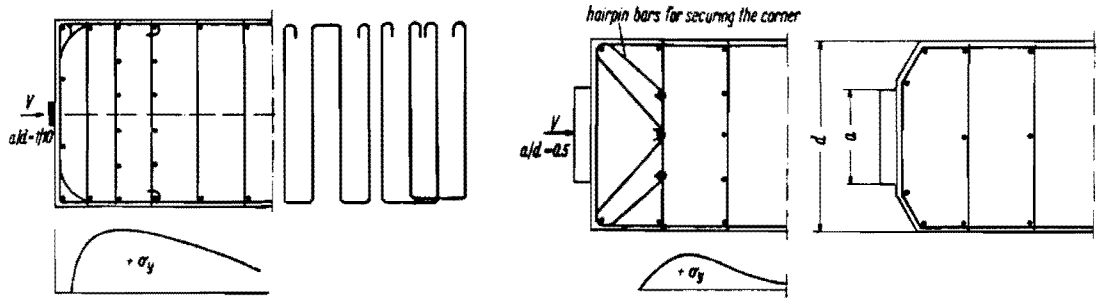
where  $Z$  denotes the total splitting force

$F$  is the concentric prestress load

$a$  is the width of the anchor plate

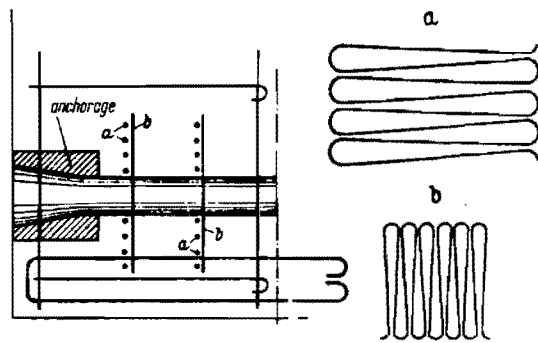
$h$  is the width or height of the member, depending on the orientation to be considered

This expression was derived by integrating the distribution curves of the bursting transverse tensile stresses which were previously determined analytically. The reinforcement should be designed to resist that total force. Placement should follow the elastic distribution curve of transverse tensile stresses. Practical arrangement of reinforcing such as shown in Fig. 2.31 was suggested. It



Suitable arrangement of the vertical reinforcement (horizontal reinforcement depends on  $b'/b$ ) behind an anchor plate for which  $a/d = 0.10$

Suitable arrangement of the vertical reinforcement behind an anchor plate for which  $a/d = 0.50$ . If the corners are chamfered, the hairpin bars are omitted



The type of reinforcement normally installed behind Freyssinet anchorages in France (from Guyon)

Fig. 2.31 Detailing of reinforcement as recommended by Leonhardt (from Ref. 26)

should be noted that at this point in time spiral reinforcement had been used occasionally, but most recommendations were in the form of closely spaced grids of orthogonal reinforcement.

2.3.2 Guyon. Guyon [5] recommended the following design procedure for single straight tendon anchorages:

For spalling stresses:

$$T_s = 0.04P + 0.20 \left( \frac{a - a_1}{a + a_1} \right)^3 P \quad (2.9)$$

where

$T_s$  = Total spalling force to be resisted by reinforcement.

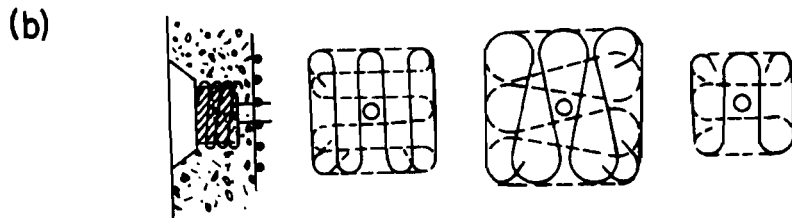
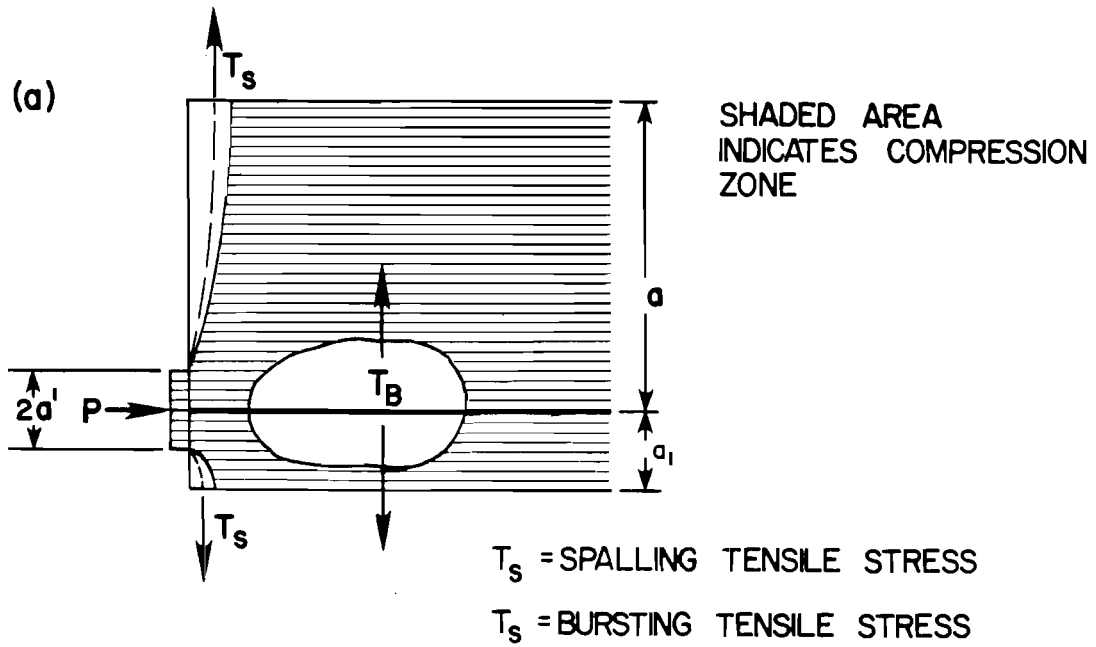
$P$  = Prestress force

$a, a_1$  are defined in Fig. 2.32a.

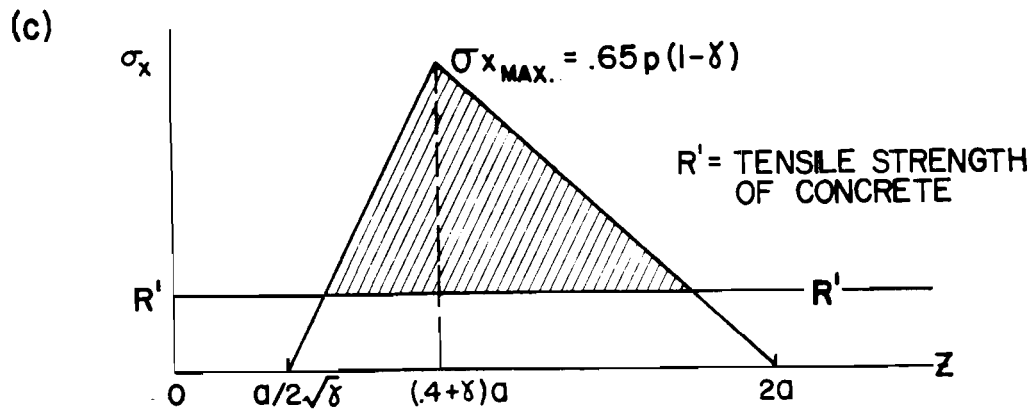
Guyon states that the term  $0.04P$  should be resisted by mesh reinforcement placed immediately behind the anchor as illustrated in Fig. 2.32. The second term reflects the increase in spalling stress with increasing eccentricity. For this term large vertical bars (parallel to the end face) should be located immediately behind the mesh reinforcement. These should be sufficiently long so as to develop the full strength of the bar.

For bursting stresses Guyon reduced the tensile portion of the bursting distribution to a triangular geometry which yielded approximately the same total bursting force as well as the magnitude and location of the peak stress, as shown in Fig. 2.32c. The total tensile force is:

$$T_b = \frac{P}{3} (1 - \gamma) \quad (2.10)$$



Mesh reinforcement immediately behind anchors



Approximate bursting distribution

Fig. 2.32 Anchorage zone reinforcement design as per Guyon (from Ref. 5)

where  $T_b$  = Total bursting tensile force

$P$  = Prestress load

$\gamma$  =  $2a'/2a_1$  (as defined in Fig. 2.33a);  $2a'$  = width of the anchor plate;  $2a_1$  is the depth of the symmetric prism

The line marked  $R'$  in Fig. 2.32c represents the tensile stress that can be resisted by the concrete alone. The peak bursting stress is given by the formula:

$$\sigma_{x_{\max}} = 0.65 p(1 - \gamma)$$

where  $p = P/\text{cross-sectional area}$

2.3.3 Rhodes and Turner. Based on the data from the extensive physical testing program of Zielinski and Rowe, Rhodes and Turner [6] in 1966 developed a series of expressions, using an approach similar to that of Guyon, where the total amount of reinforcement required to resist the bursting stresses could be easily calculated.

A fairly detailed explanation of the Rhodes and Turner design recommendations is included since this has been the most specific method thus far presented for the design of reinforcement to resist anchorage zone tensile stresses based upon experimental study.

In the Rhodes and Turner method, using notation similar to that used by Guyon, the first step is to determine the dimensions of the effective prism, usually assumed square with the load being applied through a square anchorage. Examples are shown in Fig. 2.33. A square anchor of side  $2a_1$  is assumed to act on a prism of side and depth  $2a$ . The dimension  $2a_1$  is equal to the side length and width of the proposed anchor. The dimension  $2a$  is found by inspection; it is usually assumed to be the least distance between the center line of the anchor and the edge of the concrete or half clear distance to the neighboring anchor.

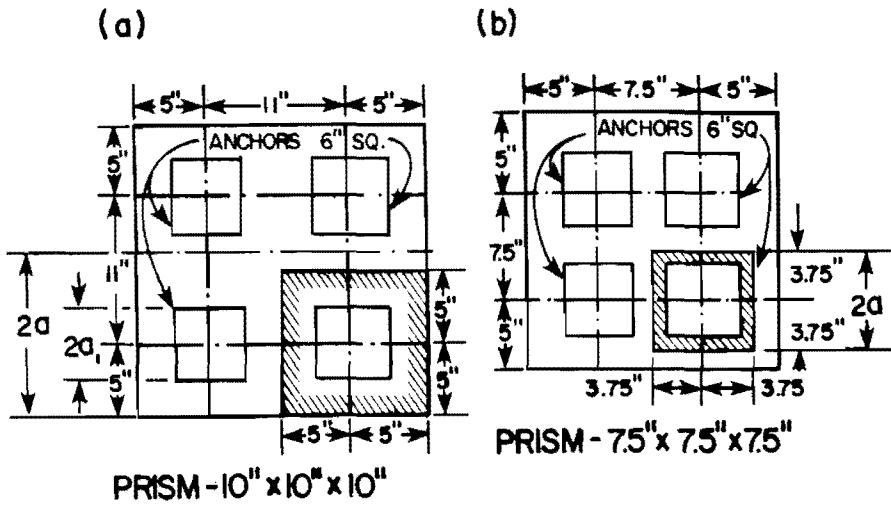


Fig. 2.33 Determination of prisms for end blocks-- Rhodes and Turner

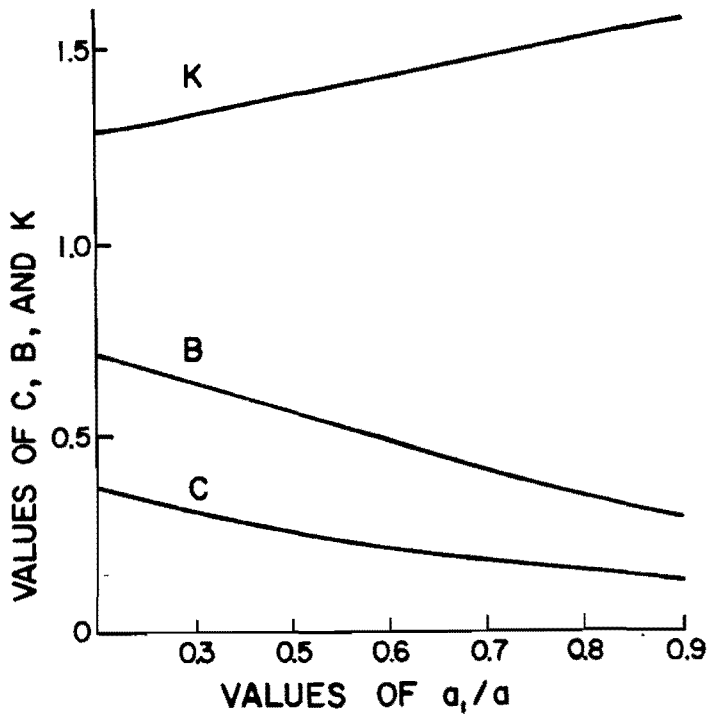


Fig 2.34 Values of coefficients B, C, and K for Rhodes and Turner equations

Similarly, a rectangular anchor with a dimension of  $2a_1$  by  $2b_1$  is assumed to act on a rectangular prism of cross section  $2a$  by  $2b$ . In this case two ratios  $a_1/a$  and  $b_1/b$  can be computed, giving different tensile forces in two perpendicular directions. Similarly, the prism will have a theoretical depth of  $2a$  for tension in one direction and  $2b$  for tension in the other direction. Circular anchors are assumed to act on square prisms, in which  $2a_1 = \sqrt{\text{area of anchor}}$ .

For each prism

$$f_c = P/A_c \quad (2.11)$$

in which  $f_c$  is the uniform direct stress in the prism;  $P$  is the maximum prestressing force, and  $A_c$  is the cross-sectional area of the prism minus the area of the tendon duct. The maximum tensile stress in a direction normal to the central axis of the prism and parallel to  $a_1$  (or  $b_1$ ) can be expressed as

$$f_n = Bf_c \quad (2.12)$$

and the total bursting tensile force can be expressed as

$$T = CP \quad (2.13)$$

in which  $B$  and  $C$  are parameters which vary with the ratio  $a_1/a$  and which have been determined by experiment (see Fig. 2.34).

The distribution of tensile stress in the longitudinal direction (along the tendon path) can be approximated by a triangle, as shown in Fig. 2.35. If a permissible tensile stress is specified then the theoretical length requiring reinforcement can be limited to the shaded length in Fig. 2.35. With the concrete resisting part of the tensile force, the tension  $T_R$  to be resisted by the reinforcement is given by:

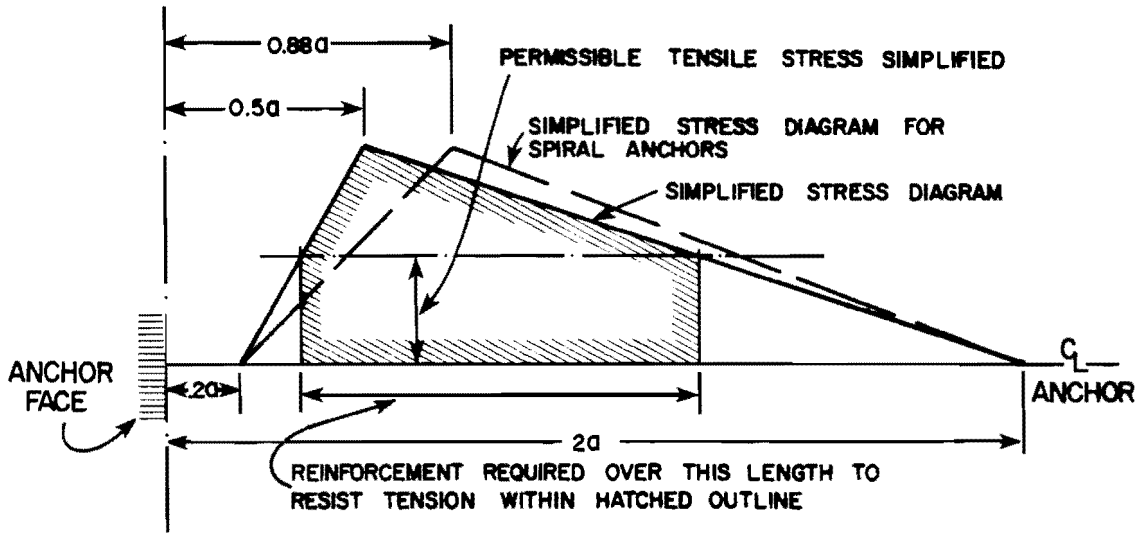


Fig. 2.35 Approximate bursting stress distribution--Rhodes and Turner

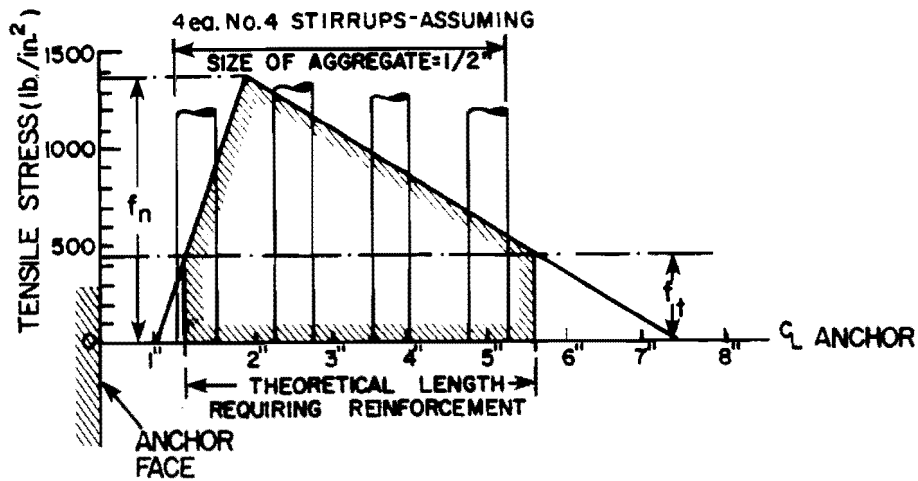


Fig. 2.36 Placing of reinforcement--Rhodes and Turner

$$T_R = T \left[ 1 - \left( \frac{f_t}{f_n} \right)^2 \right] \quad (2.14)$$

in which  $f_t$  is the permissible tensile stress.

Zielinski and Rowe found that the strains which occur in end blocks prior to cracking correspond to apparent tensile strength in excess of the splitting tensile strength of the concrete. The ratio of apparent strength to splitting strength is a function of the ratio  $a_1/a$  and is denoted by the coefficient  $K$  (see Fig. 2.34). The permissible tensile stress  $f_t$  is therefore assumed to be equal to  $0.8Kr$ , in which  $r$  is the tensile splitting strength of the concrete. Tensile stresses greater than  $f_t$  must be resisted by the reinforcement, at a working stress  $f_s$  of 20,000 psi for mild steel bars or 30,000 psi for hot rolled deformed bars. The area of reinforcement  $A_s$  required in each direction, in any prism containing a single anchor is

$$A_s = T_r / f_s \quad (2.15)$$

It is not common practice to specify a tensile splitting strength for concrete, and the designer must usually relate his figures to the compressive strength. Rhodes and Turner recommend the relationship

$$r = 0.5u^{0.75} \quad (2.16)$$

in which  $u$  is the cube strength.

Substituting the values  $T$ ,  $f_t$  and  $f_n$  in Eq. 2.14 and combining with Eq. 2.15 yields:

$$A_s = \frac{CP}{f_s} \left[ 1 - \left( \frac{0.8KrA_c}{BP} \right)^2 \right] \quad (2.17)$$

Assuming suitable values for  $r$  and  $f_s$ , it is possible to plot a family of curves relating the area of reinforcement to the ratio  $a_1/a$  for particular values of  $P$ . Since the coefficients  $C$ ,  $B$ , and  $K$  all depend on  $a_1/a$ , the only remaining unknown is  $A_c$ . Fortunately, for any particular prestressing force there is little variation in the sizes of the anchors, and the value of  $2a_1$  for any prestressing force is practically constant. The curves in Fig. 2.37 were calculated for square prisms, but Rhodes and Turner state they may also be used for rectangular prisms, for which the results will be slightly conservative. The graphs are based on the assumption that  $r = 450$  psi and  $f_s = 20,000$  psi. The values of  $2a_1$  and the areas of the ducts assumed for various prestressing forces are shown in Fig. 2.37. Values of  $K$  for ratios of  $a_1/a$  exceeding 0.7 were obtained by extrapolation.

They assumed that the absolute maximum value of the service level prestressing force for any anchor would not exceed 85 percent of the guaranteed ultimate tensile strength of the tendon. No allowance for the area of the duct need be made when calculating the ratio  $a_1/a$  but in order to determine  $f_c$  the area of the duct must be deducted from the area of the prism. For an ordinary anchor plate, the diameter of the duct to be incorporated in the calculation is that at the point of maximum tension, that is, at a distance of  $0.5a$  from the face of the anchor. However, many multi-strand anchors utilize a metal "trumpet" and the force is transmitted into the concrete by the combined end plate and tube. In such cases, they suggested it is acceptable to adopt the diameter of the sheath as the dimension to be used in design.

The foregoing considerations related to conditions at working load. It is also necessary to ensure that ultimate load conditions are satisfactory, that is, that sufficient reinforcement is provided to resist the tensile forces induced by a load equal to the guaranteed tensile strength of the tendon multiplied by a suitable load

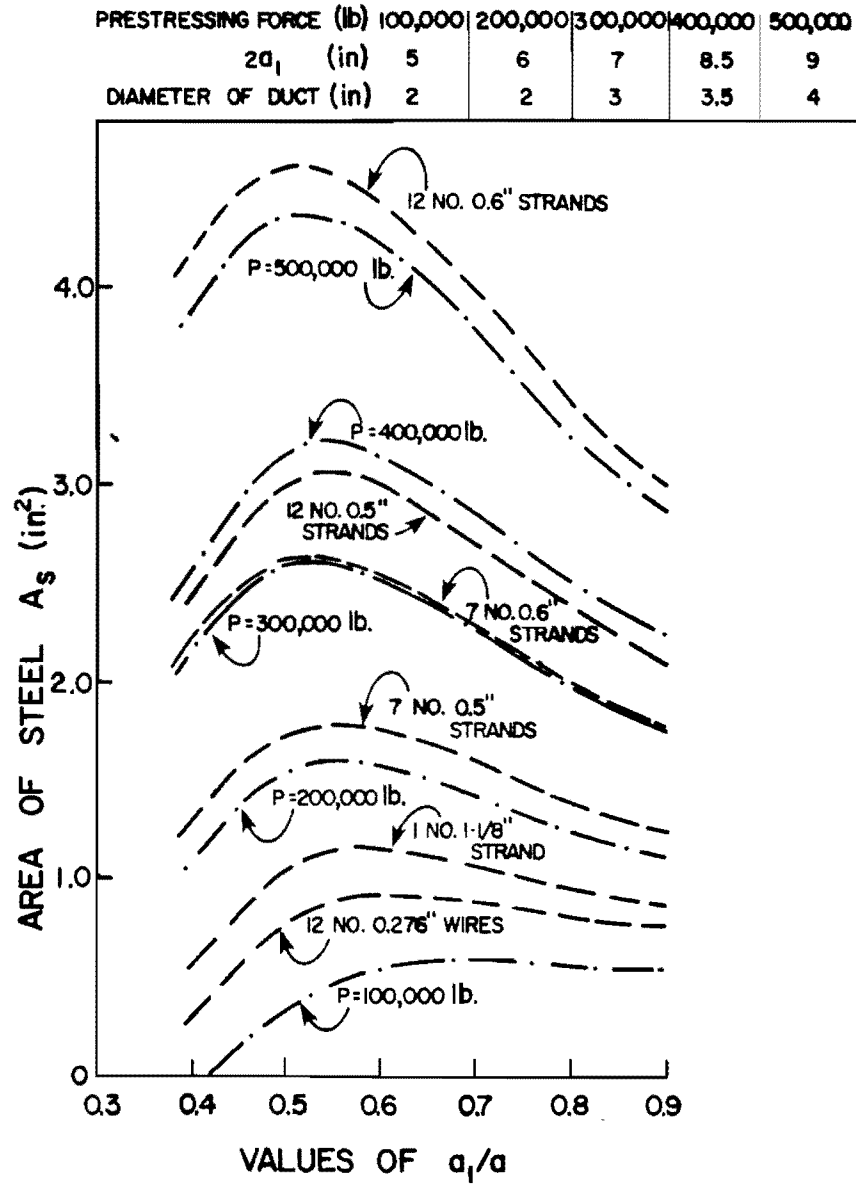


Fig. 2.37 Proportioning steel for Rhodes and Turner equations

factor. Rhodes and Turner recommend a value of 1.1 for the latter and the stress in the reinforcement must then not exceed the yield stress.

Rhodes and Turner also noted the presence of, and necessity of reinforcing for, the spalling stresses.

Additional tensile stresses are also produced between the anchors near the loaded face. The magnitudes of these stresses depend on the loads, the distance between the anchors and the shape of the end block. A precise determination of these stresses can not be made (in Zielinski and Rowe's tests), but they can be allowed for by providing the reinforcement for each separate prism as near as practicable to the face of the end block.

As an example of how one would normally apply these recommendations, Rhodes and Taylor presented the example shown in Fig. 2.33b. A prism 7-1/2 in. square with an anchor having a flange of 6 in. square has a duct with a diameter of 2 in. The value of cube strength  $u$  is assumed to be 6000 psi so that  $r$  is 450 psi. The tendon has seven 1/2 in. strands of 250 ksi steel.

$$P = 7 \times 37,000 \times 0.85 = 220,000 \text{ pounds}$$

$$\frac{a_1}{a} = \frac{2a_1}{2a} = \frac{6}{7.5} = 0.8$$

$$\text{area of the duct} = 3.14 \text{ in.}^2$$

$$A_c = (7.5)^2 - 3.14 = 53 \text{ in.}^2$$

$$f_c = \frac{P}{A_c} = \frac{220,000}{53} = 4,140 \text{ psi}$$

$$f_n = Bf_c = 0.34 (4140) = 1,408 \text{ psi}$$

and occurs at a distance of  $0.5a = 1.87$  in. from the face of the anchor.

$$T = CP = 0.15(220,000) = 33,000 \text{ lb.}$$

$$f_t = .08Kr = 0.8(1.52)(450) = 547 \text{ psi.}$$

$$\begin{aligned} T_r &= T[1 - (f_t/f_n)^2] \\ &= 33,000[1 - (547/1408)^2] = 28,300 \text{ lb.} \end{aligned}$$

$$\text{Hence } A_s = \frac{28,300}{20,000} = 1.42 \text{ in.}^2$$

This can be achieved with eight #4 bars ( $A_s = 1.38 \text{ in.}^2$ ) or four #4 stirrups placed as shown in Fig. 2.36. Alternatively, the same area could be found from Fig. 2.37 for  $a_1/a = 0.8$  and seven 0.5 in. strands.

The Rhodes and Taylor procedures were based on tests of concentric straight tendons, but were used by the post-tensioning hardware supplier for design of the anchorage zone reinforcement in the Corpus Christi bridge segments. These segments had inclined, curved, eccentric tendons. The anchorage zones were reinforced according to the provisions of Rhodes and Turner but cracked substantially even though the general results of elasticity theories would indicate the bursting stresses for the eccentric tendons would be less than the nominal bursting stresses for concentric tendons. This questions the applicability of the Rhodes and Turner method to other than concentric straight tendons.

2.3.4 ACI. Presently the major American building code [38] provides extremely little information to aid the engineer in designing or checking the adequacy of an effective reinforcing system for post-tensioned anchorage zones. Section 18.13 of ACI 318-77 requires:

18.13.1--Reinforcement shall be provided where required in tendon anchorage zones to resist bursting, splitting and spalling forces induced by tendon anchorages. Regions of abrupt change in section shall be adequately reinforced.

18.13.2--End blocks shall be provided where required for support bearing or for distribution of concentrated prestressing forces.

18.13.3--Post-tensioning anchorages and supporting concrete shall be designed to resist maximum jacking force for strength of concrete at time of prestressing.

18.13.4--Post-tensioning anchorage zones shall be designed to develop the guaranteed ultimate tensile strength of prestressing tendons using a strength reduction factor of 0.90 for concrete.

The Commentary for Section 18.13 gives the following equations to size tendon anchorages based on permissible bearing stresses:

Immediately after tendon anchorage:

$$f_b = 0.8f'_{ci} \sqrt{\frac{A_2}{A_1}} - 0.20 \leq 1.25 f'_{ci} \quad (2.18)$$

or after allowance for prestress losses:

$$f_b = 0.6f'_{ci} \sqrt{A_2/A_1} \leq f'_{ci} \quad (2.19)$$

where  $f'_{ci}$  = cylinder strength of concrete at time of loading

$A_1$  = bearing area of the post-tensioning anchor plate

$A_2$  = maximum area of the portion of the anchorage surface that is geometrically similar to, and concentric with, the area of the anchor plate.

$f_b$  = permissible concrete bearing stress under the anchor plate of the post-tensioning tendons with the end region adequately reinforced.

No recommendations are made for satisfying the bursting and spalling zone reinforcement. No guidance is provided the designer except to note that the actual stresses are quite complicated around post-tensioned anchorages and a "refined strength analysis" should be used whenever possible.

The origin of the ACI formula came originally from the recommendation proposed by Billig in 1948. As discussed in the previous section, corrections to the formula were suggested by Komendant and later by Middendorf. The square root formula was eventually adopted in the 1973 ACI specifications for prestressed concrete in lieu of any other available information.

2.3.5 CEB. In a similar fashion the Comité Euro-International du Béton (CEB) and the Federation Internationale de la Precontrainte (FIP) [7] prescribe that for the case of a reasonable uniform distribution of the applied pressures, the local resisting force shall be determined as follows:

$$F_{R_{du}} = f_{cd} \sqrt{A_{cl} A_{cd}} \leq 3.3 f_{cd} A_{cd} \quad (2.20)$$

where

$$f_{cd} = f_{ck} / \gamma_c$$

$f_{ck}$  = characteristic strength of concrete under compression

$\gamma_c$  = coefficient of safety applicable to concrete

$A_{cd}$  = the loaded area

$A_{cl}$  = the largest area which is geometrically similar to  $A_{cd}$ , with the same center of gravity, lying totally within  $A_c$ , in the plane of  $A_{cd}$

$F_{R_{du}}$  = ultimate resisting force for design

Since the coefficient of safety applicable to concrete ( $\gamma_c$ ) is normally equal to 1.5, the CEB/FIP formula can be rewritten as:

$$\frac{F_{R_{du}}}{A_{cd}} = 0.67 f_{ck} \sqrt{A_{cl} / A_{cd}} \leq 2.2 f_{ck} \quad (2.21)$$

Therefore, both ACI and CEB-FIP codes have the same type of formula for admissible bearing stresses, except with respect to the upper limit of applicability and factor of safety. The CEB bearing stresses are substantially higher.

For the anchorage zone transverse reinforcement, the CEB-FIP recommendations suggest the following expression, developed by Leonhardt:

$$N_{std} = 0.3F_{s du} (1 - a_o/a_1) \quad (2.22)$$

where

$N_{std}$  = total tensile force (bursting) to be resisted

$F_{s du} = 1.2\sigma_{\rho_{max}} A_{ps}$  maximum force in prestressing steel

$a_o$  = the side of the area  $A_{cd}$  measured parallel to a

$a_1$  = depth or width of the symmetrical prism, whichever governs.

The resisting force in the reinforcement is

$$N_{R_{td}} = f_{yd} \cdot A_s \quad (2.23)$$

where

$f_{yd} = f_{yk}/\gamma_s$

$f_{yk}$  = characteristic yield stress of steel

$\gamma_s$  = coefficient of safety applicable to steel.

Equating Eqs. 2.22 and 2.23 yields the required steel area. In a general statement the CEB-FIP Code recommends:

The determination of the additional reinforcement may be based on the theory of elasticity or on the equilibrium and compatibility of a rational internal system of forces. In both cases, the method used must be proven experimentally.

2.3.6 AASHTO. The current AASHTO [39] Specifications Section 1.6.6(b)4, limits the anchorage bearing stress to 3000 psi (but not  $> 0.9 f'_{ci}$ ) which seems to be extremely conservative. One popular commercial anchor will normally develop unit stresses at transfer of approximately 6500 psi. The cylindrical anchorages on the Hood Canal Bridge had bearing stresses in the 10,000 psi range. Middendorf reported compressive stresses under bearing plates in some of his studies as high as  $4f'_{ci}$ . AASHTO section 1.5.36 permits substantially higher bearing stresses on reinforced concrete at ultimate since it includes  $\sqrt{A_2/A_1}$  factor. Clearly, the lack of definitive research on post-tensioned anchorage zones is echoed here in gross conservatism. The anchorage zone "state-of-the-art" could probably best be summed up in a statement from the 1977 AASHTO Specifications, Sec. 1.6.15:

. . . In post-tensioned members a closely spaced grid of both vertical and horizontal bars shall be placed near the face of the end block to resist bursting stresses. Amounts of steel in the end grid should follow Recommendations of the Supplier of the Anchorage. Where such recommendations are not available, the grid shall consist of at least #3 bars on 3 in. centers in each direction, placed not more than 1/2 in. from the inside face of the anchor bearing plate.

Closely spaced reinforcement shall be placed both vertically and horizontally throughout the length of the end block in accordance with accepted methods of end block stress analysis. . .

For the situation of thin web or low cover post-tensioned applications, it is clear the designer is given little guidance and the constructor is at the mercy of his suppliers. No Commentary exists to document the "accepted methods of end block stress analysis."

2.3.7 PTI. The PTI [40] post-tensioning manual, Section 3.1.7, provides the same formula as the ACI 318-77 Commentary, but goes slightly further in stating:

Manufacturers' standard bearing plates and other standard anchorage hardware should be used in all but special applications. Reinforcement should be placed behind the anchor plates to resist bursting and spalling stresses in the concrete.

They then go on to refer to Leonhardt [26] and Guyon [4] for the design of this reinforcement.

#### 2.4 Summary

The comprehensive literature review undertaken reflects the state of published analytical and test data on post-tensioned anchorage zones. Various post-tension systems have conducted extensive investigations and full-scale tests to determine proper uses for their hardware products. These tests are ordinarily not published in this highly competitive and proprietary field. Certainly, no post-tension system supplier would want to have its system utilized in an application where anchorage zone cracking would threaten the strength or serviceability of the structure. Yet the continuing demand for new applications brought on by innovation and development requires constant extrapolation of limited data to new circumstances.

Most published analyses and test data are for straight, concentric tendons. It was shown in discussion of the widely accepted "Symmetrical Prism" method of Guyon that when applied to eccentric tendons as in Fig. 2.6, the theory indicates trends directly opposed to test results. None of the published literature treats significant inclinations or curved tendons. The design codes and standards used in American design--AASHTO, ACI, PTI--are limited to conservative (and often impractical) bearing stress formulae and performance language telling the designer to resist bursting, splitting, and spalling forces but giving no guidance on how to do it. It was shown that one practical method (Rhodes and Turner) was based exclusively on straight tendon tests and when applied in a major bridge structure with inclined, eccentric tendons was unable to adequately prevent cracking. It is obvious further information is needed on this complex problem.

## C H A P T E R 3

### ANALYTICAL STUDY USING FINITE ELEMENTS

#### 3.1 Introduction

The most important visible benchmark in the behavior of a post-tensioned anchorage zone under load is the formation of the longitudinal tendon path crack. From a serviceability standpoint, there is no concern before cracking. From a strength standpoint, cracking always seems to occur at a load somewhat under the ultimate capacity and hence serves as a warning indicator. Until shortly before the formation of the crack, the measurements made by the internal strain gages used in this study show that the load-strain relationships of the concrete are nearly linear. With proper vibration the concrete itself can be assumed to act as a homogeneous, elastic material up to the point of crack initiation. Thus, an approximate linear-elastic analysis of the anchorage zone stress state is a reasonable approximation prior to cracking.

This chapter details the selection and calibration of the static, linear-elastic finite element program used in this study. Comprehensive program details and examples of coding are given in Ref. 41.

3.1.1 Finite Element Models. It is not possible to obtain analytical mathematical solutions for all engineering problems. An analytical solution is a mathematical expression that gives the values of the desired unknown quantity at any location in a body. Analytical solutions of anchorage zone stresses can be obtained only for certain simplified situations such as the uniform concentric post-tensioning load on a rectangular prism solved by Guyon. For problems involving complex geometrics, material

properties, and boundary conditions, the engineer must resort to numerical methods that provide approximate, but acceptable, solutions. In most numerical methods, the solutions yield approximate values of the unknown quantities only at a discrete number of points in the body. One way to discretize a structure is to divide it into an equivalent system of smaller elements. The assemblage of such elements then represents the original body. Instead of solving the problem for the entire structure in one operation, the solutions are first formulated for each smaller unit and then combined to obtain the solution for the original structure. Although the analysis procedure is thereby considerably simplified, the amount of data to be handled depends on the number of smaller bodies considered. For a very large number of subdivisions computation by hand is unworkable and automated electronic computation is used.

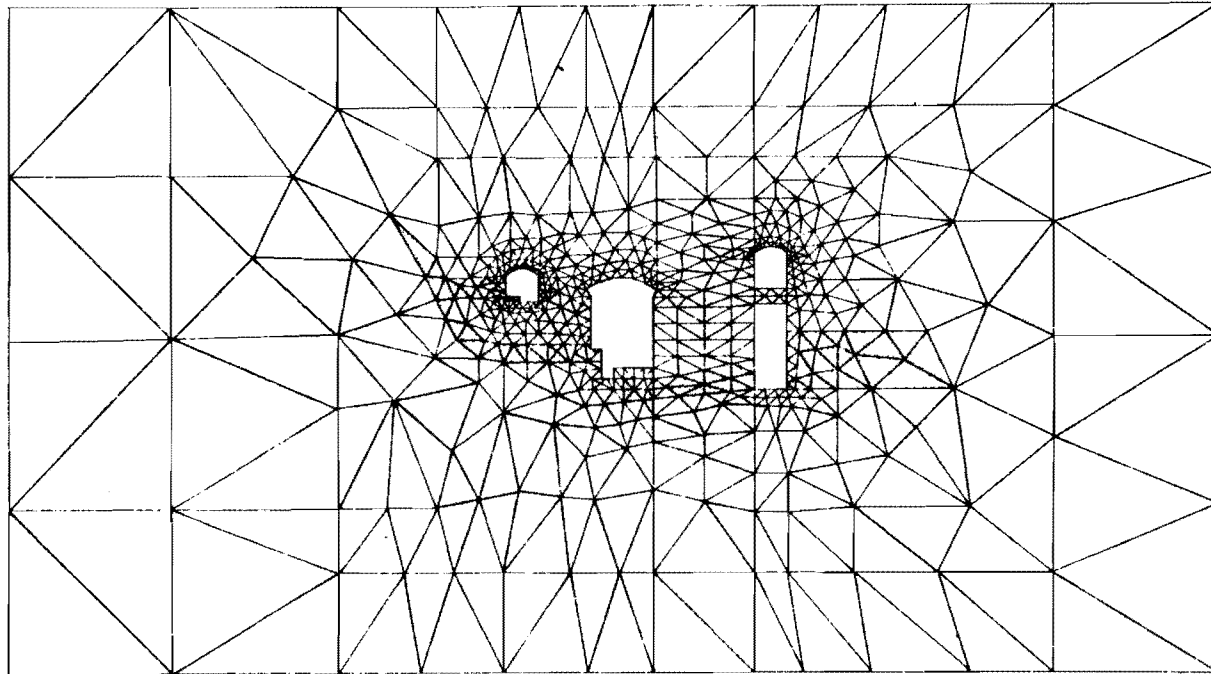
The finite element method is essentially a product of the electronic digital computer age. The method can be systematically programmed to accommodate such complex and difficult problems as nonhomogeneous materials, nonlinear stress behavior, and complicated boundary conditions. It is this advantage in boundary condition modeling capabilities which led to the choice of a finite element approach for the solution of the post-tensioned anchorage zone stress state with realistic variables such as tendon inclination, eccentricity, and curvature.

3.1.2 Mesh Generation. In early finite element programs, analyses were confined to two-dimensional plane stress and plane strain problems such as shown in Fig. 3.1a. Inputting the coordinates at each node and the connections between nodes was very time-consuming. Innovative methods for automatically defining sets of nodal points, called mesh generators, shortened the painstaking generation process. Until recently, these mesh generation schemes were usually limited to rectangular, regular, uniform arrays of points. For the more complex three-dimensional structures shown in

Fig. 3.1b, the input difficulties are a magnitude greater. One of the most powerful mesh generation schemes available was developed by Becker for use in the program TEXGAP [43]. This extensive pre-processor permits the user to generate one, two, and three-dimensional arrays of nodes. Automatic mesh generation was an absolute prerequisite for solution of the complex, three-dimensional system of block-outs, curved tendons and flanges associated with a typical post-tensioned box girder anchorage zone.

3.1.3 Accuracy. In dealing with complex geometries where the stress field may change rapidly, there are theoretically two approaches which can be used to achieve an accurate solution--mesh refinement or the use of higher order elements. Practical limits on computational time set limits on the level of mesh refinement possible. Higher order elements have several attributes which make them a desirable choice for modeling three-dimensional problems. The displacement field across the element is simulated by an analytical expression, usually a polynomial, known as a displacement model. If the exact solution is a linear displacement field, then this field is precisely replicated by a finite element using a linear displacement model. However, in any complex problem the true displacement field is not likely to be linear. In such a case the linear model is only approximate. Higher order displacement models yield more accurate, faster converging, approximations to the true solution.

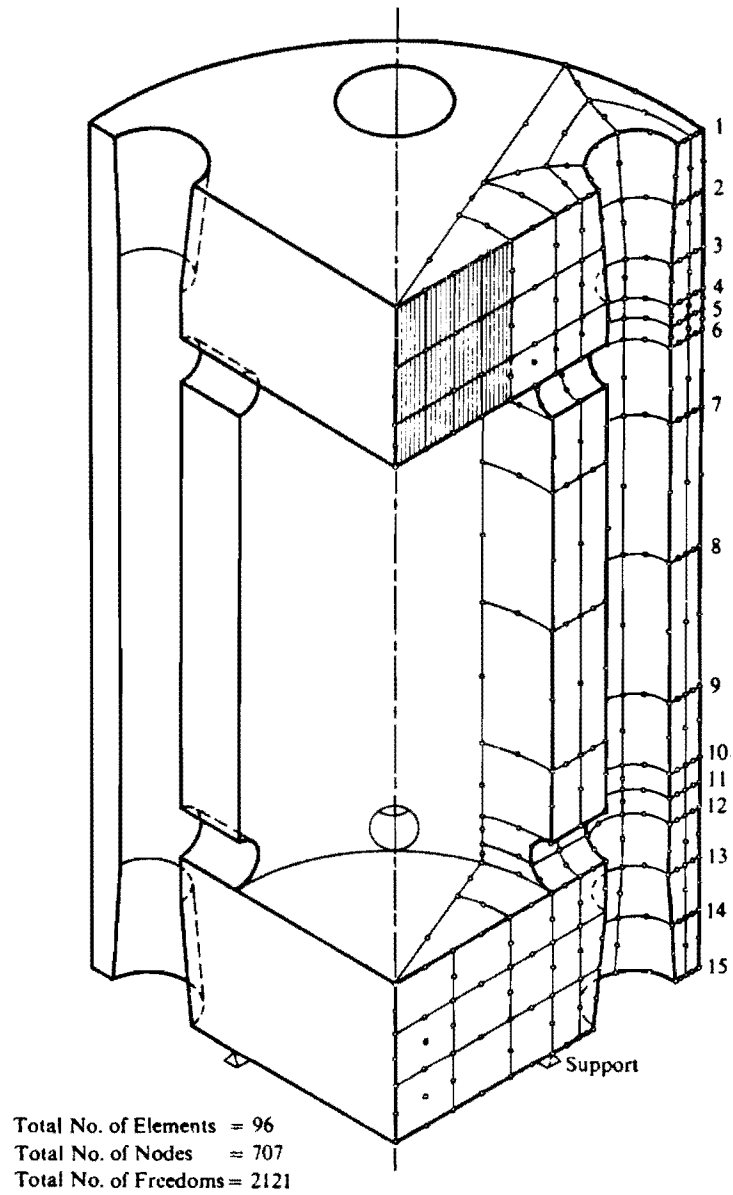
Likewise, the physical geometry of the problem must be considered. If only rectangular objects are to be modeled, a linear geometry model for the element will be sufficient. If, however, curved boundaries are involved, these can only be modeled precisely by a higher order geometric model. The formulation of displacement models and the calculation of element stiffnesses is greatly simplified if the geometry and displacements of the element are described in terms of the same parameters and if these parameters are of the



An underground power station. Mesh used in analysis.

a) Two-dimensional plane strain problem with irregular mesh (Ref. 42)

Fig. 3.1 Typical irregular meshes



Three dimensional analysis of a pressure vessel

b) Three-dimensional mesh (Ref. 42)

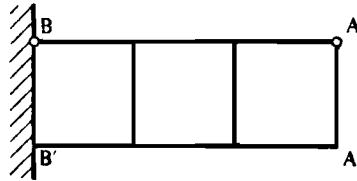
Fig. 3.1 (continued)

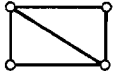
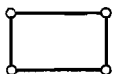
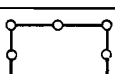
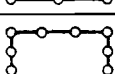
same order. This is known as the isoparametric element concept. The improvement in accuracy associated with higher order element formulation is readily seen from Fig. 3.2 where a cantilever beam is modeled with elements of various order.

For many years the methodology has existed to permit the solution of complex three-dimensional stress analysis problems using higher order finite elements. That there are only a few such codes and that these are infrequently used is basically due to two problems. The first is the difficulty associated with programming the problem for execution. Mesh generation and element definition are much more difficult for higher order elements. The second complication is the actual solution of the equilibrium equations. When higher order elements are used, the size of the overall computational problem might easily exceed the capabilities of most systems. In the early 1970's when Yettam and Robbins [22] were using finite element models for simple anchorage zone problems, nearly all programs used banded in-core gaussian elimination equation solvers. This imposed a severe restriction on the number of elements that could be used. Thus, most codes used the first order 8-node brick for their primary element.

The recent development of the frontal equation solver by Irons [44] permits expansion of the number of elements, thus making feasible the large scale use of higher order elements.

In choosing a suitable program for the current project the field was quite narrow. In fact only one program was found which had the mesh generation and higher order element capabilities to make feasible an accurate solution of the post-tensioned anchorage zone problem. That program was TEXGAP, developed by Becker and Dunham [43].



Type of element	Vertical Load of A		Couple at AA'	
	Max. defl. at AA'	Max. stress BB'	Max. defl. at AA'	Max. stress BB'
	0.26	0.19	0.22	0.22
	0.65	0.56	0.67	0.67
	0.53	0.51	0.52	0.55
	0.99	0.99	1.00	1.00
	1.00	1.00	1.00	1.00
EXACT	1.00	1.00	1.00	1.00

A cantilever in plane stress analysed by various elements. Accuracy improvement with higher order elements

Fig. 3.2 Accuracy improvement with higher order elements (Ref. 42)

### 3.2 Capabilities of TEXGAP

3.2.1 General. TEXGAP-2D and TEXGAP-3D are linear elastic finite element codes for solution of static continuum problems. Before outlining the specific capabilities of the three variations of the code used, the general limitations and assumptions common to all are summarized.

In a linear elastic program, isotropic material behavior is defined by  $E$  (Young's Modulus) and  $\nu$  (Poisson's Ratio). The program can vary either to model orthotropic materials. As the anchorage zone for a post-tensioned girder is principally concrete, the results will not be precise for extremely large strains, since concrete is a nonlinear material at high strains. However, most of this nonlinearity occurs with high compression. The tensile behavior may be assumed as nearly linear to cracking. Thus, it is assumed that the program will yield reasonable results up to first cracking.

Concrete is composed of a mixture of aggregates of varying sizes and mechanical properties which are bound together with a fine mortar paste. With proper uniform vibration, the mixture assumes a reasonably homogeneous character. The computer program assumes the material to be ideally homogeneous.

In modeling the anchorage zone, the program assumes perfect bond between adjacent elements, regardless of material properties. Thus, the program assumes an unbreakable, continuous contact between the steel anchorage plate and the concrete. Because of the extremely high friction forces which exist beneath the plate, this assumption should lead to negligible error.

Local anchorage and shear reinforcement have not been included in the finite element model. In fact, this reinforcement has little effect on the behavior of the system until cracking has occurred. After cracking the analysis has little validity since the linear elastic assumption is no longer valid.

3.2.2 TEXGAP-2D: Two-Dimensional Program. Since modeling in two dimensions is an order of magnitude easier than working in three dimensions, both computationally and visually, the possibility of using a two-dimensional program to model the anchorage zone behavior was investigated. While certain things such as curved tendon ducts could not be modeled in two dimensions, the trends for some variables, as shown in Fig. 3.3, could be examined. Also, since previous photoelastic tests by Sargious and Vaughn utilized relatively thin plastics, a two-dimensional state of plane stress was a reasonable assumption for checking these studies. Indeed, calibration runs indicated excellent agreement with such tests.

The program TEXGAP-2D is a linear elastic code for analysis of plane or axi-symmetric bodies. The grid of nodal points is generated separately from the elements. This permits the user to experiment with a large number of nodal points. A large number of nodal points can be generated with a very few cards of input since TEXGAP generates nodes by parts or regions of the grid using an isoparametric scheme instead of just by lines. Difficult curved boundaries can be accurately described using the cubic isoparametric generation scheme. Nodal points can be concentrated in the vicinity of a corner of special interest by utilization of a gradient specification. The primary elements used were an 8-node quadrilateral and a 6-node triangle, both of which can assume curved sides as shown in Fig. 3.4.

TEXGAP uses the frontal solution technique of Irons [44] in which the stiffness equations are processed on an element basis. As soon as all contributions to a particular degree of freedom are assembled, that degree of freedom is condensed from the system. This usually keeps the number of active unknowns at a minimum and reduces the solution time. The frontal method allows extensive programming flexibility by permitting a variable number of degrees of freedom at nodal points.

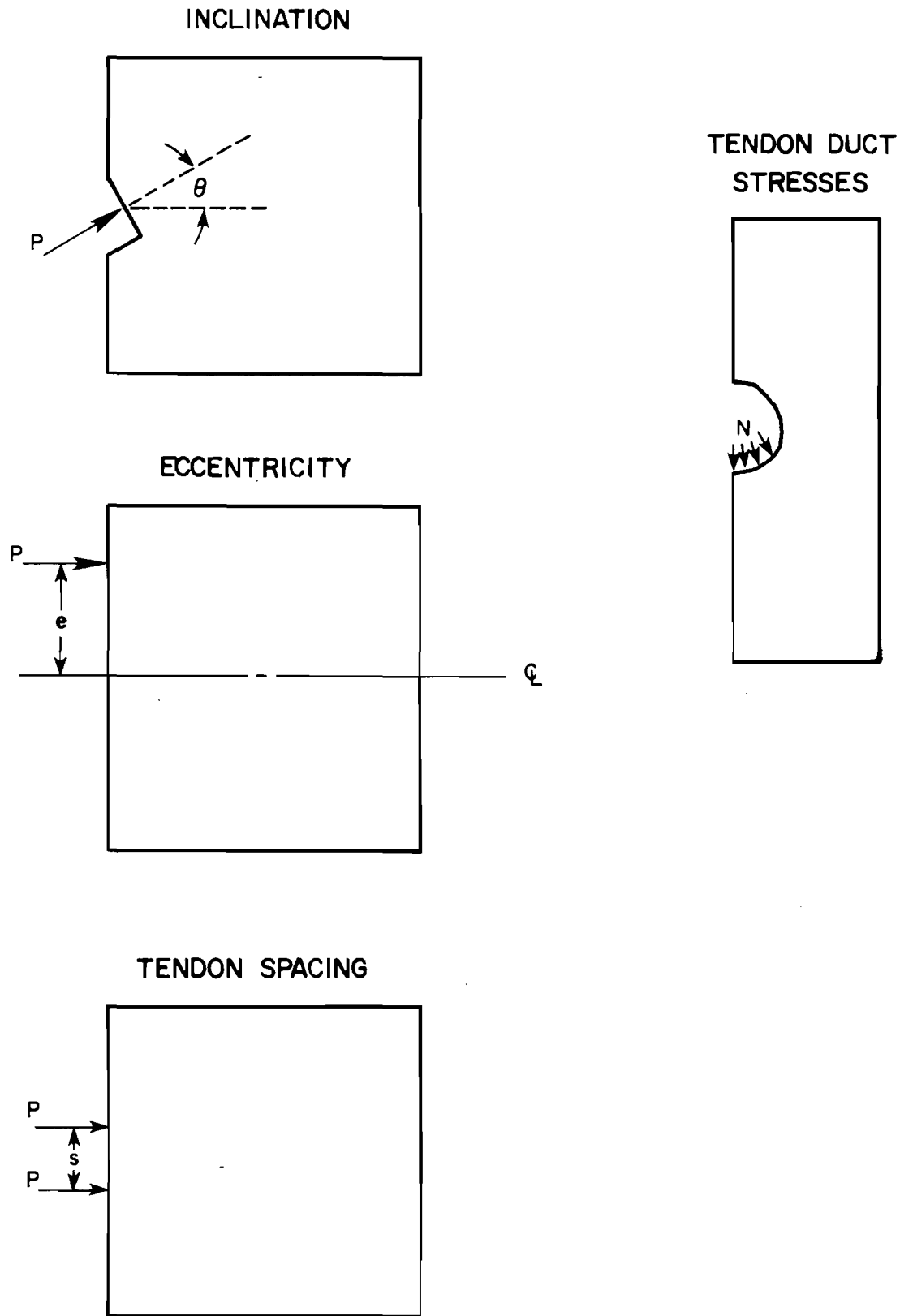


Fig. 3.3 Two-dimensional modeling capabilities for post-tensioned anchorage zones

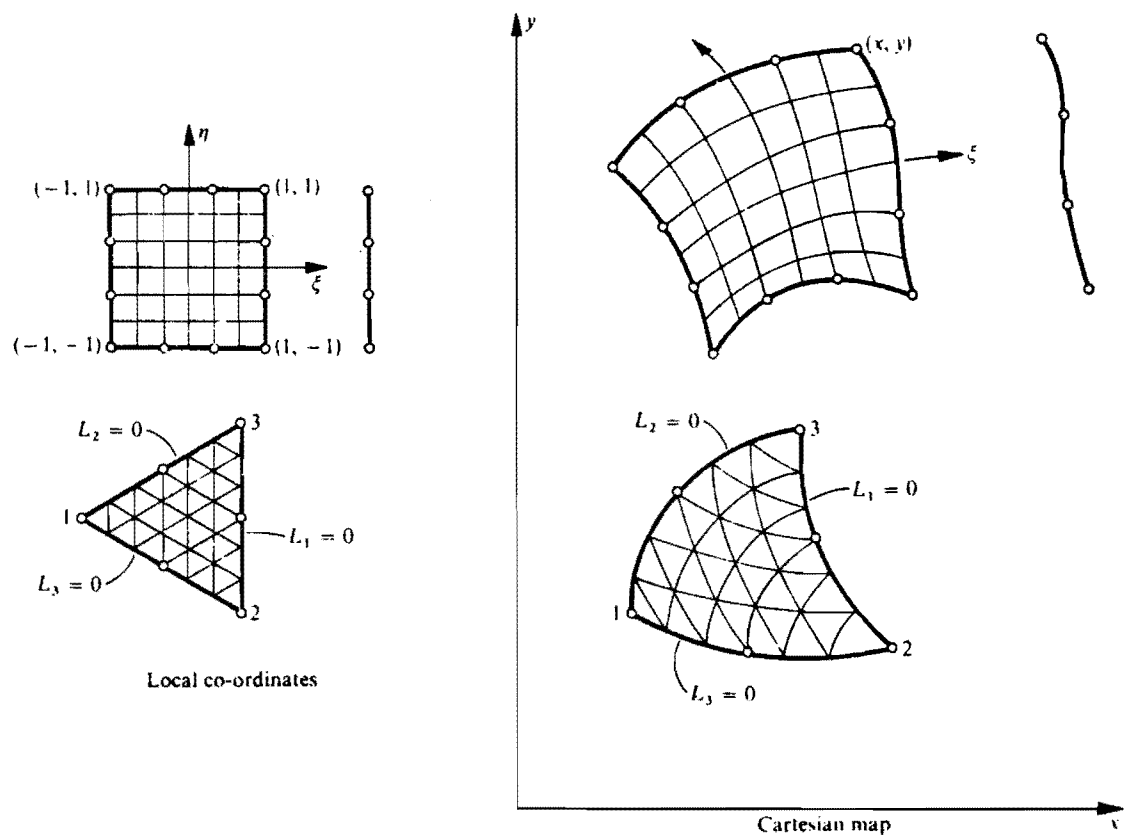


Fig. 3.4 2D isoparametric elements used to model anchorage zones (from Ref. 42)

In addition, **TEXGAP** has the unique and powerful capability to take a coarse grid finite element solution and subdivide a portion of the coarse grid into a very fine grid. The fine grid is resolved to achieve highly accurate results in localized regions at very low computational costs. Debugging of the mesh before solution is done via an interactive graphics package which permits the viewing of the grid on a standard Tektronix terminal. A typical mesh for solution of duct stresses due to tendon normal (radial) loads is shown in Fig. 3.5. As the loads are applied along a relatively long surface with respect to the width of the web section in the actual girder, a plane strain assumption is used.

3.2.3 **TEXGAP-3D: Three-Dimensional Program.** As was pointed out in Chapter 2, the actual post-tensioned anchorage is very much a three-dimensional entity. Although inclined loads can be modeled in two dimensions, the inclined post-tensioned system cannot. Large normal and friction forces are usually generated along the tendon duct which cannot be ignored. This requires that a cylindrical, parabolic, or sometimes cubically curved tendon duct be modeled through the rectangular shell of the web section. The boundary conditions satisfying the pressure and friction distribution along the duct must be applied. Since the duct is a three-dimensional entity, the cover concrete which surrounds it must be modeled as well. Physical tests to investigate the effect of cover by using variable web thickness indicated that the three-dimensional model yielded results closely matching the experimental data, while the two-dimensional program yielded consistently high results. For these reasons the more accurate three-dimensional program was adopted after the calibration stage. Besides the capability of modeling the duct, cover, and web thickness, it is also possible to consider the effect of bearing stress by examining different size anchor plates under the same loading.

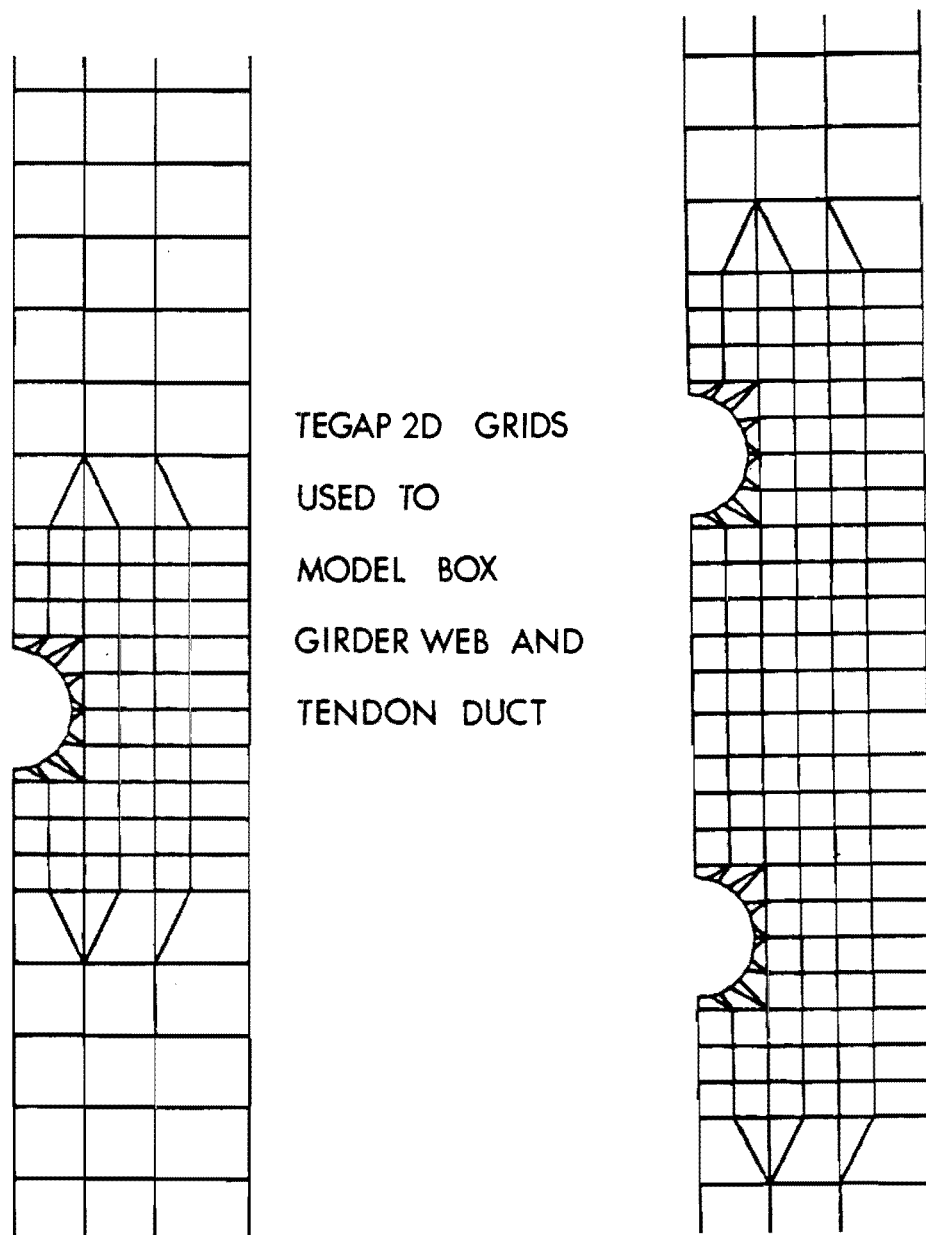


Fig. 3.5 2D grids used to model box girder web and tendon duct

TEXGAP-3D is a linear elastic finite element code that solves static three-dimensional continuum problems. It is not a general purpose code because it does not contain other element types such as beam, plate, and shell elements. It is well suited for analysis of a post-tensioned anchorage zone. In order to make the program more fail-safe, easier to use, and more convenient to code, only quadratic, isoparametric elements are included in the element library. The elements can have curved edges with quadratic interpolation being used for both the displacements and the geometry. Three basic element configurations were used: bricks, tetrahedrons, and triangular prisms, as shown in Fig. 3.6. All three element types can be anisotropic compressible or isotropic incompressible.

The preprocessor and postprocessors coded for TEXGAP3D are perhaps the most powerful such packages available today in a continuum three-dimensional program. The major features of the preprocessor include options to permit the definition of global and local coordinate systems of Cartesian, Cylindrical, Spherical, or Toroidal types. Nodes may be generated in these systems on arcs, curved surfaces, or three-dimensional blocks using linear, quadratic, or cubic interpolation with gradient control. Points on the intersection of coordinate systems can be computed as well as connections or Laplacian filling of points between previously defined points. Elements and boundary conditions can be easily defined using data defined looping and default nodal connectivities. Boundary conditions involve pressure, traction, spring, normal roller, and degree-of-freedom tying as well as the usual nodal point force and displacement values. Material properties may be isotropic, orthotropic, and anisotropic. Local properties may be transformed to the global systems in several convenient ways, including the use of the locally defined coordinate systems.

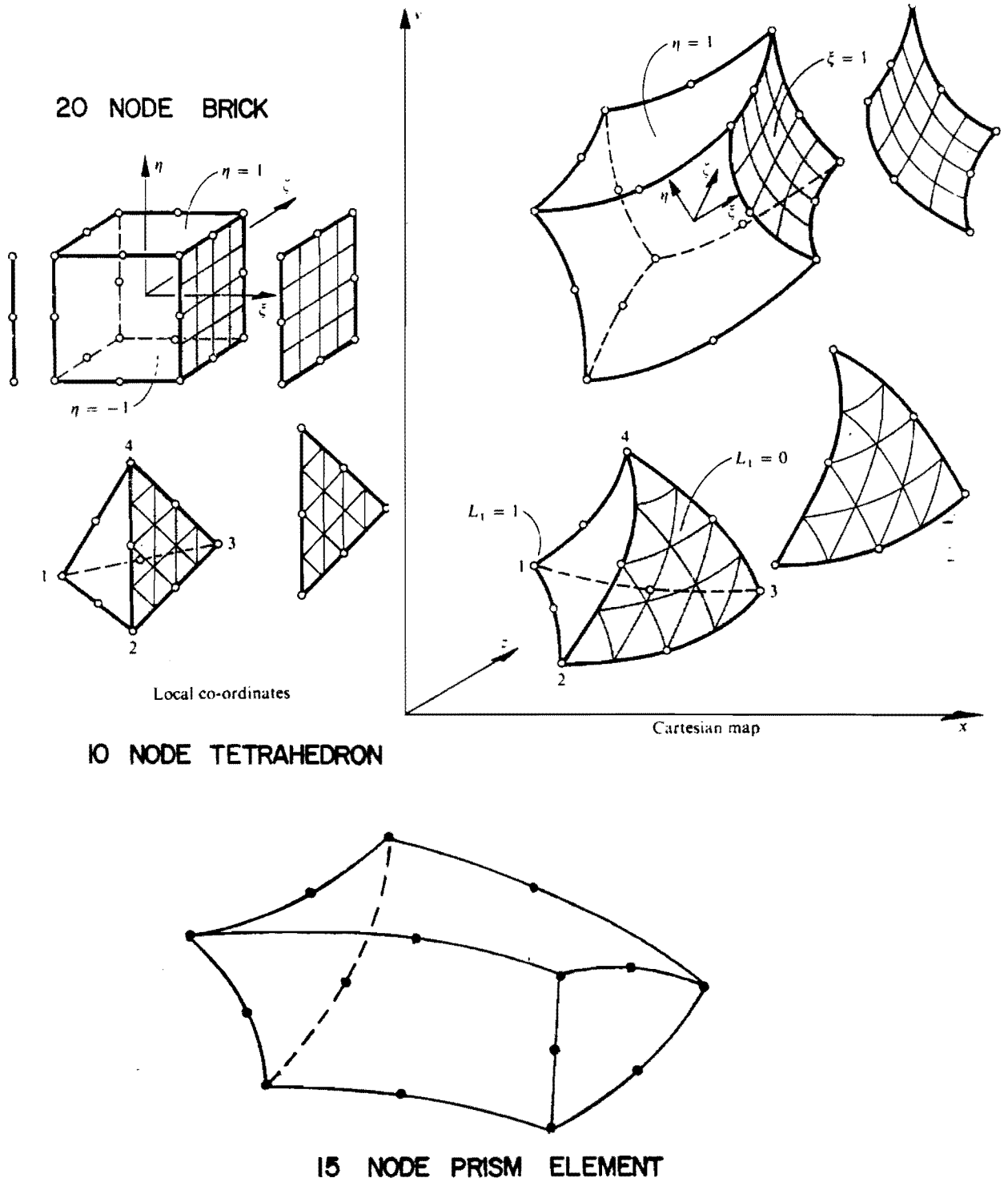


Fig. 3.6 TEXGAP-3D general elements--all isoparametric (from Refs. 42 and 43)

The major features of the postprocessor include user control over the points within an element at which stresses and strains are computed. Either the built-in options or user-defined points may be used. Bounds are available to limit the processed region either by Cartesian or connectivity limits or both. Processing can be done on an entire block of elements, or on a layer, or on connecting planes. Isoparametric element plots and deformed grid plots as well as isoparametric and deformed plane plots are available. Plots of the location of stress points by number are also available. Contour point plots can be made for stresses and/or strains on connectivity planes.

Also worthy of note is that the program has the powerful option of rezoning or subdividing coarse grid elements to achieve more accurate definitions of stress and deformation in local regions of interest. Only brick elements can be rezoned.

Because of the complexity of debugging difficult three-dimensional meshes, an interactive graphics plotting routine allows the user to quickly view sections of the mesh in different spatial orientations. If desired, surface plots using hidden line removal techniques are available.

TEXGAP-3D was the main program base used for all three-dimensional finite element modeling throughout the course of the project. However, extensive modifications were made to facilitate modeling of the prototype specimens. These modifications are discussed in the following section.

3.2.4 Program PUZGAP-3D. One of the chief obstacles to the use of higher order elements in the early 1970's was the actual solution of the system of equations for the nodal displacements. The magnitude of the system to be solved for even a relatively small problem using 20 node isoparametric bricks could easily exceed the central memory capacity of a large computer. This was because at that time almost all codes used gaussian elimination "band solvers."

Consider a relatively large three-dimensional mesh such as that shown in Fig. 3.7a. If the solution used 20 node bricks, the node numbering for the first layer would be as shown in Fig. 3.7b, c, and d. The total number of nodes in the problem is thus the sum of  $11 \times 96$  corner nodes per layer (1056) plus  $10 \times 36$  midside nodes per layer (360) or a total of 1416. Since there are three degrees of freedom per node, 4248 unknowns must be solved. A closer look at element number 1 in Fig. 3.7e shows that the maximum bandwidth is 152 nodes or  $152 \times 3 = 456$  degrees of freedom. The storage capacity required for the banded stiffness matrix would thus be  $456 \times 4248 = 1,937,088$  base ten characters. The maximum available core on the large CDC 6600 at the University of Texas is 220k base eight, or 73,728 base ten. To store the banded form of this stiffness matrix for in-core solution would thus require 26 times the limiting storage capacity of this large computer.

Early efforts at solving problems such as this led to elementary substructuring of the band by partitioning. The methods of partitioning varied but in all methods as the upper partitions were eliminated they were removed to disk and the next partition brought into core. For the case of one general purpose program, SAP IV, two partitions are in core for solution at any given time. The main disadvantage of this procedure, particularly with problems with large bandwidths, is that the massive transfer of I/O from disk to core results in inordinate amounts of computer time required for solution.

In 1970, Irons introduced the frontal or wavefront technique. The stiffness matrix is assembled on an element by element basis, rather than by the usual technique using nodal point numbering. The technique allows for extremely rapid solution times as only a relatively small amount of core storage adequate to retain the "front" is needed. Details are given in Ref. 41. In the example shown in Fig. 3.7, the maximum front width occurs when the final element for a given face is being reduced. For that situation, 96

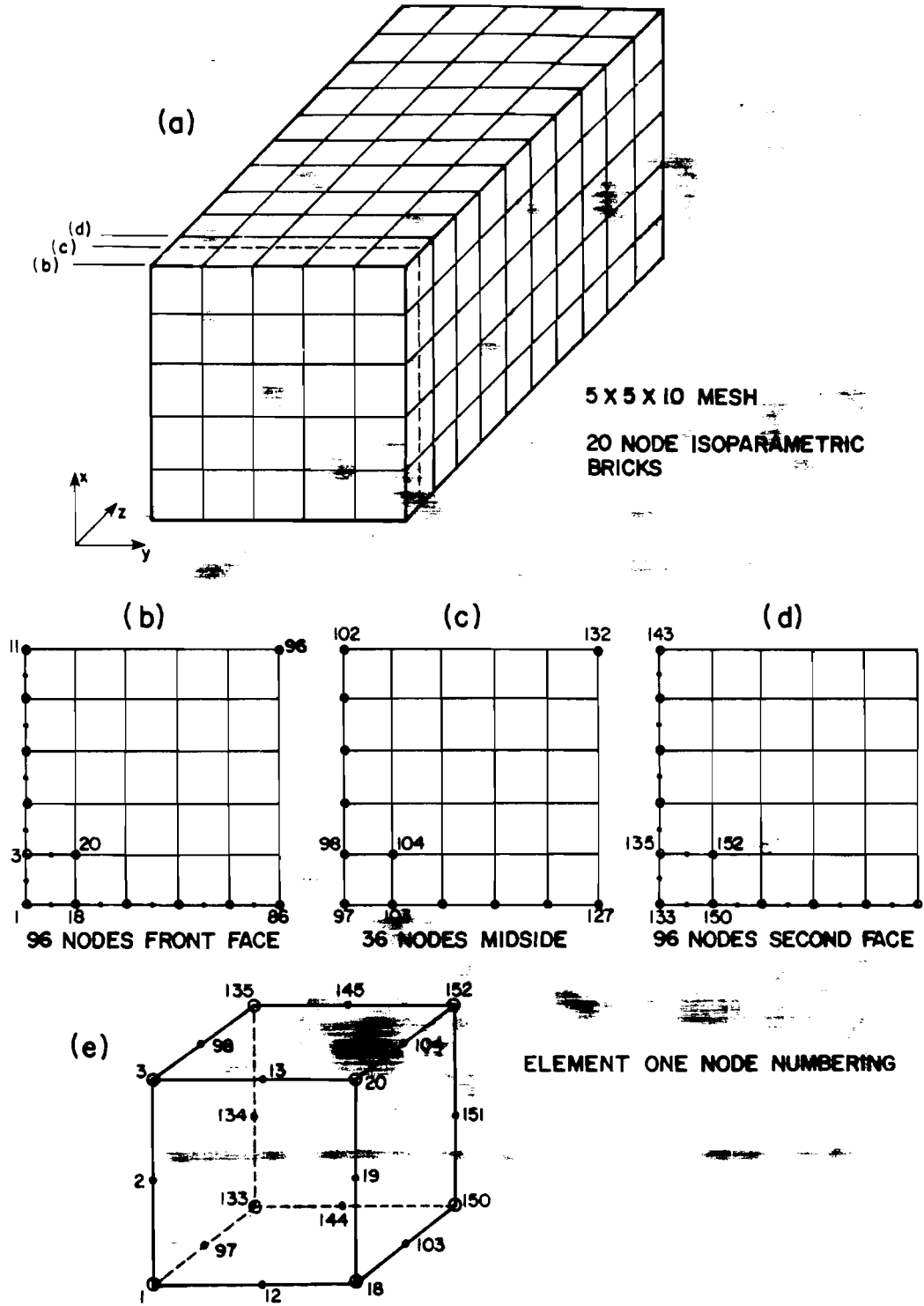


Fig. 3.7 5 x 5 x 10 mesh--3D problem

nodes on the next face to be processed are retained in core, plus an additional 12 nodes from the final element from the previous face. That totals to 108 nodes or 324 degrees of freedom (DOF), since each node represents three translational DOF's. The required in-core storage for the front is  $324 \times 325/2 = 52,650$ . This is less than the 73,728 base ten word capacity of most major computers such as the CDC 6600 and thus the program can execute directly in core using the frontal technique, whereas the band solver will require substantial partitioning.

The refined mesh for a box girder web containing a 30 degree inclined, curved post-tensioning tendon running through the middle required 500 elements of 20 node bricks, arrayed in such a manner that at times the maximum front width approached 600. The in-core storage requirement using the frontal technique would be  $600 \times 601/2 = 180,300$  words. This value exceeds the 73,728 available for the CDC 6600. The solution exceeded the capabilities of the frontal equation solver used in TEXGAP.

At that point in time C. P. Johnson of The University of Texas had done extensive work [45] in the area of multi-level substructuring techniques based upon a frontal equation solution. While the primary use of his program--PUZZLE--had been geared toward substructure reduction of complex grids for dynamic analysis, the provision had been made for the general solution of large systems of finite element equations.

PUZZLE operates on three levels of programming strategy: Level one is activated when the front can be stored in the available core. Except for programming methodology, this level is identical to that of TEXGAP's frontal equation solver. Level two is activated when the front associated with a given element cannot be stored. It does require that the portion of the front associated with the degrees of freedom to be eliminated can be stored in-core. This

portion is held in-core while the remainder of the front is processed in blocks whose size depends on the remaining available core. An additional level is available for those fronts which cannot be accommodated by the first two levels. Level three processes a given front by repeated application of level two. This provides virtually unlimited solution capacity.

The successful interfacing of the two programs TEXTGAP and PUZZLE by Becker, Johnson and Stone [41] formed the hybrid program PUZGAP 3D, and presented an extremely powerful tool for the solution of the post-tensioned anchorage zone problem. PUZGAP 3D was used for all three-dimensional analysis discussed in this report. [Copies of program PUZGAP 3D can be obtained from Dr. E. B. Becker, c/o TICOM, Department of Engineering Mechanics, The University of Texas at Austin, Austin, Texas 78712.]

### 3.3 Calibration

The ultimate objective in the use of any analytical model is to be able to replicate as closely as possible the behavior of the physical prototype. Once the model is shown to produce accurate results for a variety of conditions, it can be used to extrapolate and yield solutions to complex problems where physical testing would be time-consuming and economically prohibitive. Such a process of verification is termed calibration.

At the beginning of the calibration phase the available material for calibration consisted of a few photoelastic tests reported in the literature, experimental results from Zielinski and Rowe, and the photoelastic studies being done concurrently by Vaughn. Most of the comparisons with that data as outlined in Secs. 3.3.1 and 3.3.2 proved quite acceptable. However, it was felt that none of the existing data realistically represented the anchorage zone stress state for a thin web post-tensioned anchorage. In particular, it

should be remembered that the maximum transverse tensile stress in a three-dimensional problem decays rapidly from its peak along the center line towards the side face. This was amply demonstrated by Yettram and Robbins [22]. All tests performed by Zielinski and Rowe [9] presented transverse stress distributions based on surface strain measurements only. For this reason it was felt that the most positive method of calibration would be to compare the analysis results with physical measurements of the internal strain along the line of maximum transverse stress in a physical model. The gages in the model would ideally be located at the integration points of the elements along that line, but locations close to the nodes would also be acceptable. With this scheme, a precise means of calibrating the program would be available. These calibration procedures are detailed in Secs. 3.3.3 and 3.3.4.

Detailed coding for TEXGAP and PUZGAP 3D for all calibration examples is presented in Ref. 41.

3.3.1 Literature Comparisons. Most anchorage stress studies in the past have been two-dimensional analyses, so the first comparisons used the two-dimensional program.

Sargious [25] performed a number of photoelastic tests, as described in Sec. 2.2.1. A computer run was made to model Sargious' test with an eccentricity of  $2a/6$  and an angle of inclination of approximately 6 degrees. The results for the bursting and spalling distributions are shown in Figs. 3.8a and 3.9. For this typical case, there is very good agreement between Sargious' experimental data and the finite element predictions. A plane stress assumption was used for the model. Stress contour plots generated by the program are shown in Fig. 3.10. Figure 3.10a clearly shows the spalling and bursting transverse tensile stress zones.

In addition to the calibration run, a number of different runs were made to investigate the effects of the various geometric variables such as eccentricity and inclination of the tendon. In

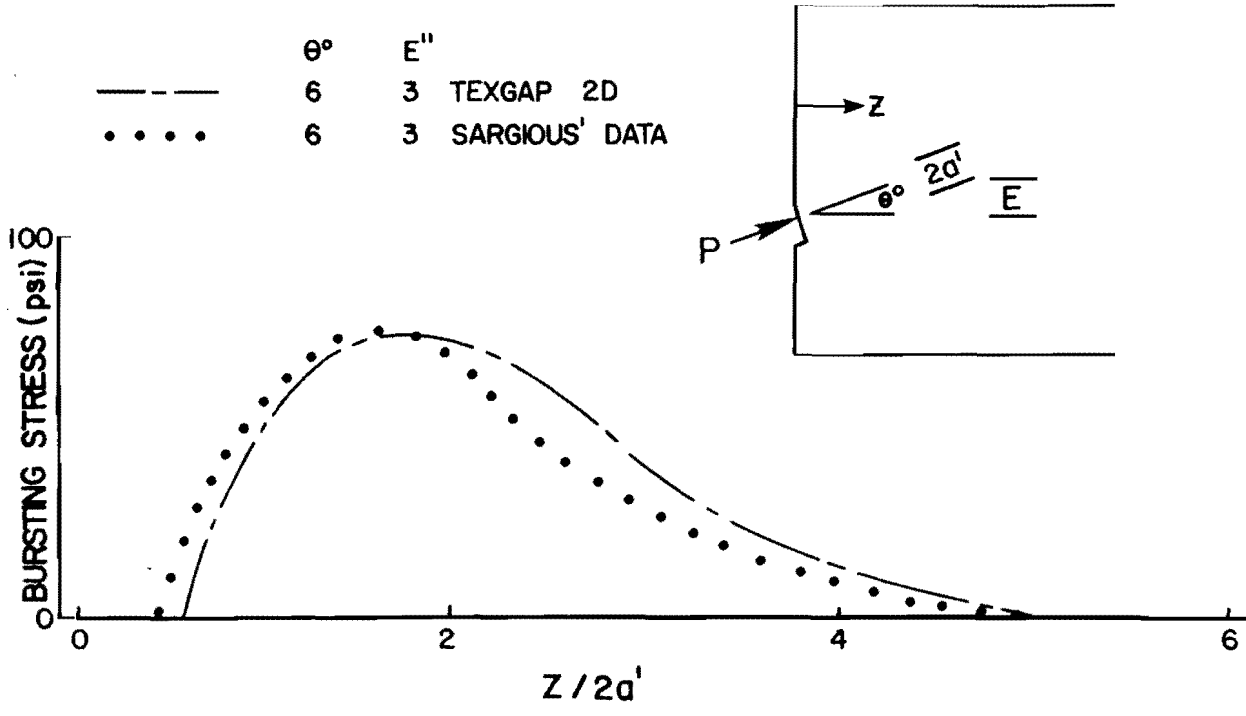


Fig. 3.8 Bursting stress comparison--2D-FEM vs Sargious

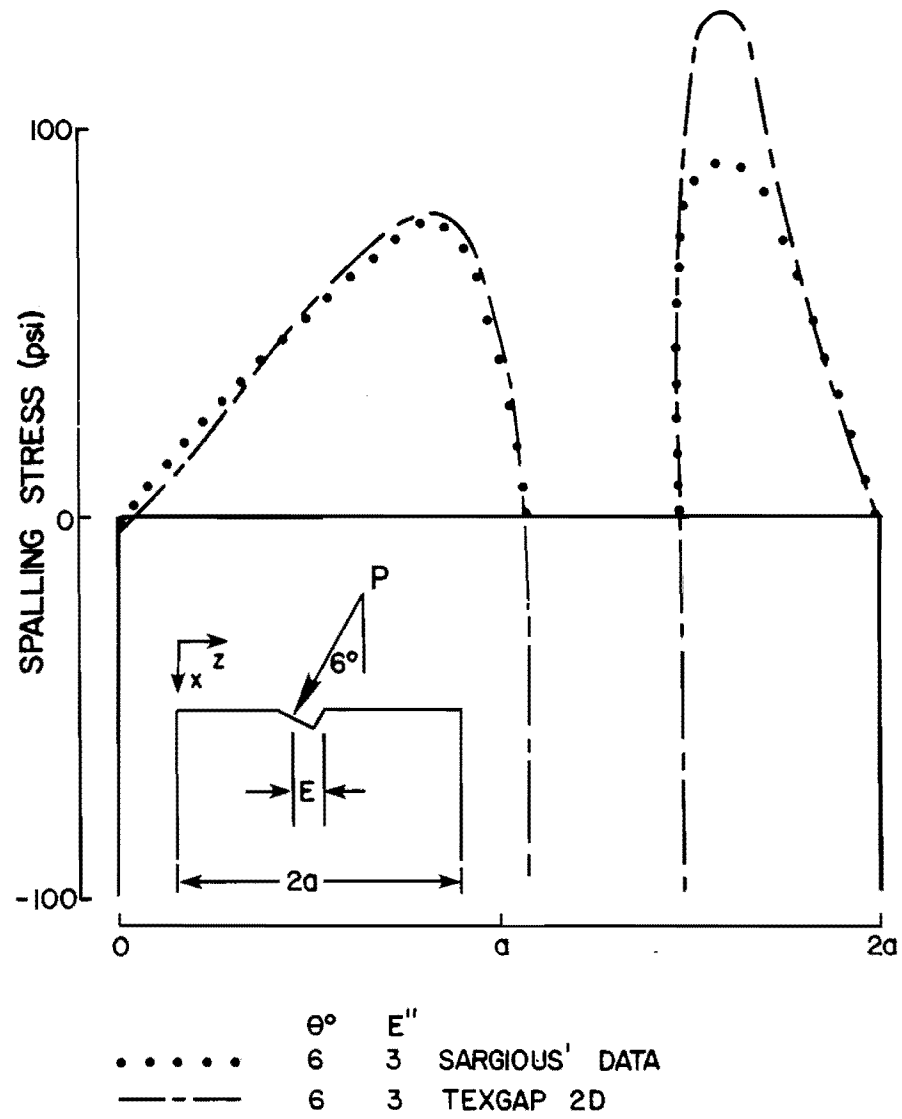
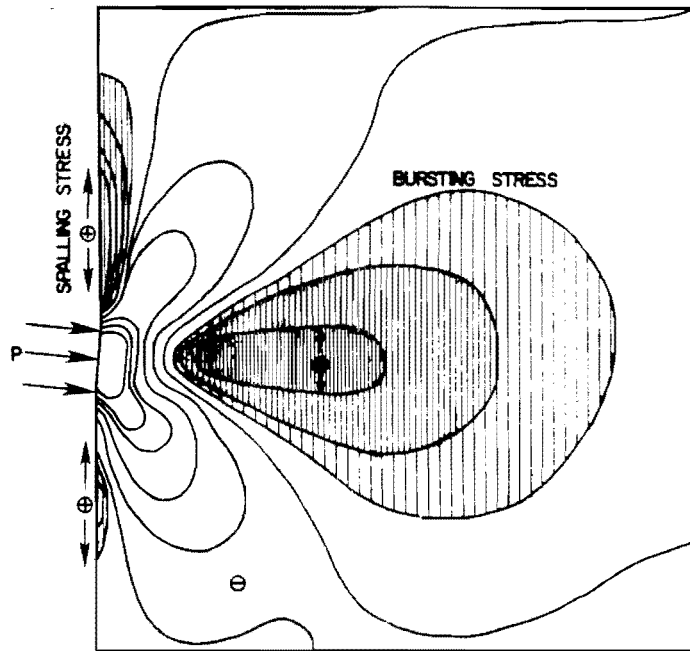
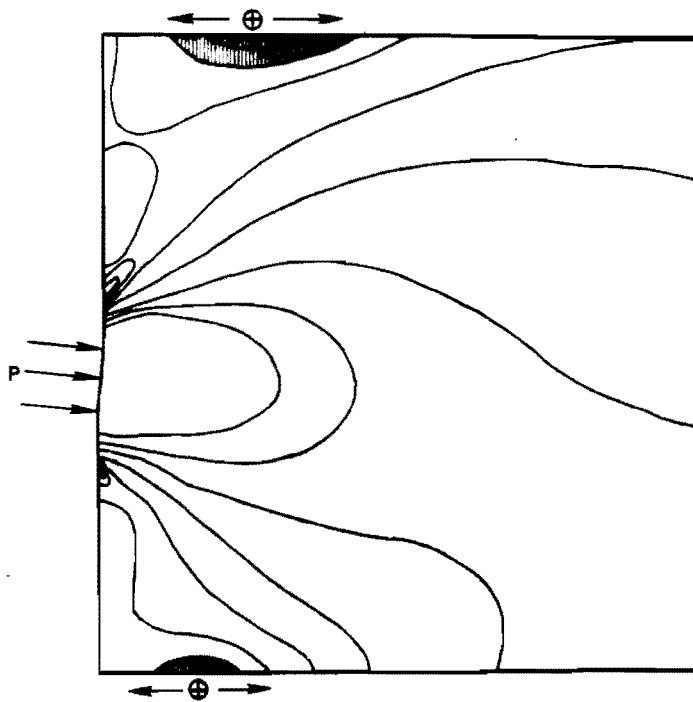


Fig. 3.9 Spalling stress comparison--2D-FEM vs Sargious



a) Transverse stress



b) Longitudinal stress

Fig. 3.10 Stress distributions for Sargious' problem--  
2D-FEM

general, the effects of change of eccentricity or inclination from the symmetrical centroidal loading configuration can be seen from Figs. 3.11 and 3.12. In Fig. 3.11 it can be seen that for any loading configuration other than centroidal, the maximum bursting stress decreases. Conversely, in Fig. 3.12 the maximum spalling stress increases rapidly for even slight changes in inclination and eccentricity. Main trends from these types of variable studies will be discussed in later reports in this series.

In a second calibration series a number of tests performed by Zielinski and Rowe [9] were modeled to check the three-dimensional code. A typical example would be the  $6 \times 6 \times 6$  prisms. Figure 3.13 shows the finite element mesh used for modeling the block. These figures were generated using an interactive mesh debugger and were taken directly from a Tektronix 4010 terminal. Note that the mesh shown represents only one-quarter of the prism tested by Zielinski and Rowe. Wherever possible, advantage of geometric symmetry was taken. In general, concentric, straight tendon problems have four-fold symmetry. Eccentric and inclined tendon problems have two-fold symmetry. Care must be taken to supply the proper boundary conditions for these reduced models as shown in Fig. 3.14. The results for the bursting transverse strain distribution are shown in Fig. 3.15. These values are for the transverse surface strain taken along the prism face center line. It can be seen that the curves are similar in shape, although the FEM solution gives appreciably lower values than obtained by Zielinski and Rowe.

3.3.2 Photoelastic Comparison. At the time the first 20 calibration runs were being made, Vaughn [27] was nearing completion of a series of nine photoelastic tests. This provided a wealth of raw data to work with. Six of the nine tests were modeled using the two-dimensional finite element program. A typical mesh for a concentric single straight tendon with a bearing-type anchor is shown in Fig. 3.16. Figure 3.5 shows a section of the meshes used to

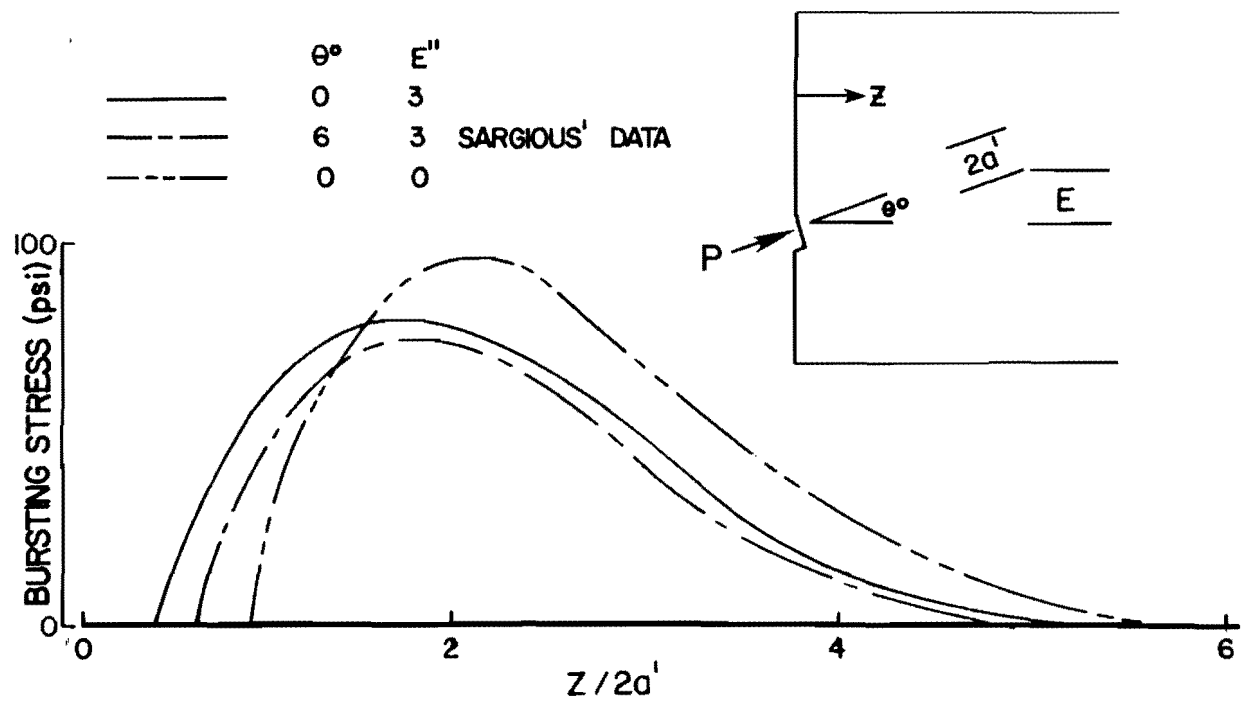


Fig. 3.11 Bursting stress distribution variable check--  
2D-FEM

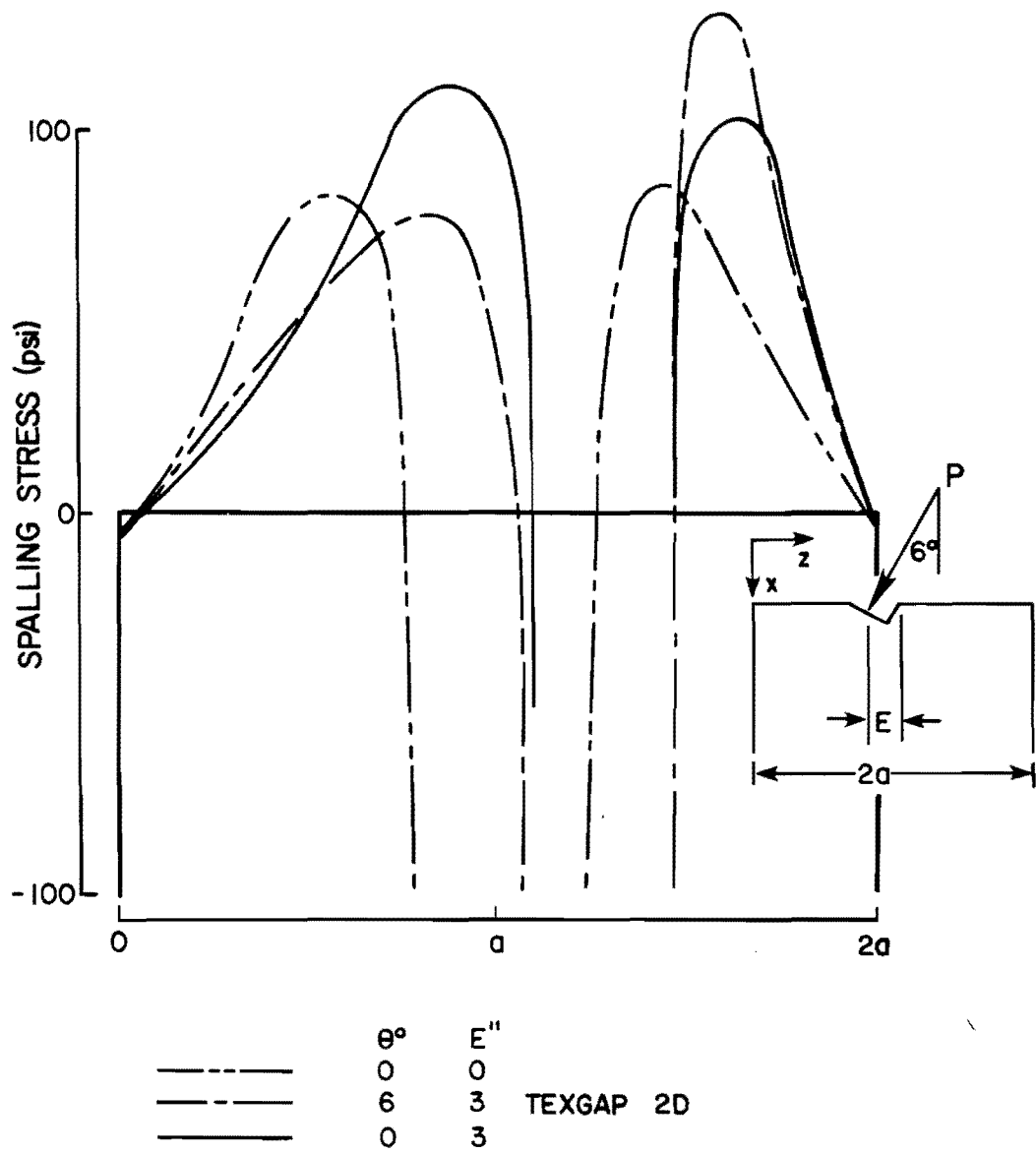
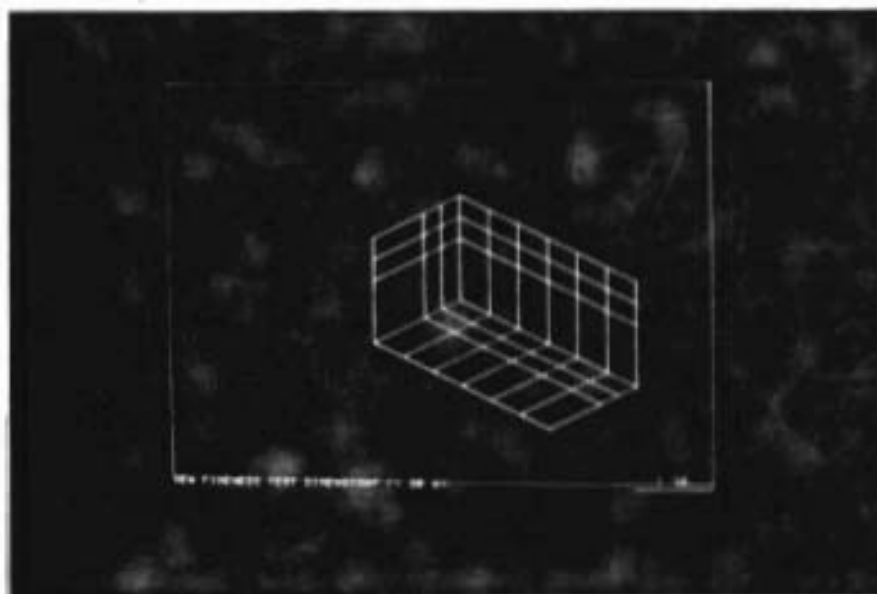
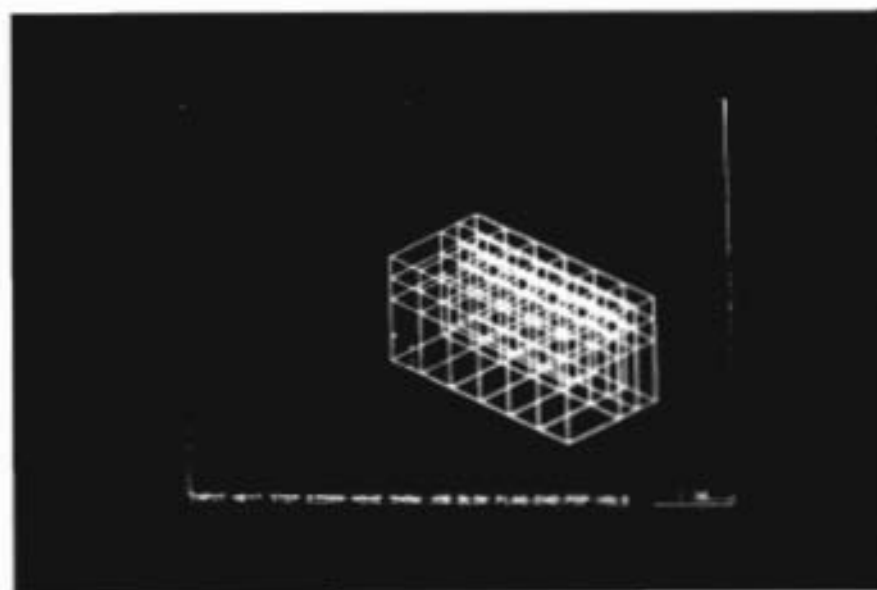


Fig. 3.12 Spalling stress distribution variable check--  
2D-FEM

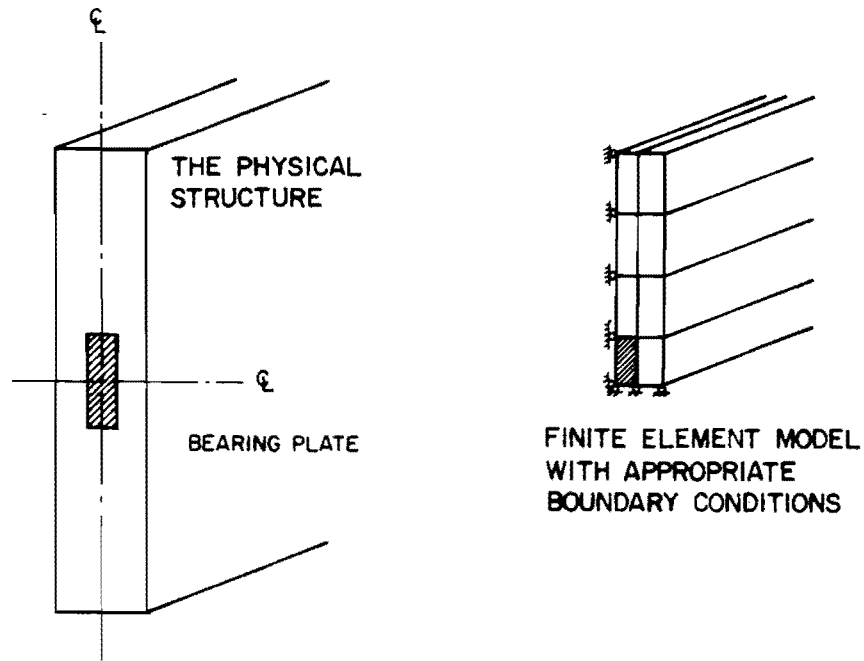


(a) Surface interactive plot--1/4 symmetric mesh of Zielinski and Rowe 6 in. X 6 in. X 6 in. prism.  $a'/a = .59$

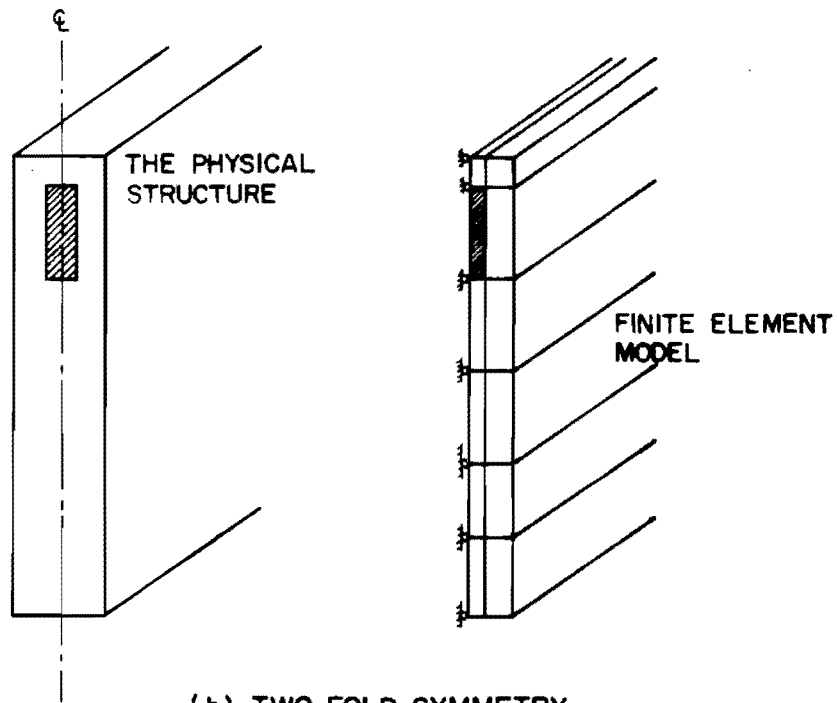


(b) Same as (a), but detailing entire mesh

Fig. 3.13 Interactive graphics plot of Zielinski and Rowe 6 in. prism



(a) FOUR-FOLD SYMMETRY



(b) TWO-FOLD SYMMETRY

Fig. 3.14 Symmetry conditions in post-tensioned structures and equivalent FEM models

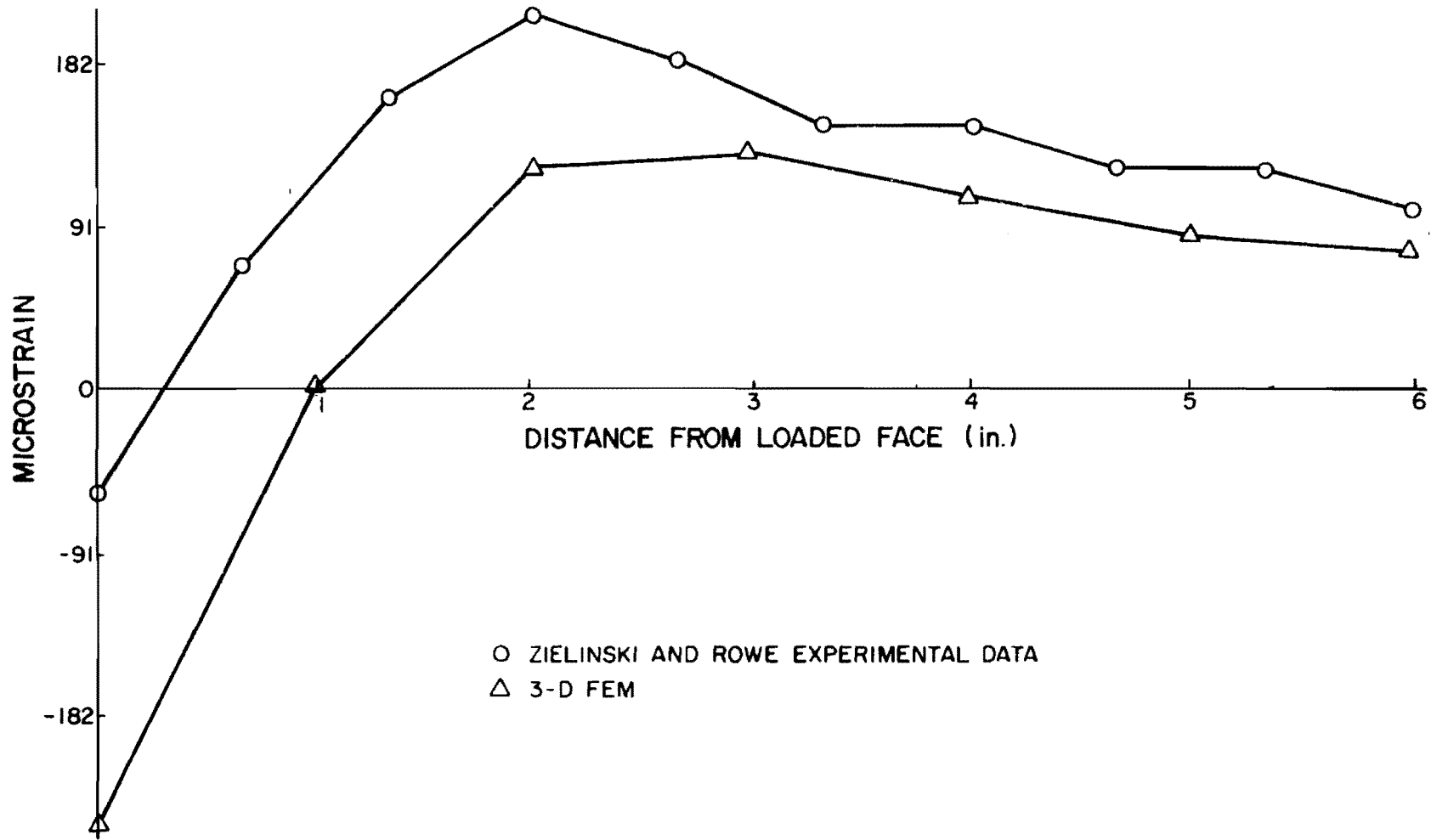


Fig. 3.15 Calibration with Zielinski and Rowe cube

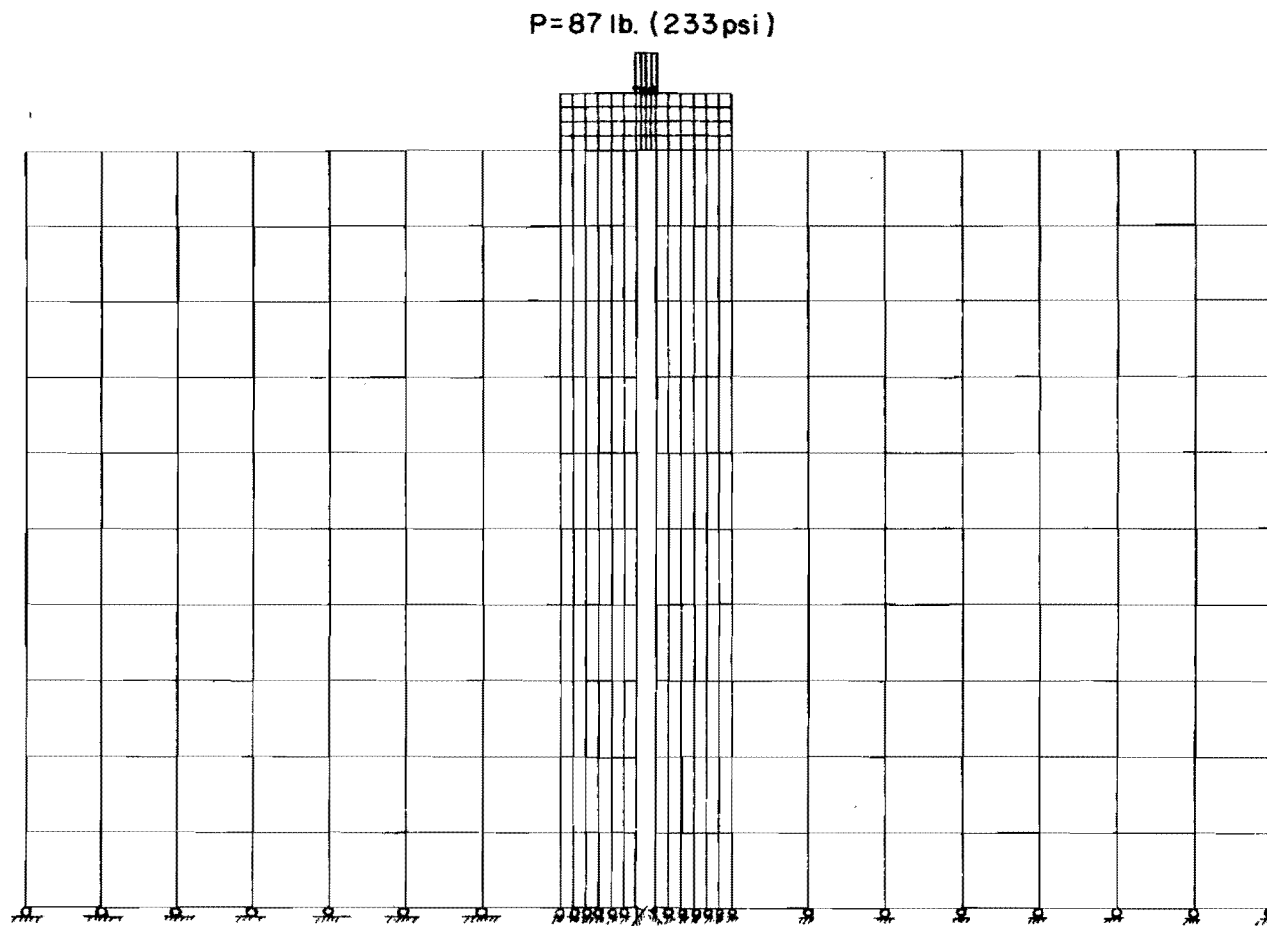
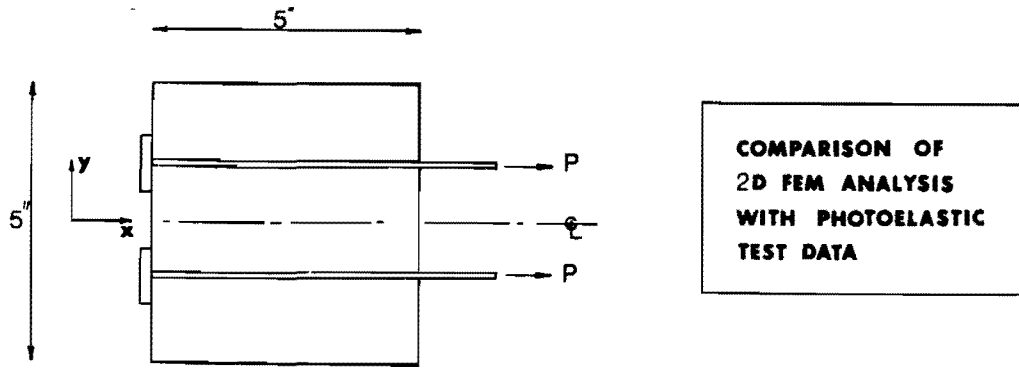


Fig. 3.16 Typical mesh used for modeling Vaughn's tests

simulate Vaughn's tests which looked at the effect of radial forces on the tendon duct in regions of sharp curvature. Figure 3.17 shows a sample comparison run with Vaughn's test #7 which had two parallel straight tendons. In most cases the transverse and longitudinal stress distributions for the photoelastic model and 2D computer program agreed quite well, as shown in Fig. 3.17. For some cases, however, the resolution of stresses in regions of high stress concentration, such as the tendon duct shown in Fig. 3.5, was not conclusive in the photoelastic tests.

3.3.3 One-fourth Scale Model Tests. Photoelastic studies are not capable of replicating the performance of a concrete anchorage zone. Thus an extensive series of model tests was begun with the dual purpose of calibrating the program with hard data from anchorage zone tests in thin web concrete sections and to do a preliminary investigation of the primary variables affecting the cracking load--cover, inclination, eccentricity and anchorage geometry. The use of one-fourth scale model specimens for the first series of physical tests in this investigation was decided upon for several reasons. The first was the economy of time and materials. It would take substantially less effort to prepare, cast, instrument, and test a one-fourth scale model than a full-scale prototype. The second reason was that extensive previous research at The University of Texas at Austin had indicated that microconcrete models could be used to accurately replicate conditions and performance seen in prototype concrete specimens. Thus, models could be used to examine a wider range of parameters than would a test program confined solely to full-scale testing.

The next step was to develop a method of instrumentation capable of measuring the transverse bursting strain inside the concrete, on the tendon center line and as near to it as possible. The design of these gages is discussed in detail in the second report in this series. The insert strain gages were then suspended from the



Vaughn's test No. 7  
 dual tendon  $t = .375'$ ;  $P = .09k$

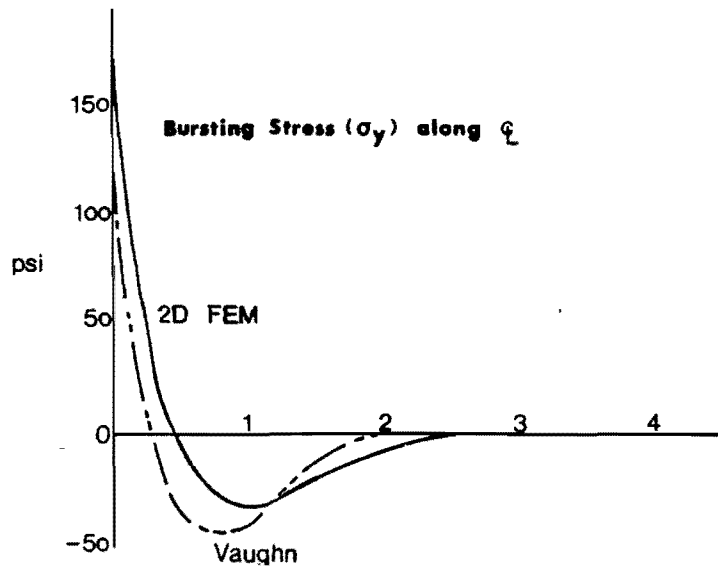
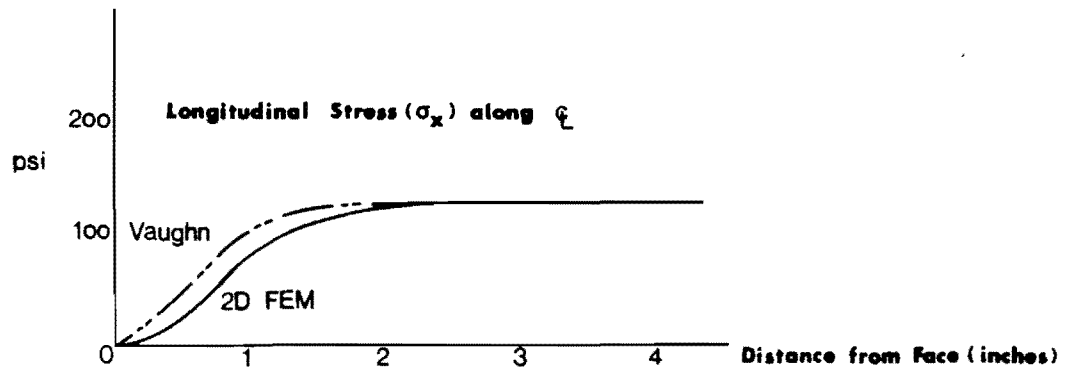


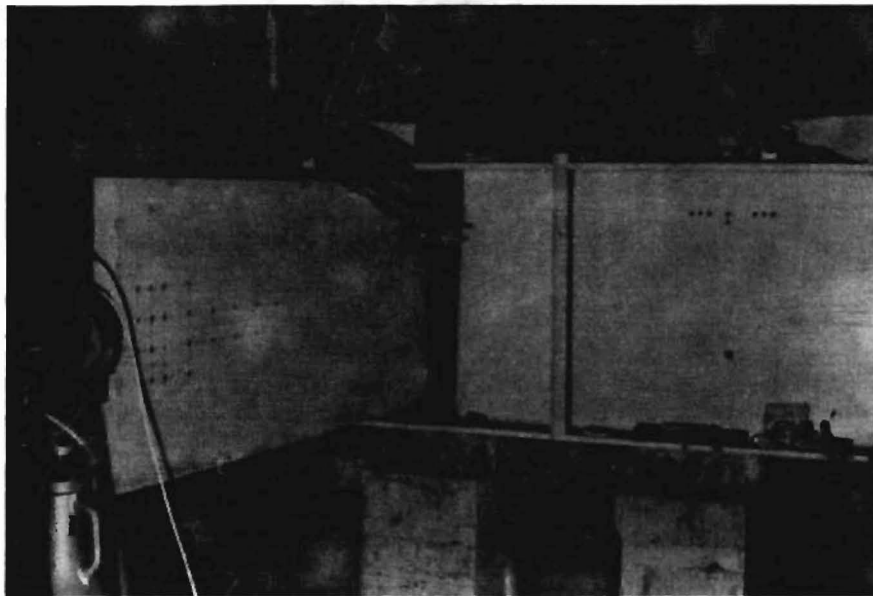
Fig. 3.17 Comparison of Vaughn's test #7 with 2D-FEM analysis

model shear reinforcement and were oriented perpendicular to the tendon so as to measure the transverse strain. Each gage thus represented one point on a typical bursting strain distribution curve. The term bursting strain (and associated stress) is emphasized here, because at the time these model specimens were being cast and tested the preponderance of literature indicated that this was the primary cause of tendon path cracking in post-tensioned anchorage zones. Thus, it was not until certain inconsistencies in this approach were noted from data analysis in the test program that it became evident that other stresses, in particular the spalling stresses, demanded an intensive study.

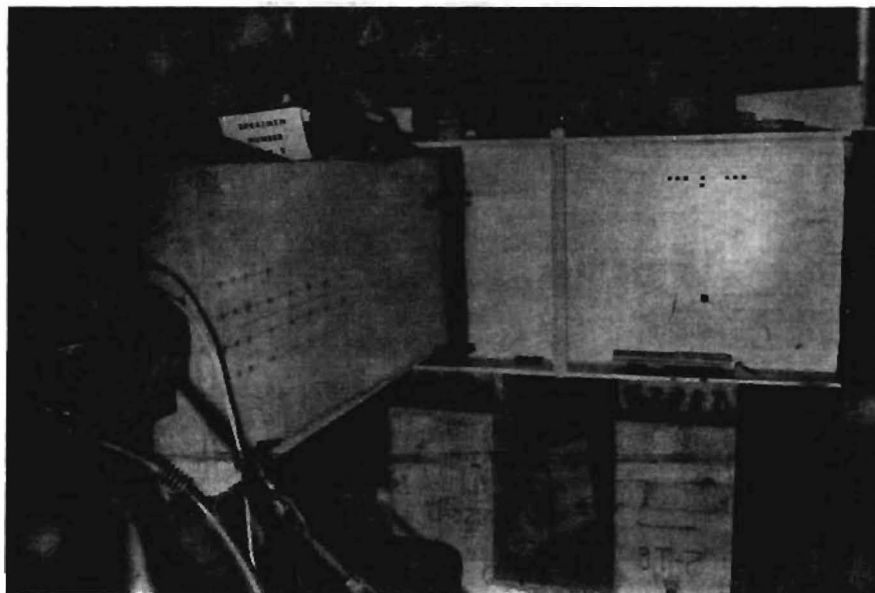
3.3.3.1 Cover Effects. A series of four one-fourth scale models were used to investigate the effect of cover concrete for concentrically loaded anchorages. Figure 3.18 shows typical specimens with widths of  $t = 2$  in. and  $t = 4$  in. Six gages were placed along the tendon path at 3 in. spacing. As this was a four-fold symmetry problem, only one-quarter of the specimen was modeled with the finite element program. The equivalent FEM meshes are shown in Fig. 3.19.

Comparative strains from the FEM model corresponding to insert gage locations were selected, as shown in Fig. 3.20.

Figures 3.21, 3.22, and 3.23 illustrate the results of the first test series and the corresponding finite element runs. With the exception of the 4 in. width model (Fig. 3.21) in which the experimental data were skewed slightly to the right, the program produced peak strains and bursting distribution shapes which could be considered to be exceptionally accurate, given the expected scatter in experimental data. For the case with  $t = 2$  in., it should be noted that the specimen was cracked at 24 ksi and, thus, to achieve a representative curve which could be scaled for comparison with the other specimens, the data were linearly scaled up from the 10 ksi load stage.

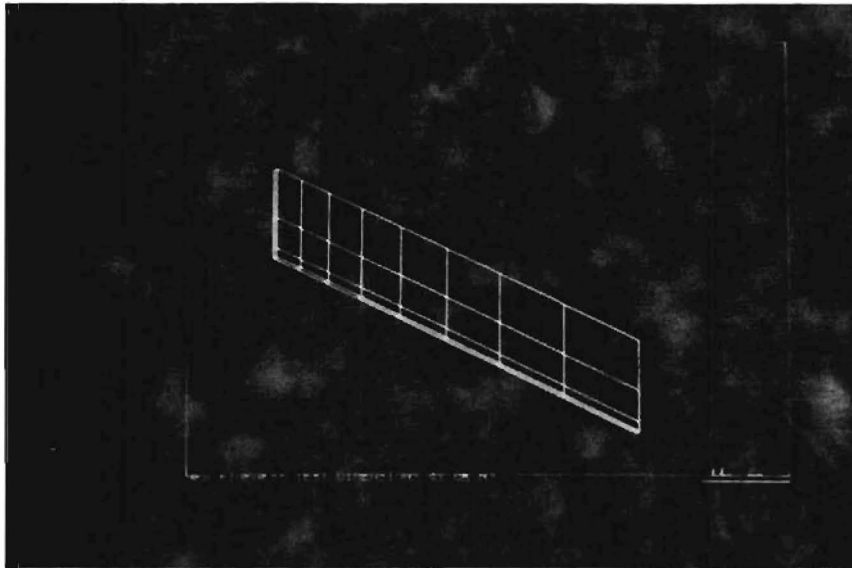


(a)  $t = 2$  in. model M3-2, physical test

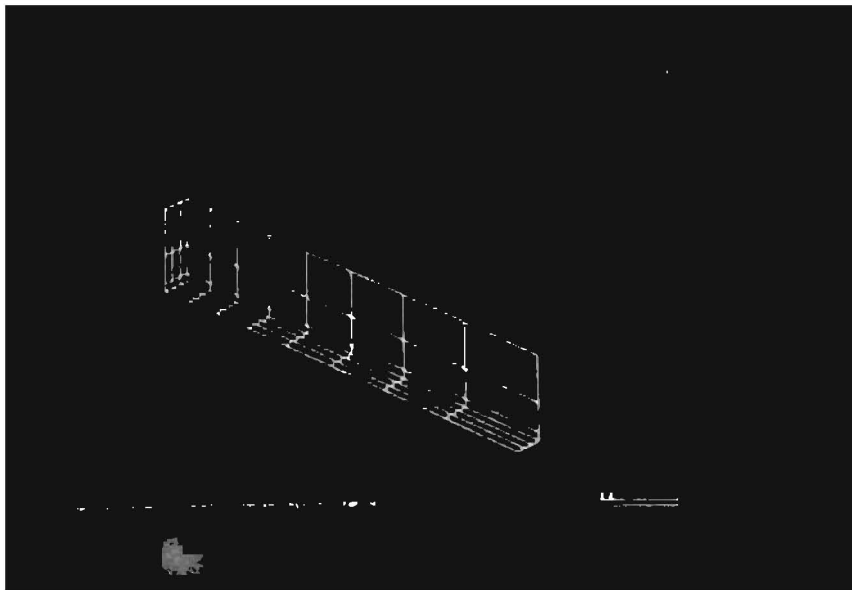


(b)  $t = 4$  in. model M2-2, physical test

Fig. 3.18 Typical physical specimens; cover series tests



(a)  $t = 2$  in., 1/4 symmetric mesh. Load applied to lower square



(b)  $t = 6$  in., 1/4 symmetric mesh. Load applied to lower left square

Fig. 3.19 Interactive plot of cover series FEM meshes

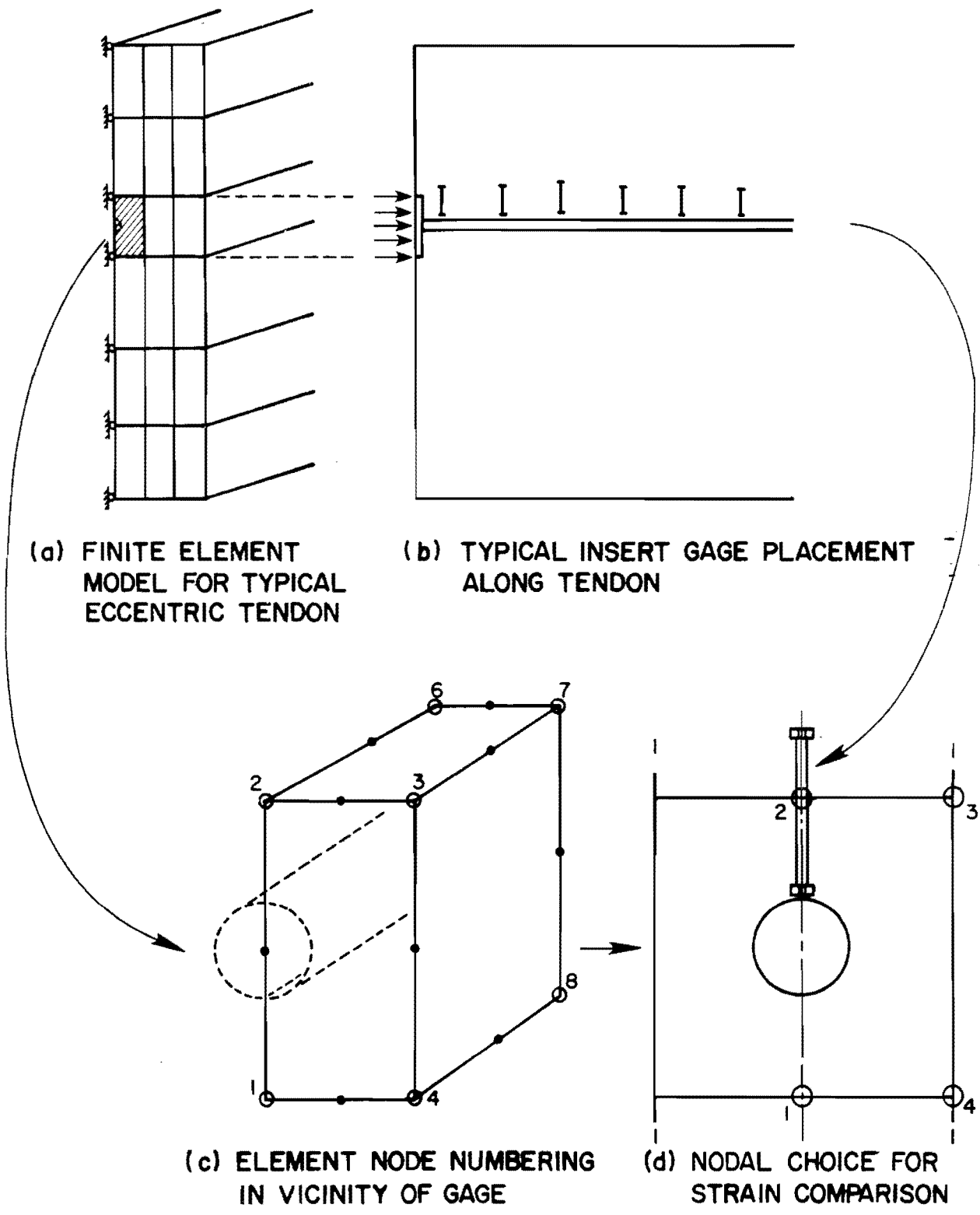


Fig. 3.20 Nodal choice for strain comparison between 3D-FEM and first model series tests

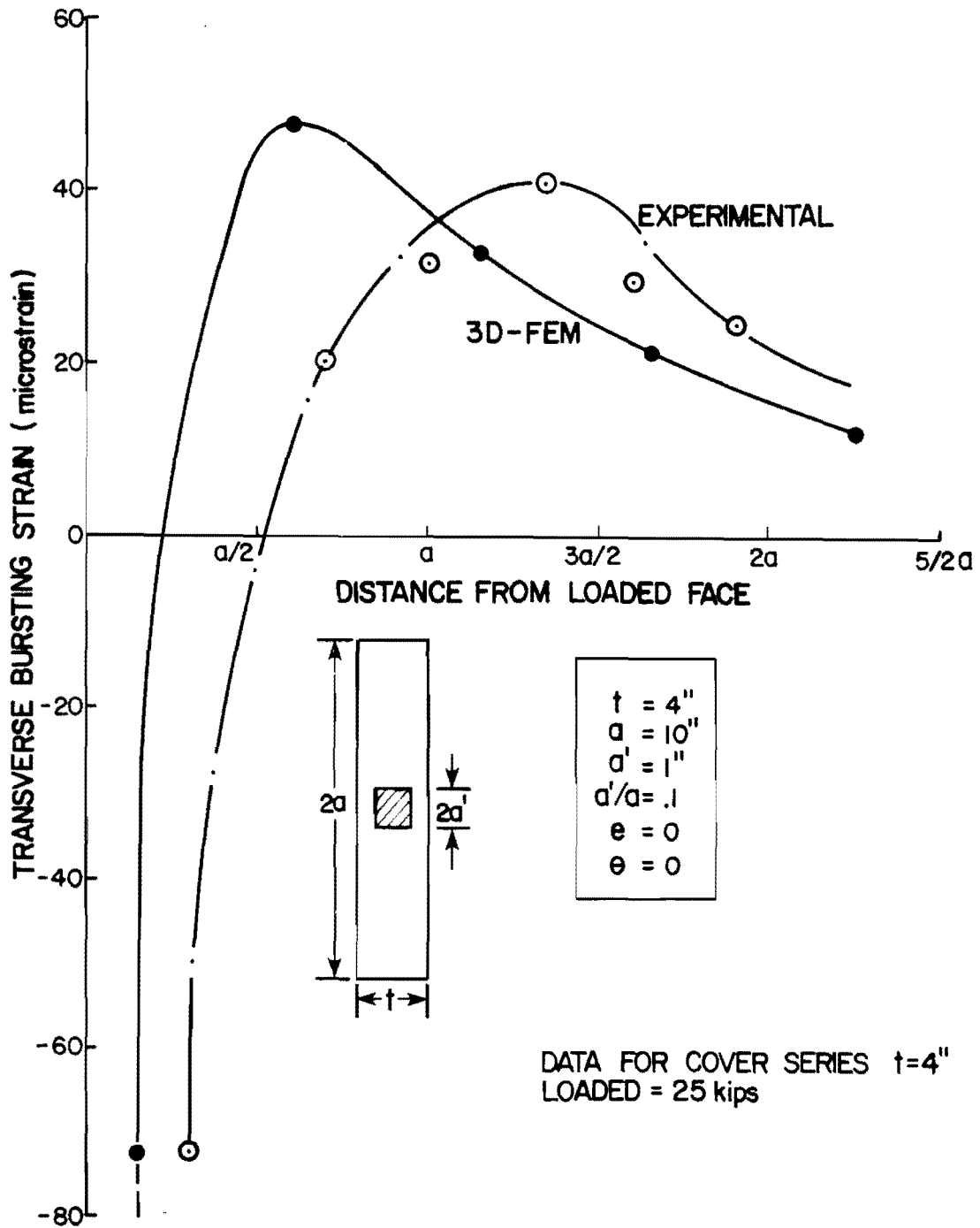


Fig. 3.21 Specimen M1-2 versus 3D-FEM transverse bursting stress distribution

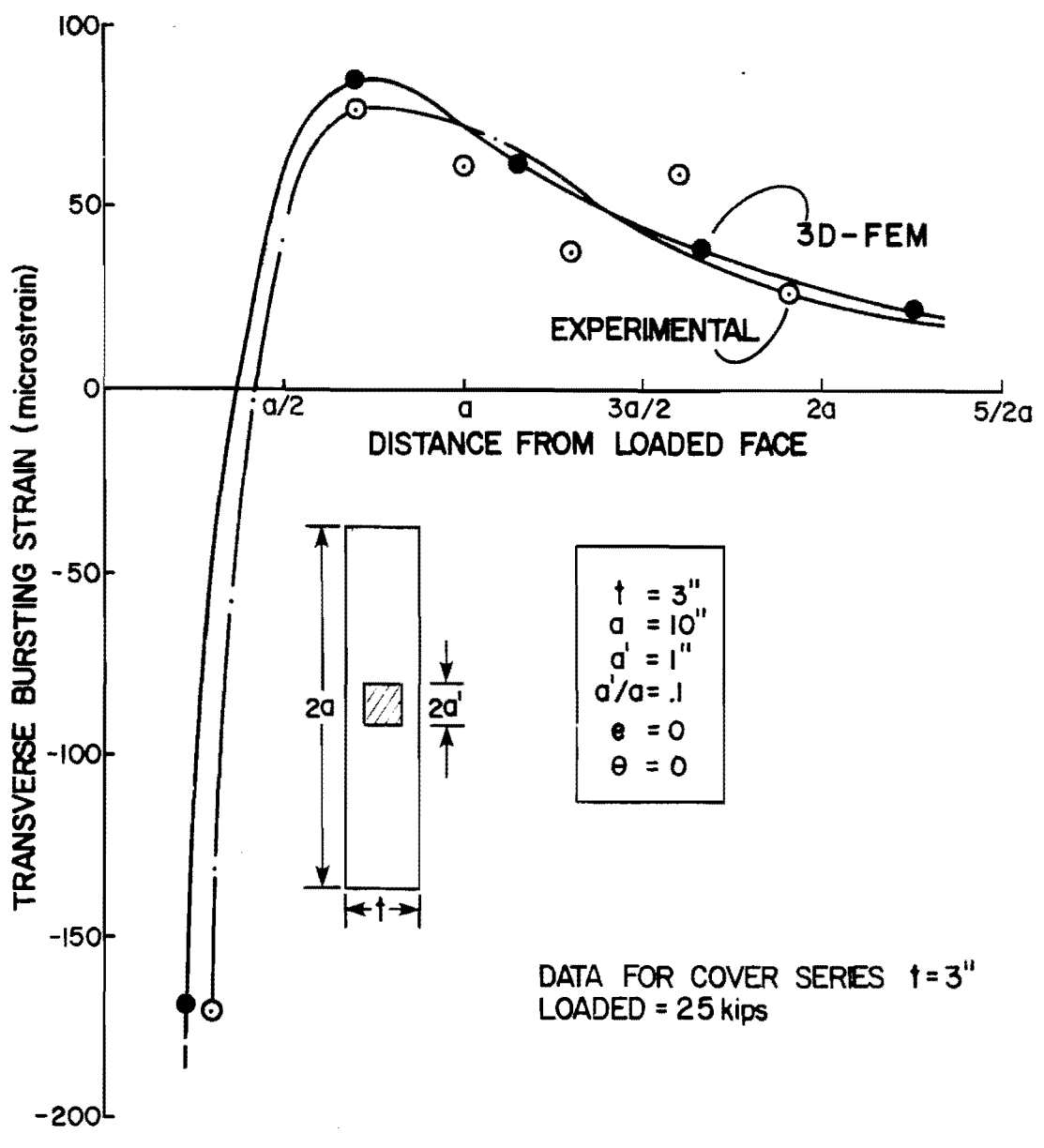


Fig. 3.22 Specimen M2-2 versus 3D-FEM transverse bursting stress distribution

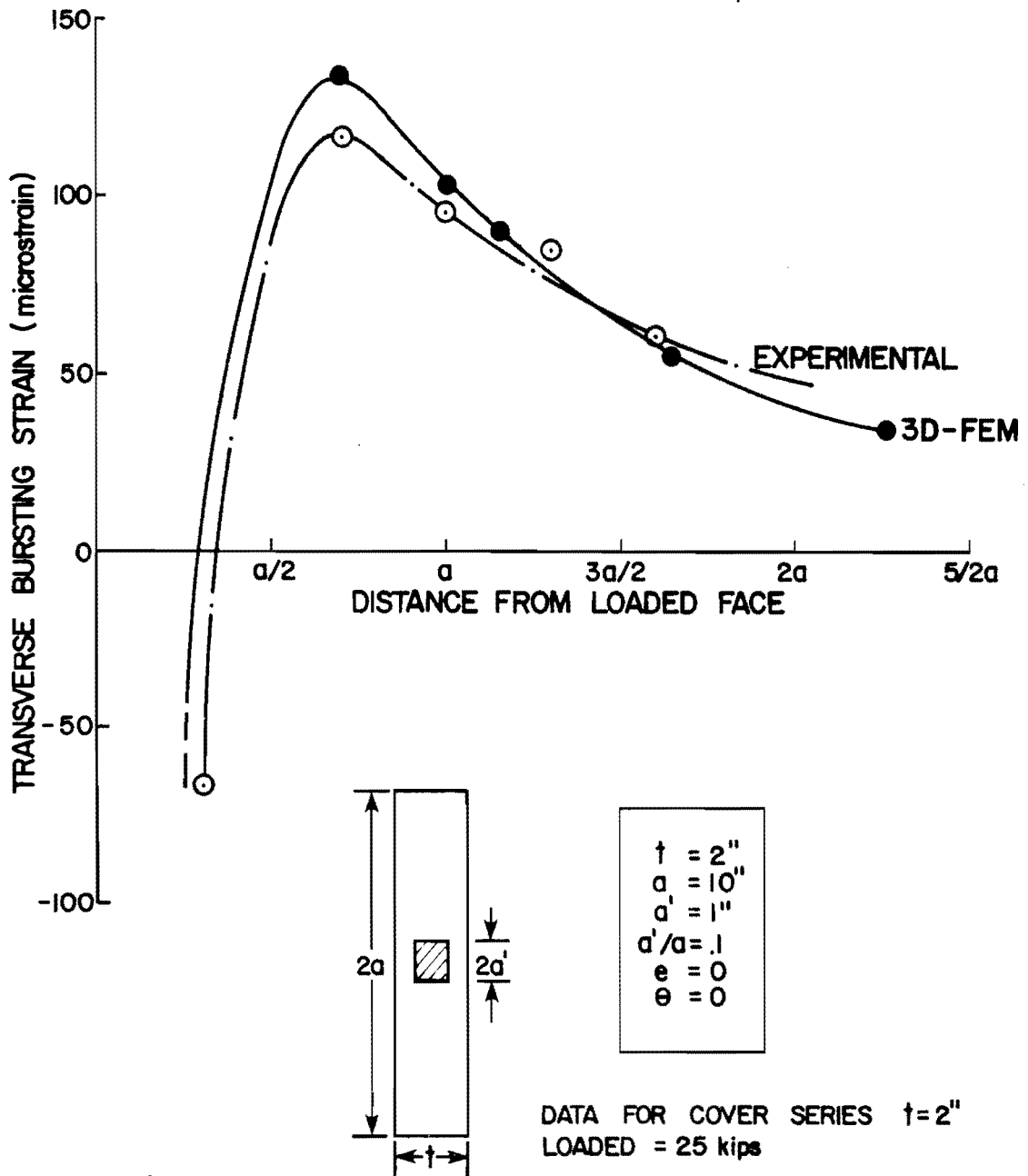
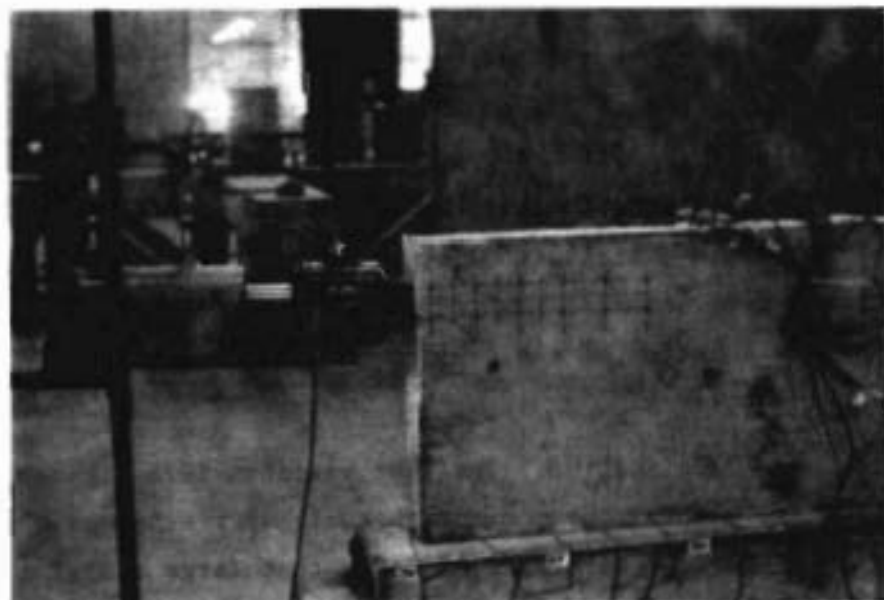


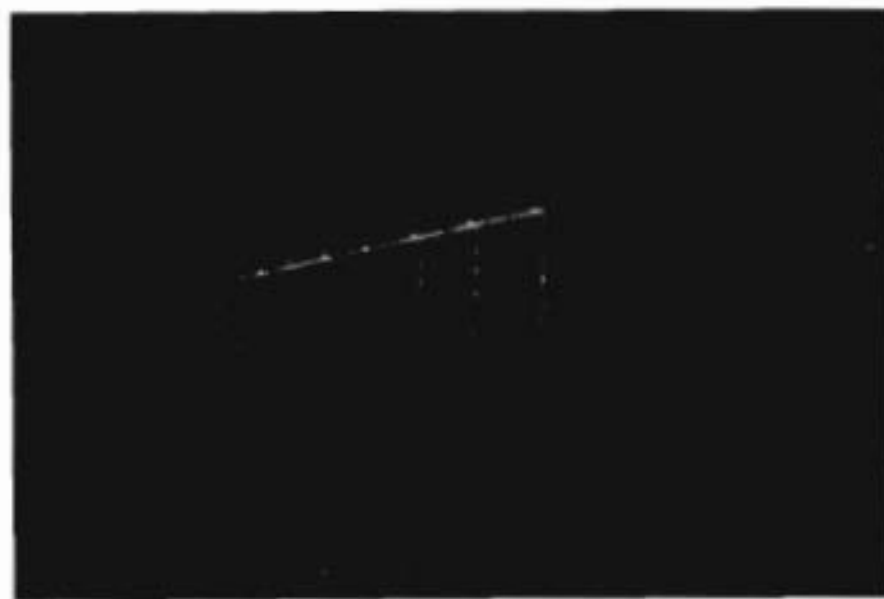
Fig. 3.23 Specimen M3-2 versus 3D-FEM transverse bursting stress distribution

3.3.3.2 Eccentricity. The eccentricity series used the same type of specimen as previously described except that the web width was set at 3 in. and the eccentricity varied from  $e = 0$  to  $e = 0.6a$  (6 in.). Both plate anchors and cone-type anchors were used in the physical tests. A typical specimen and related FEM one-half symmetric surface mesh are shown in Fig. 3.24. Figure 3.25 shows the bursting strain distribution for this specimen with both bearing-type and cone-type anchors. Maximum strains are close to those predicted but the location of the maximum strains is further along the axis than predicted.

3.3.3.3 Inclination. The last variable investigated in the calibration tests using the one-fourth scale specimens was the tendon inclination. Previous work had indicated that large radial and friction forces were generated along the tendon duct which could not be ignored in an analytical model. For the inclined tendon specimens shown in Fig. 3.26, the analytical model had to account for the anchorage blackout, the side cover, the proper geometry of the curved tendon path as well as the appropriate tendon duct and associated forces. The development of the finite element model is shown in Fig. 3.27. Specific detail of the anchorage zone is shown in Fig. 3.27c and d. For a problem of this complexity, even the mesh shown in Fig. 3.27 can be considered quite coarse. There was sufficient refinement along the tendon duct in the anchorage zone to give a reasonable approximation of the bursting strain in that region. One method of verifying this accuracy was comparison of output for interfacing nodes on two adjacent elements. If the mesh was sufficiently fine to model the actual stress field, these two values would be nearly identical. If, on the other hand, the gradient was quite sharp across a pair of elements where the mesh was too coarse, the values will differ markedly. This indicated that mesh refinement and possibly successive rezoning operations might be necessary to achieve



(a) Eccentric plate anchor with  $e = 0.6a$



(b) Interactive surface drawing of FEM mesh used to model specimen shown above

Fig. 3.24 Eccentric tendon model test and FEM mesh

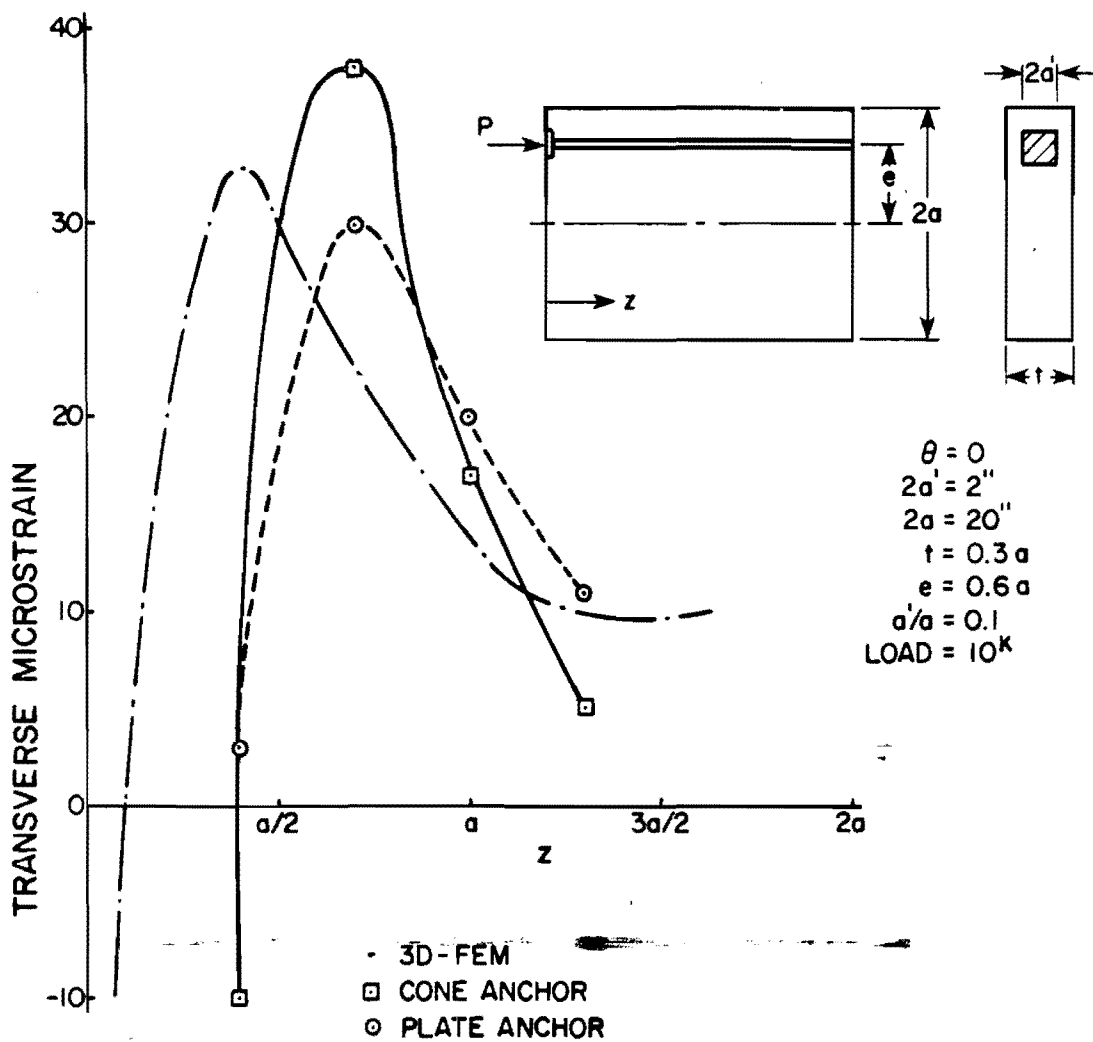
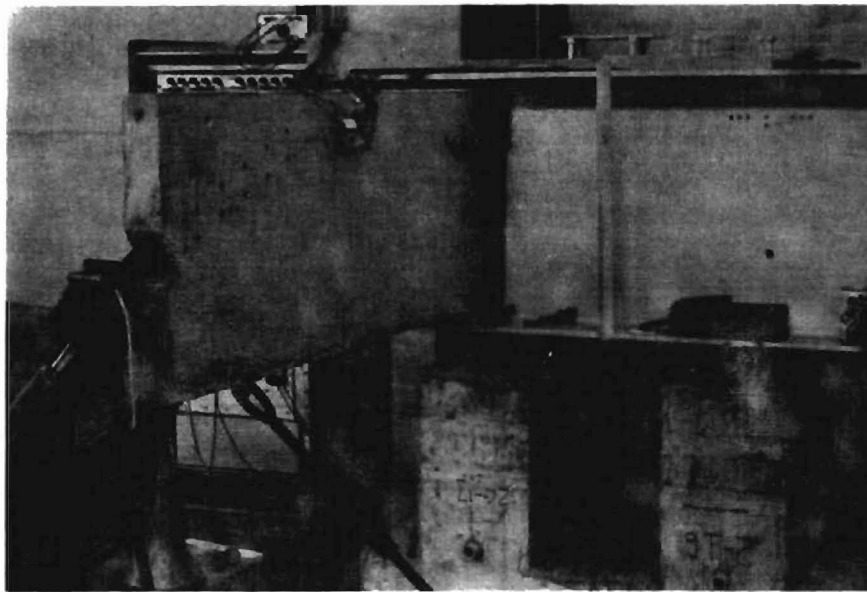
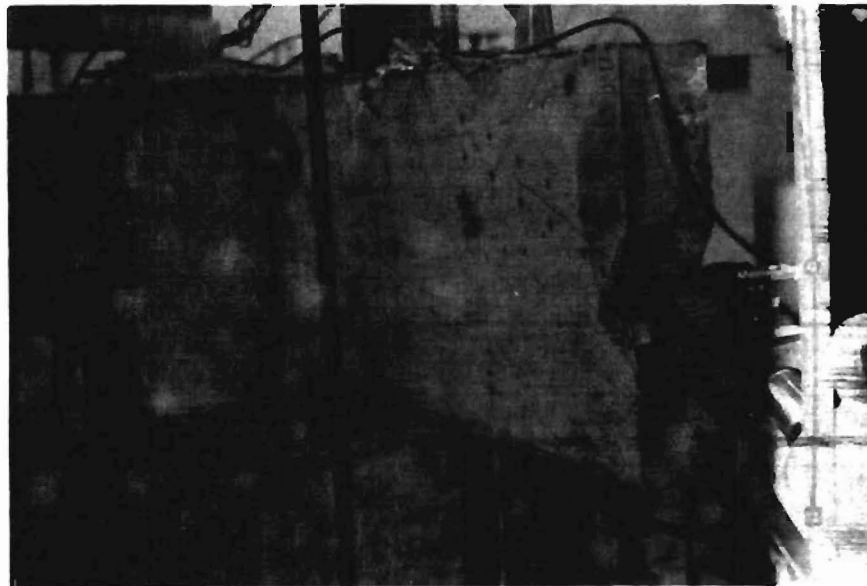


Fig. 3.25 Transverse strain along tendon path for eccentric tendon tests

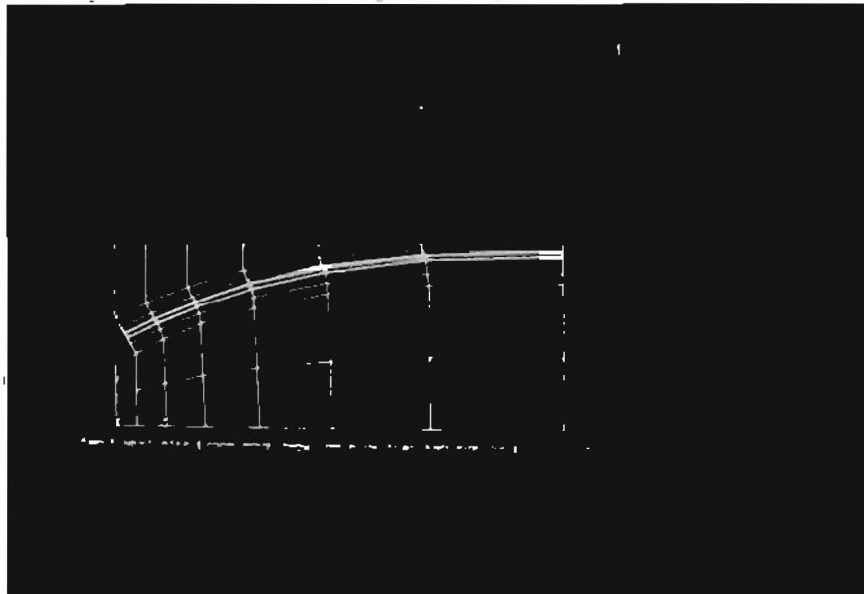


(a) Specimen M1-3, 30 degree inclined tendon

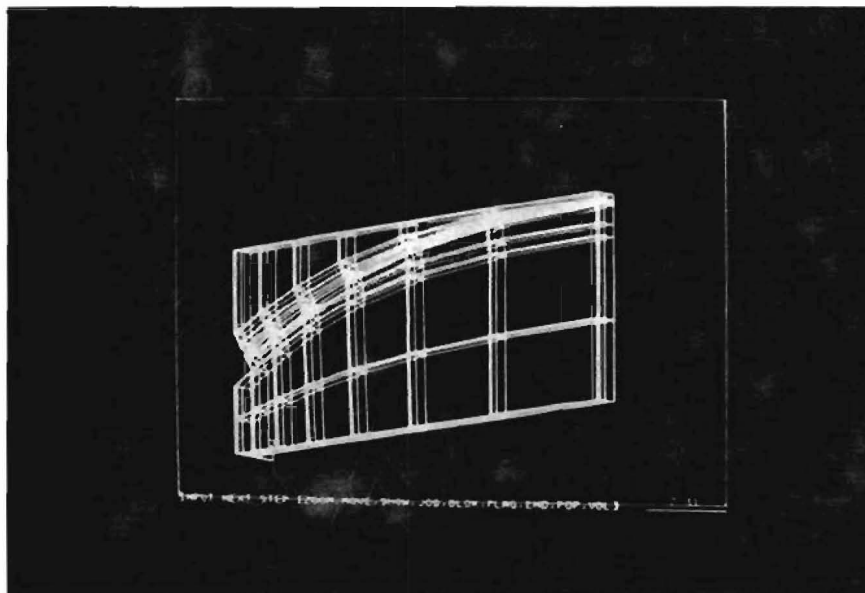


(b) Specimen M2-3, 30 degree inclined tendon

Fig. 3.26 Typical inclined tendon model tests

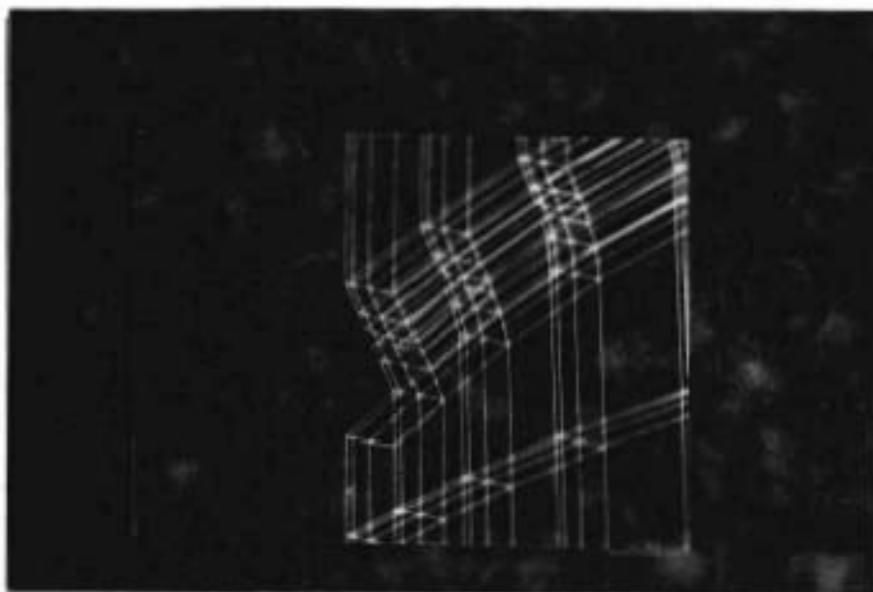


(a) Lateral view of mesh used for curved tendon models

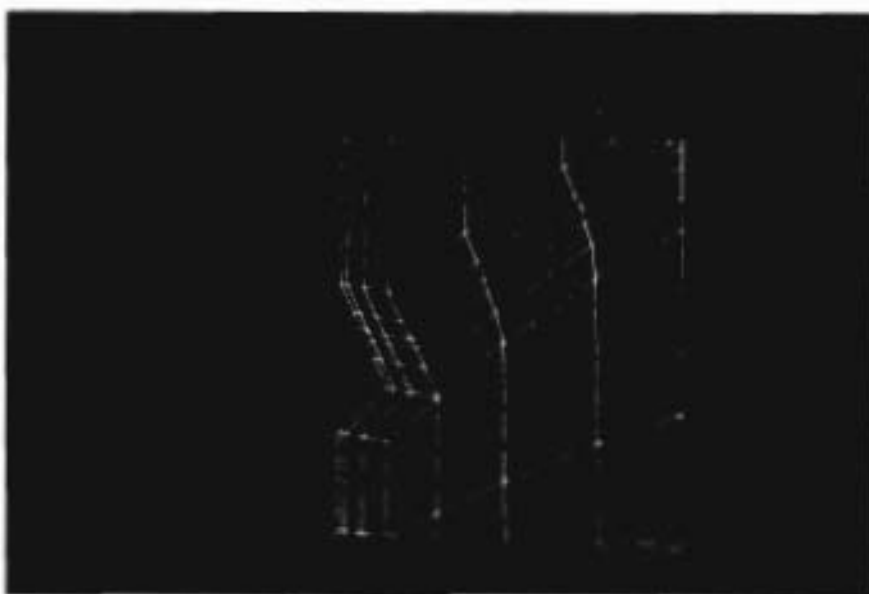


(b) Isometric view

Fig. 3.27 Interactive plot of mesh used for curved tendon models



(c) Close up of anchorage zone mesh



(d) Surface plot of mesh in vicinity of anchorage zone

Fig. 3.27 (continued)

the correct solution. The mesh shown in Fig. 3.27 was sufficiently fine to give a reasonable comparison with the experimental bursting strain distribution, as shown in Fig. 3.28. However, it was not sufficiently fine to give any reasonable estimate of the end face spalling distribution which has a very sharp gradient as one approaches the anchorage from below. During the first twenty one-fourth scale tests, no gages were placed to study the spalling distribution. To provide a solution for a sufficiently fine mesh along the tendon duct required the development of the program PUZGAP 3D. The mesh refinement capabilities made possible by partitioning the front can be readily seen in the 460 element mesh used to model the full-scale curved tendon specimen reported in Sec. 3.3.4.

3.3.4 Calibration: Full-Scale Tests. The final step in calibrating the program was to compare it against the results of the full-scale tests. There was a growing awareness of the importance of the spalling stresses in the behavior of the anchorage zone and each full-scale test specimen was progressively more heavily instrumented in that area. The mesh refinement achievable with PUZGAP permitted accurate solutions for these spalling stresses. Greater refinement was also possible along the tendon duct. This, however, complicated the problem of which node points to use for obtaining the bursting strain curve, as illustrated in Fig. 3.29. Ideal positioning of the gage is shown in Fig. 3.29a. However, the gages were fastened with somewhat flexible steel wire and the placement process was quite laborious because of the need to thread them between reinforcement and duct work. On occasion, the gages would shift slightly when the reinforcing cage was placed in the form and later during casting when vibrators inevitably hit the wires. The gages varied in location within the bounds shown in Fig. 3.29b. The variances were small--on the order of 0.5 to 0.75 in. maximum for the full-scale specimens. The choice of nodes 1, 2, 3, or 4 or the element centroid for comparison with the gage would thus be somewhat arbitrary as strain

### CURVED TENDON ANALYSIS

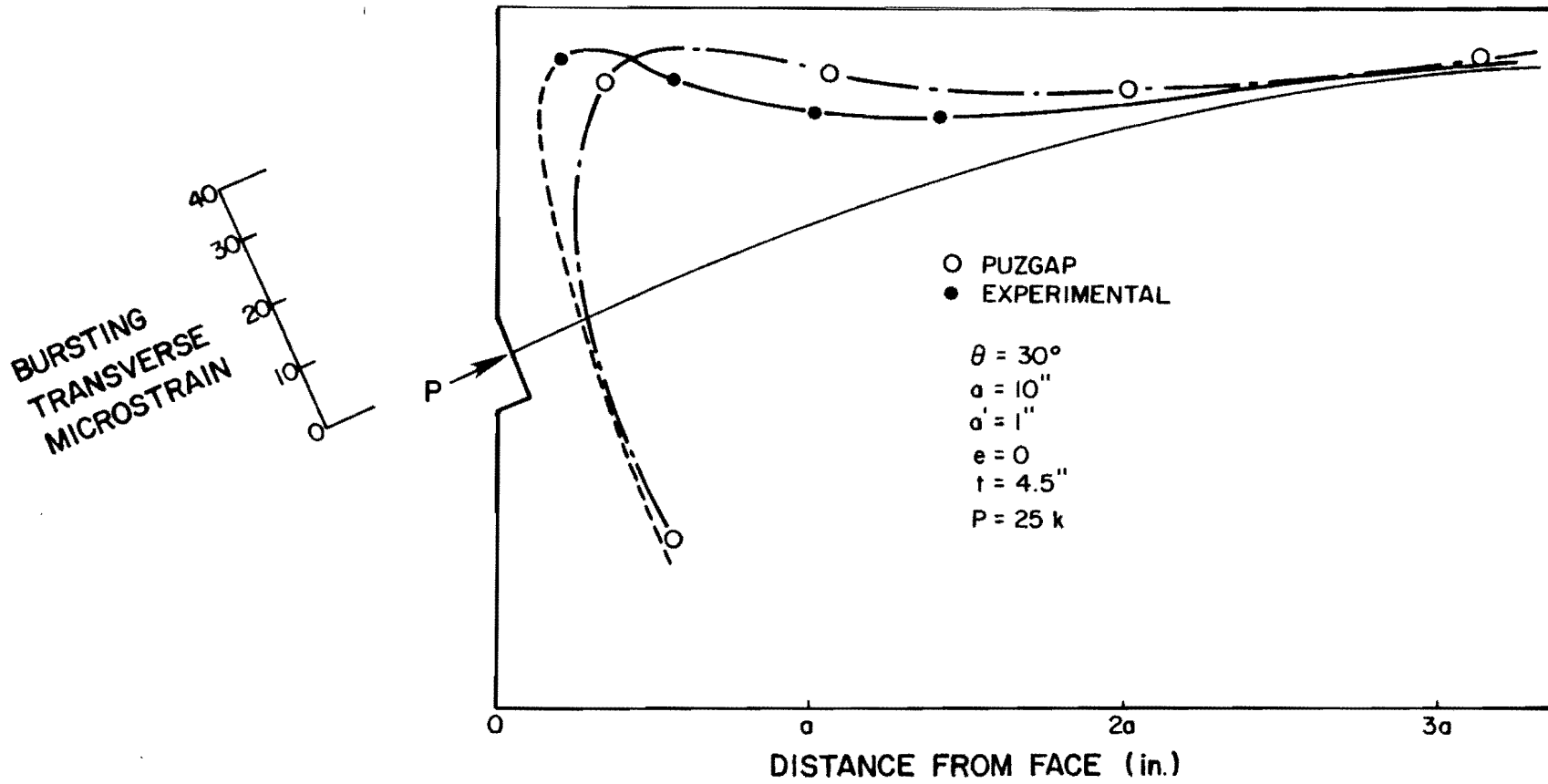
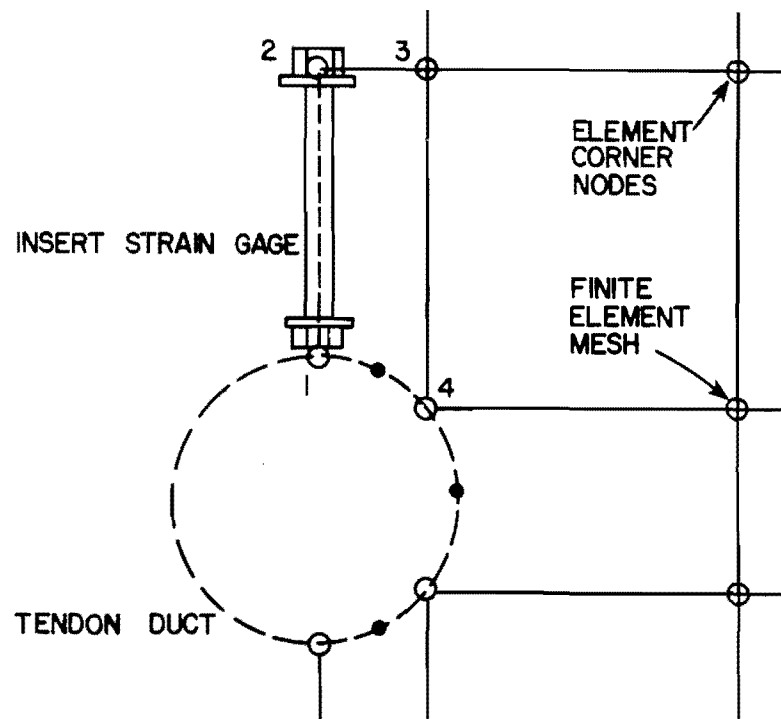


Fig. 3.28 Comparison of analytical and experimental bursting strain distribution for inclined tendon model tests

## (a) IDEAL GAGE PLACEMENT



## (b) ACTUAL POSITIONING AFTER CASTING, HANDLING

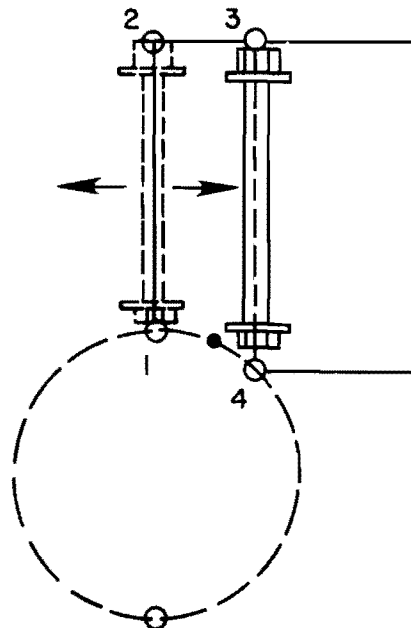
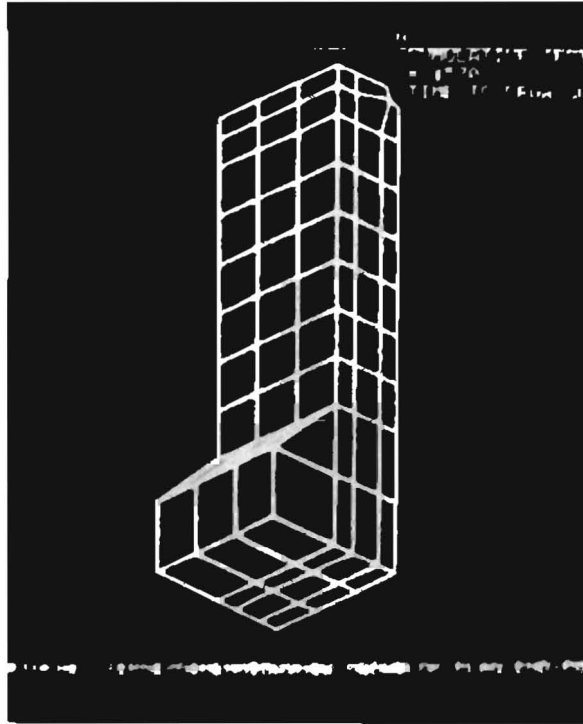


Fig. 3.29 Insert gage location for prototype specimens

data were available at all these points. The decision was made to use node 4 which consistently indicated the highest strain, thus giving a conservative solution.

Basically the full-scale specimens dealt with only two geometric variables: the size of the bearing plate and the tendon inclination. Various reinforcing schemes were tested using the 30 degree inclined tendon, so that most of the full-scale tests had this geometry. The two straight tendon tests, used to investigate bearing stress effects, were precisely replicated in the finite element model, as shown in Fig. 3.30. Note that computational advantage was taken of the four-fold symmetry. Figure 3.31 shows two of the typical curved tendon specimens. The development of the finite element model, which was assembled and debugged in stages, is illustrated in Fig. 3.32. Typical listings of input data for the straight tendon full-scale specimens and curved tendon specimens are given in Ref. 41. The nodal point definitions for the 30 degree tendon take about 150 statements in the PUZGAP version. An equivalent set of nodal definitions would have to be done on a point-by-point basis for codes such as SAP IV or NASTRAN. This would require well over 10,000 statements. The element definitions would require another 460.

For the curved tendon models shown in Fig. 3.32, it should be noted that the flanges were not included in the model. The reason for this was the extreme difficulty involved with developing a compatible mesh where the duct crosses into the flange. Before going to the "flangeless" model however, a number of runs were made to investigate the errors which would be incurred for such an assumption. As it turned out, for the situation where the anchorage is located close to the section centroid (i.e., low eccentricity) the results are virtually identical. This is not true for highly eccentric anchors in the vicinity of the flange. For these situations, if curved tendons are involved, the solution will have to be more rigorous. Fortunately, most segmental bridges that have

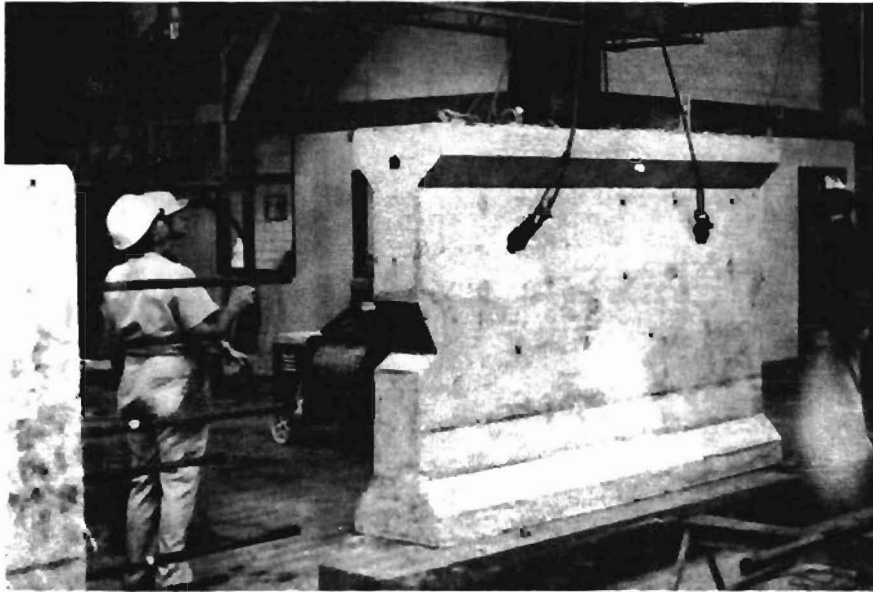


(a) FS1B 3D-FEM quarter symmetric model

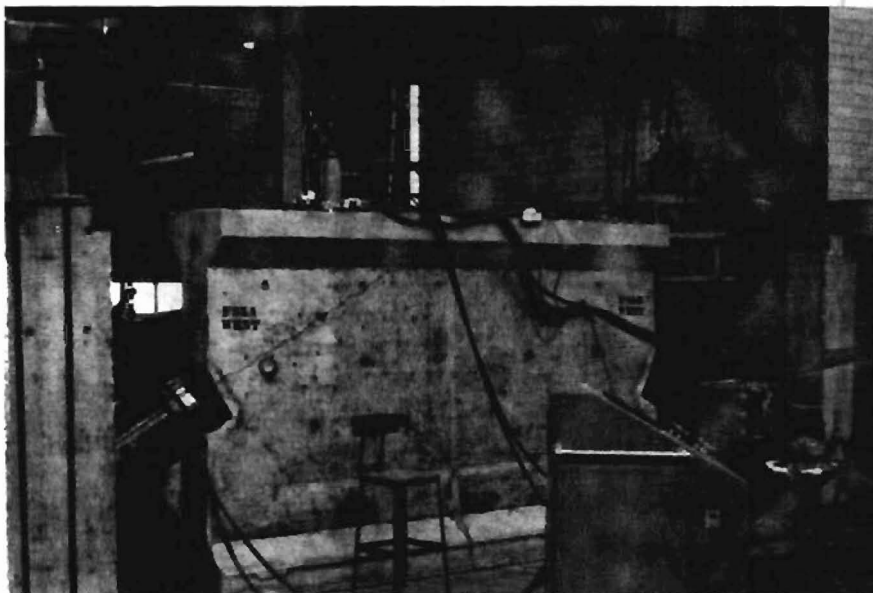


(b) FS1B physical test

Fig. 3.30 Typical full-scale specimens

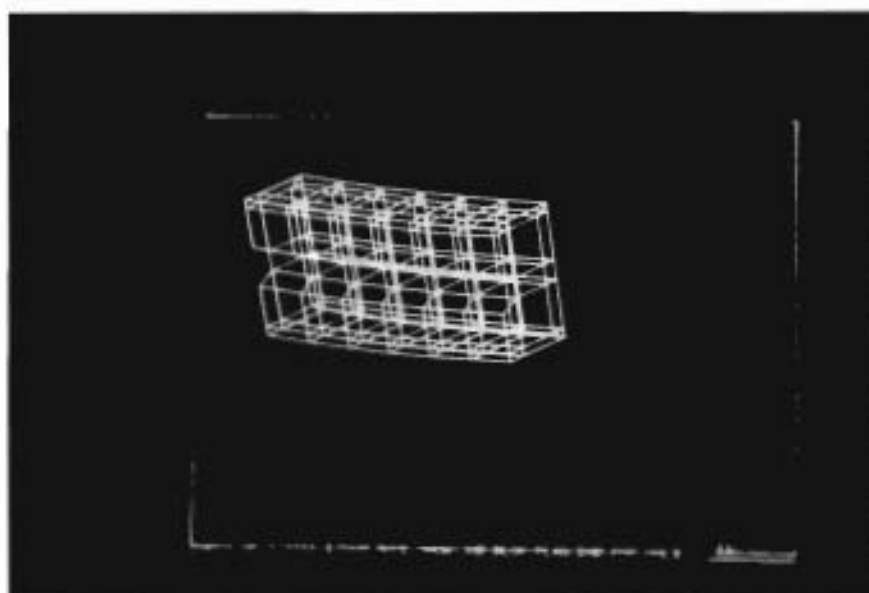


(a) Full-scale specimen FS2B and FS2A (30 and 15 degree inclined tendons)

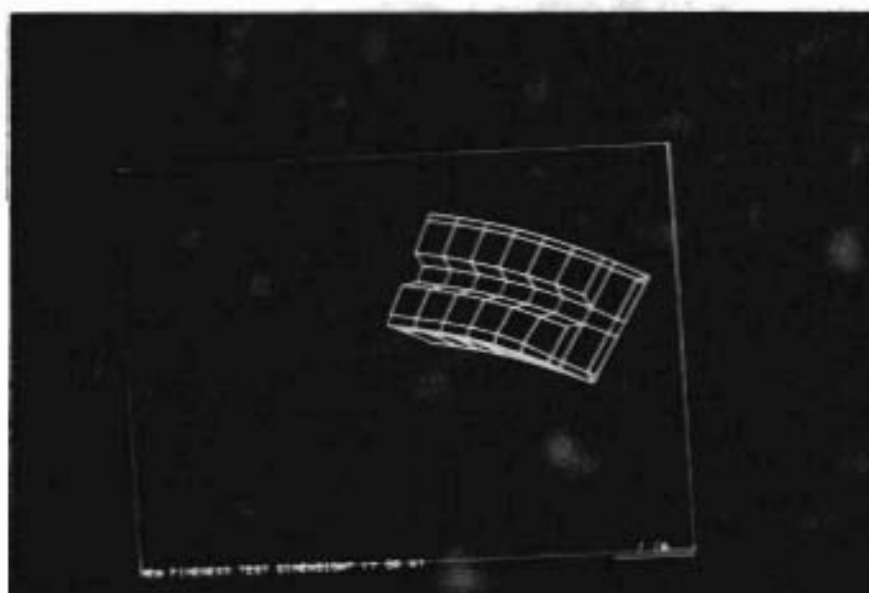


(b) FS5A 30 degree tendon with lateral prestress for maximum precompression of bursting stress

Fig. 3.31 Typical full-scale specimens

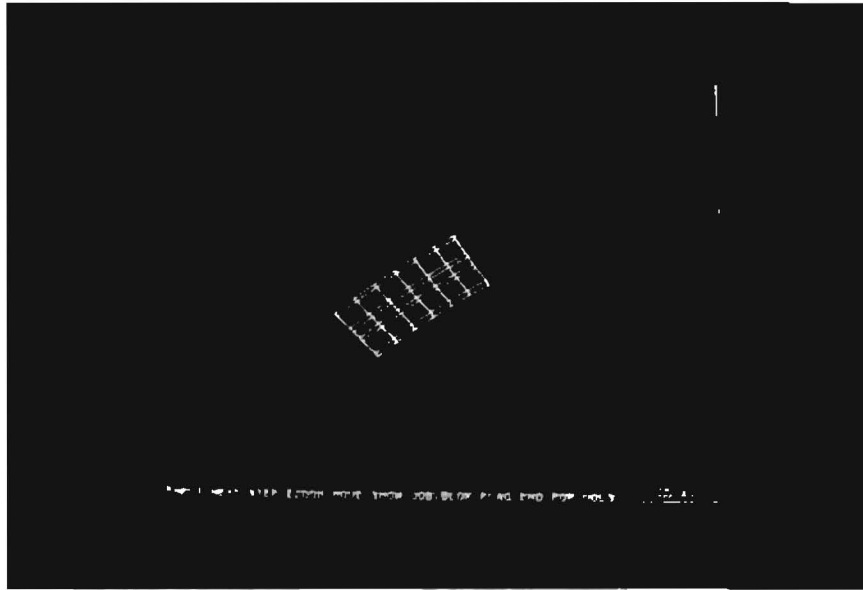


(a) Duct section near anchorage

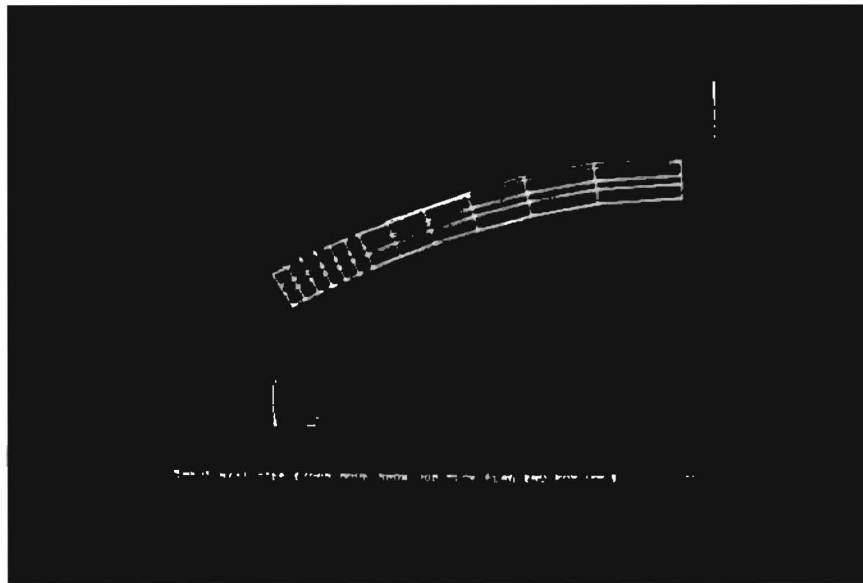


(b) Surface view showing duct near anchorage zone

Fig. 3.32 Curved tendon mesh for full-scale specimens

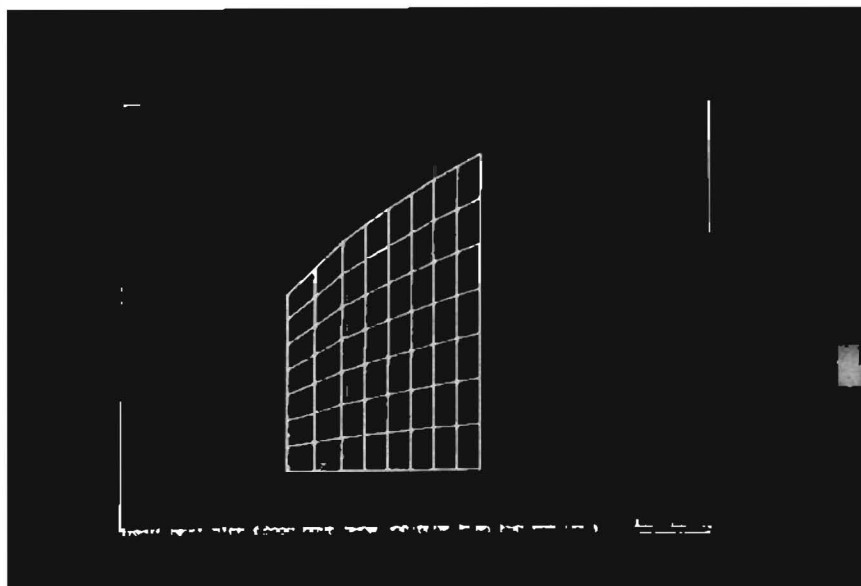


(c) Lateral view of duct mesh in vicinity of the anchorage zone

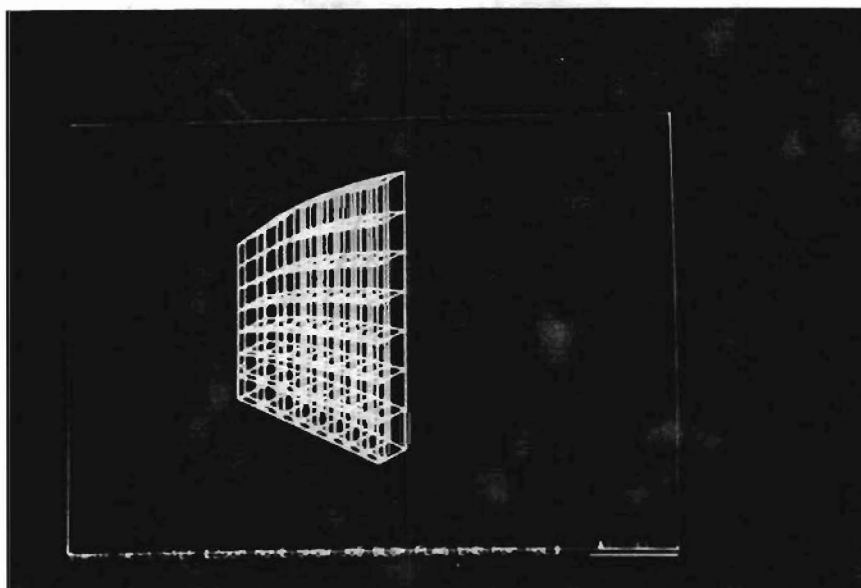


(d) Full lateral view of tendon duct mesh. Note geometry error at top of panels 7 and 8 where midside interpolation was mistyped in input

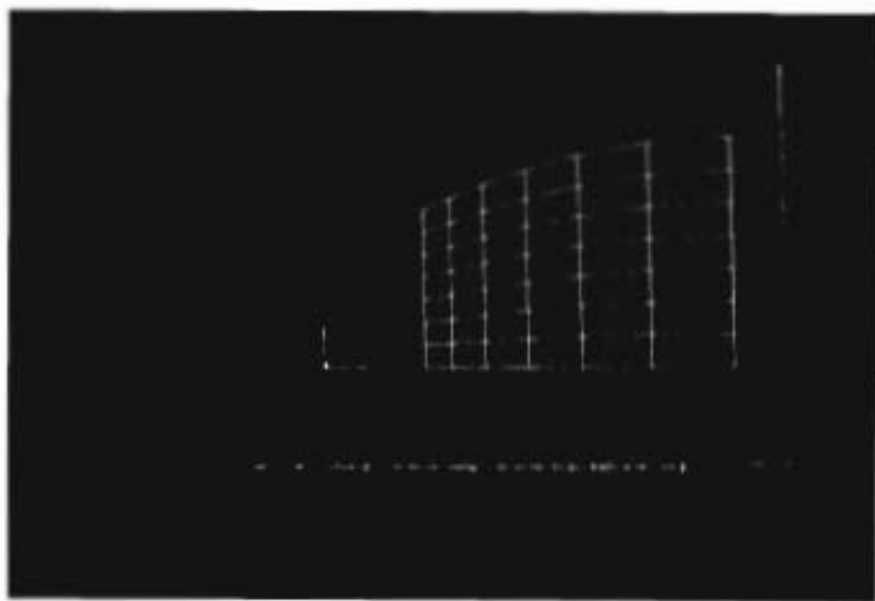
Fig. 3.32 (continued)



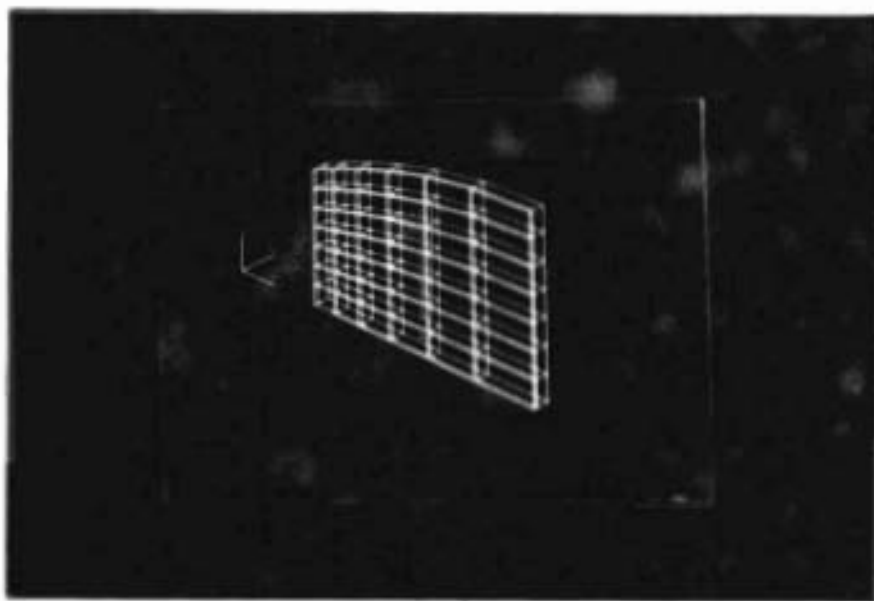
(e) Bottom mesh near anchorage zone--lateral view.  
Note mesh refinement along end face (left) compared  
to Fig. 3.27a



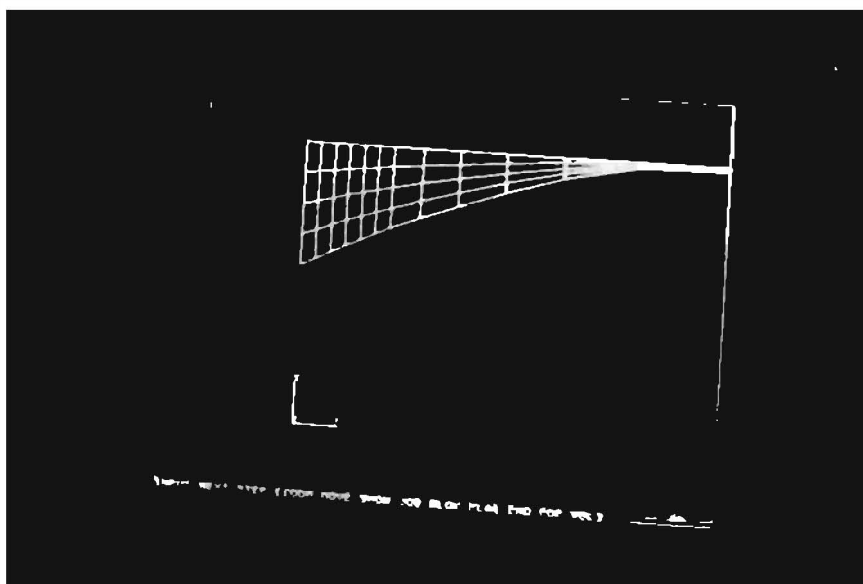
(f) Bottom mesh near anchorage zone--isometric view



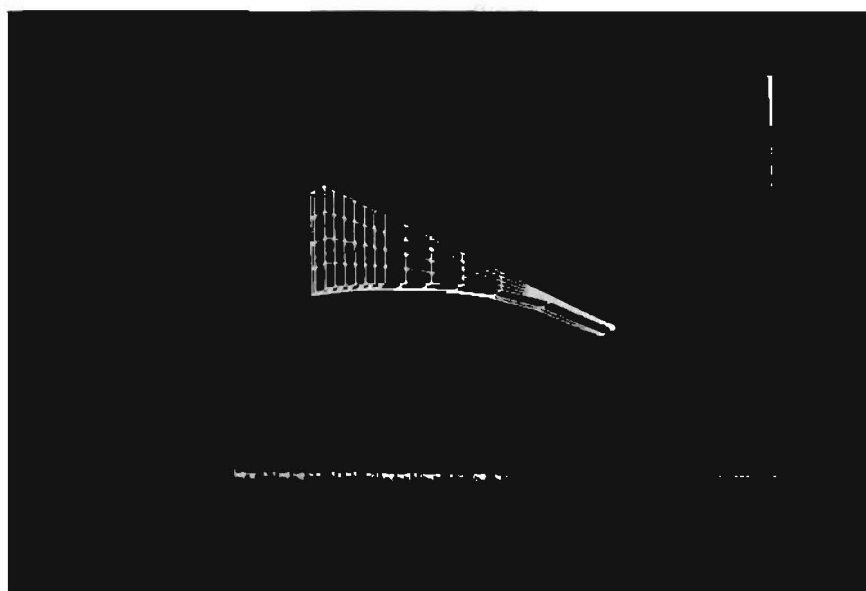
(g) Graded bottom mesh, part two--lateral view



(h) Graded bottom mesh, part two--isometric view



(i) Top mesh--lateral view



(j) Top mesh--surface plot

Fig. 3.32 (continued)

anchorages located in the flange have nearly horizontal profiles, simplifying the mesh generation.

3.3.5 Results. Figures 3.33 through 3.37 give comparisons between experimental gage data and the 3D-FEM solution for the bursting strain distribution. Given the anticipated scatter associated with strain gage data, the comparison seems to be qualitatively reasonable, the program being neither consistently low nor too high. For most cases, the three-dimensional program appears to yield fairly acceptable results for the bursting and spalling distributions measured experimentally.

Quantitatively, the term good correlation was assumed when the standard deviation of the predicted strain divided by the observed strain was less than 25 percent. Excellent correlation was assumed when the standard deviation was less than 10 percent. Figure 3.38 is a statistical summary showing typical correlations for five randomly selected specimens comparing experimental and FEM predicted strains for both bursting and spalling distributions. Most fall in the "good correlation" range. The worst case shown (Fig. 3.33) is greatly influenced by one strain gage which strongly disagrees with the theoretical predictions.

Careful attention should be paid to the strain distribution along the end face--the spalling strain. Due to the loss of several of the gages, the experimental data for specimens FS1A and FS1B were insufficient for comparison. However, Figs. 3.39 through 3.42 illustrate spalling distributions for specimens FS2B, FS2A, FS4A, and FS5A, each of which was more heavily instrumented. FS5A had dual backup gages and thus yielded the highest number of "surviving" gages after fabrication and casting. Consequently, it was not surprising that this test yielded the best comparison with the PUZGAP program (see Fig. 3.41). In viewing these particular plots the predominant feature is the "spike," predicted from the analytical study, which

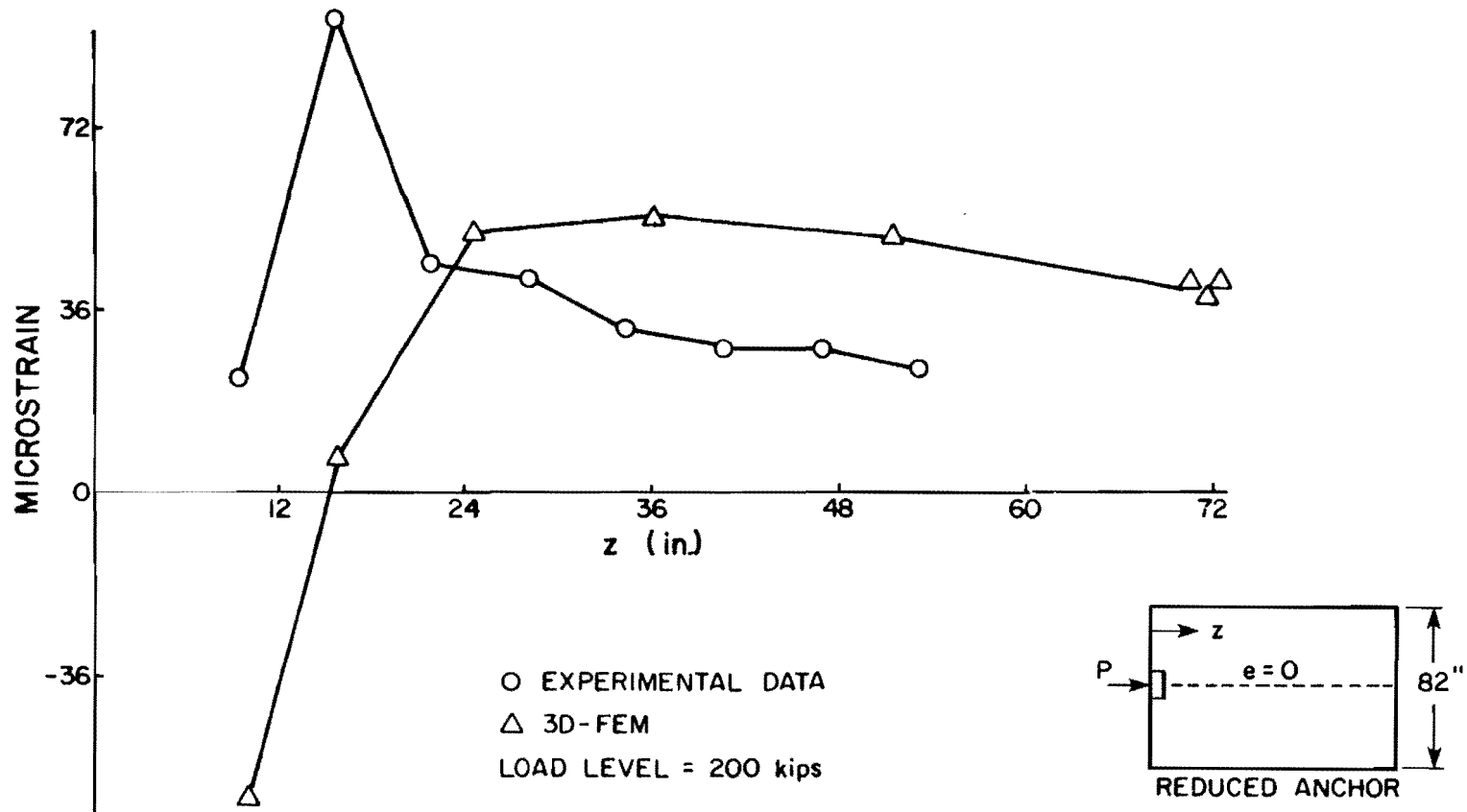


Fig. 3.33 FS1A 3D-FEM vs experimental bursting strain distribution

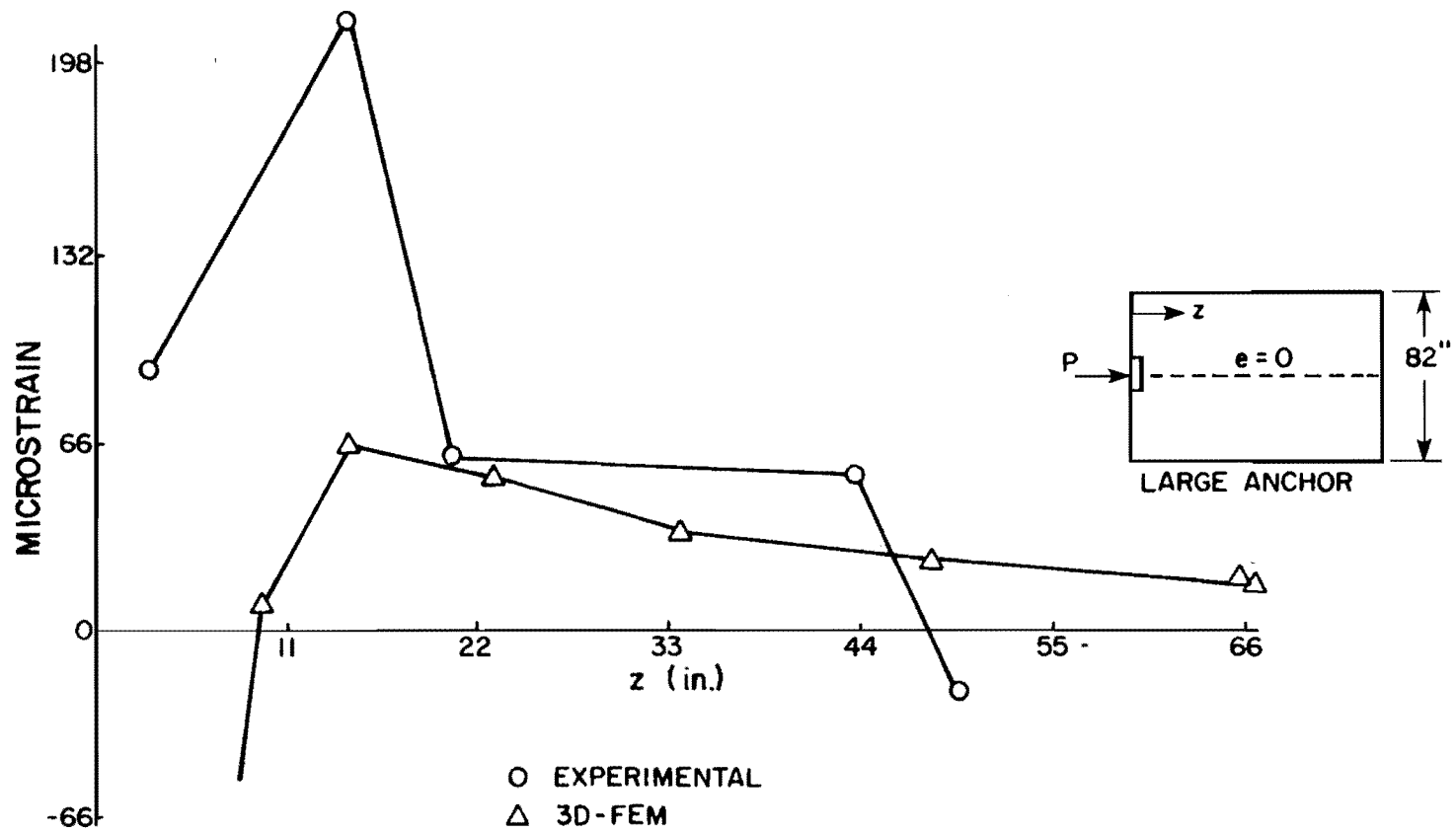


Fig. 3.34 FS1B 3D-FEM vs experimental bursting strain distribution

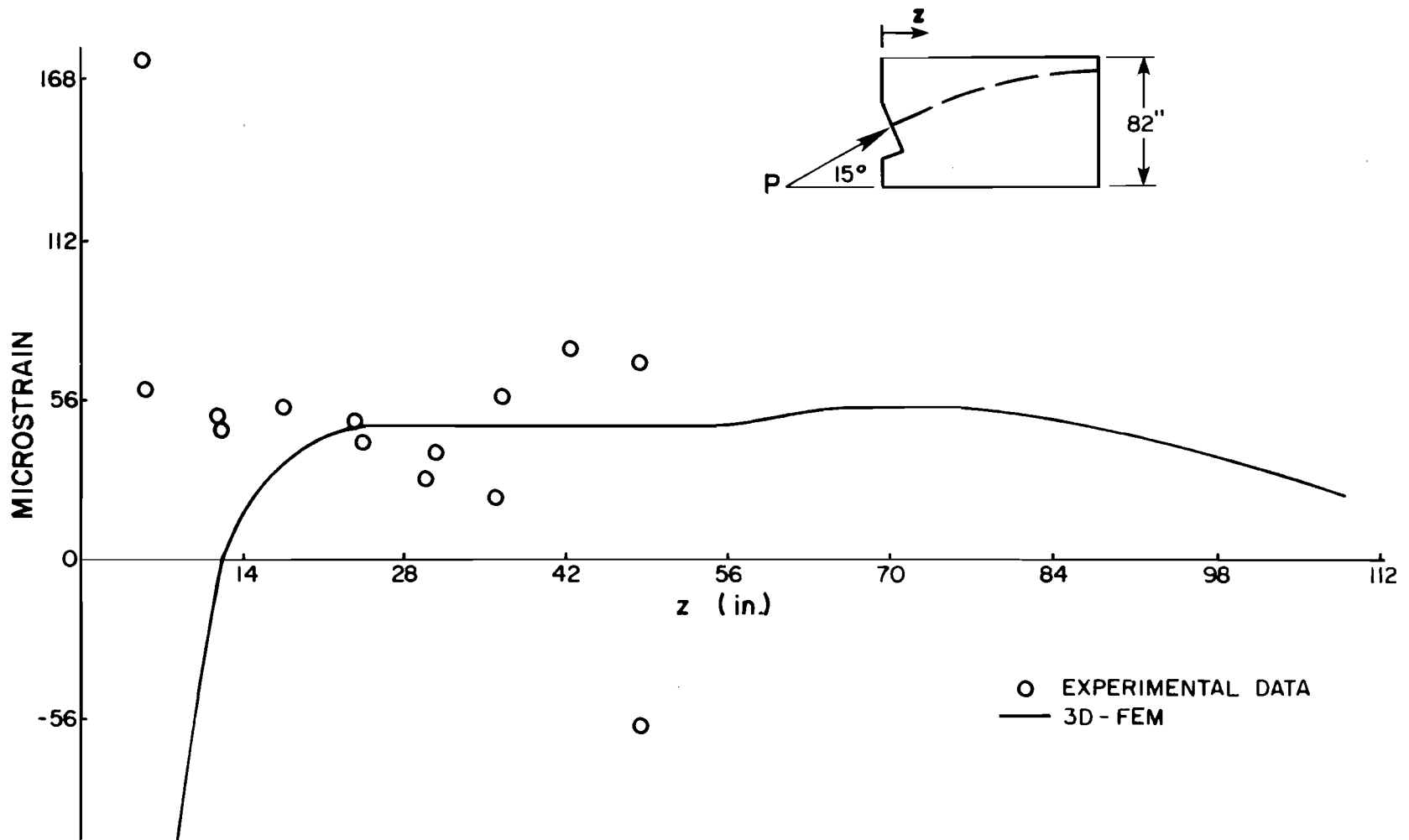


Fig. 3.35 FS2A 3D-FEM vs experimental bursting strain distribution

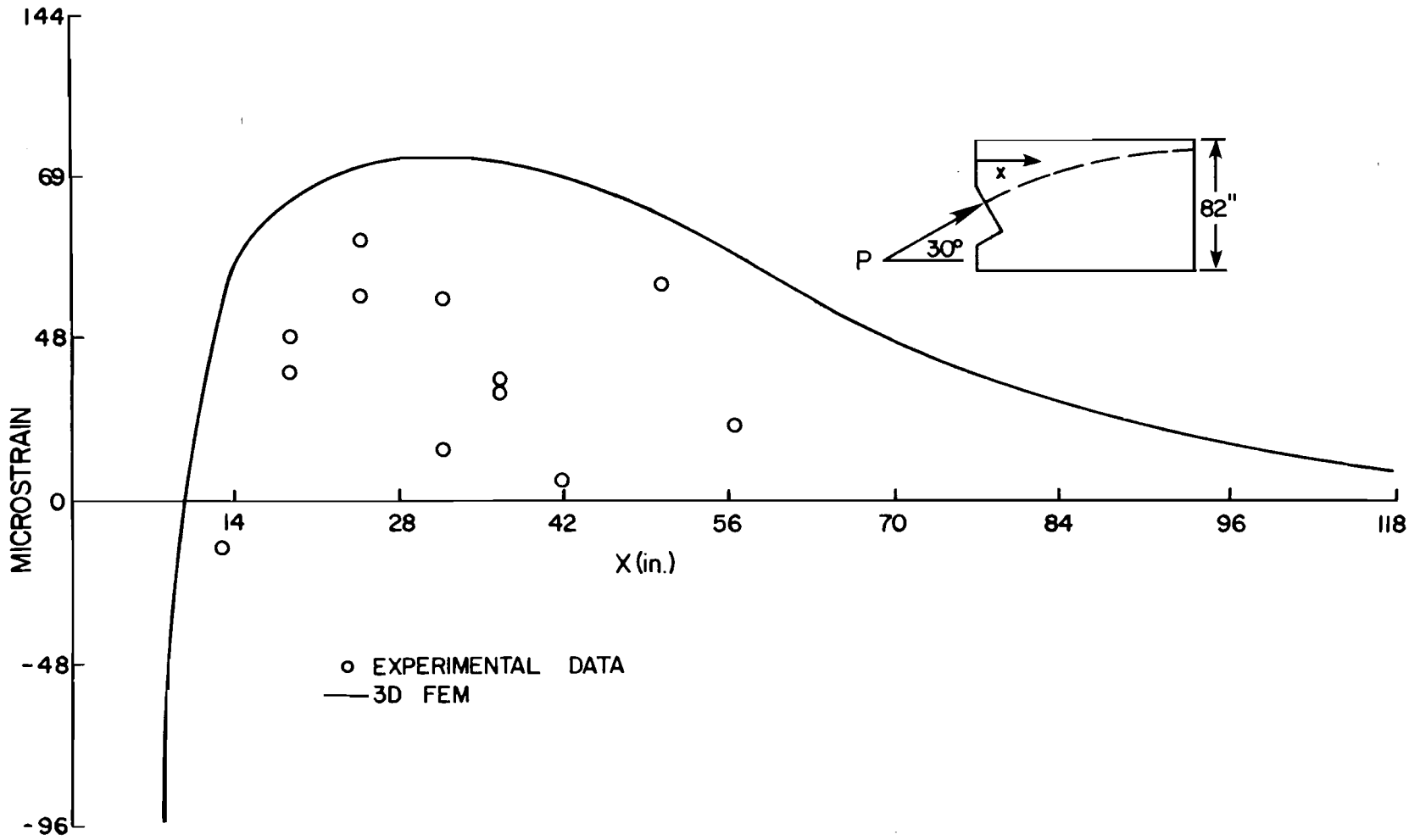


Fig. 3.36 FS2B 3D-FEM vs experimental bursting strain distribution

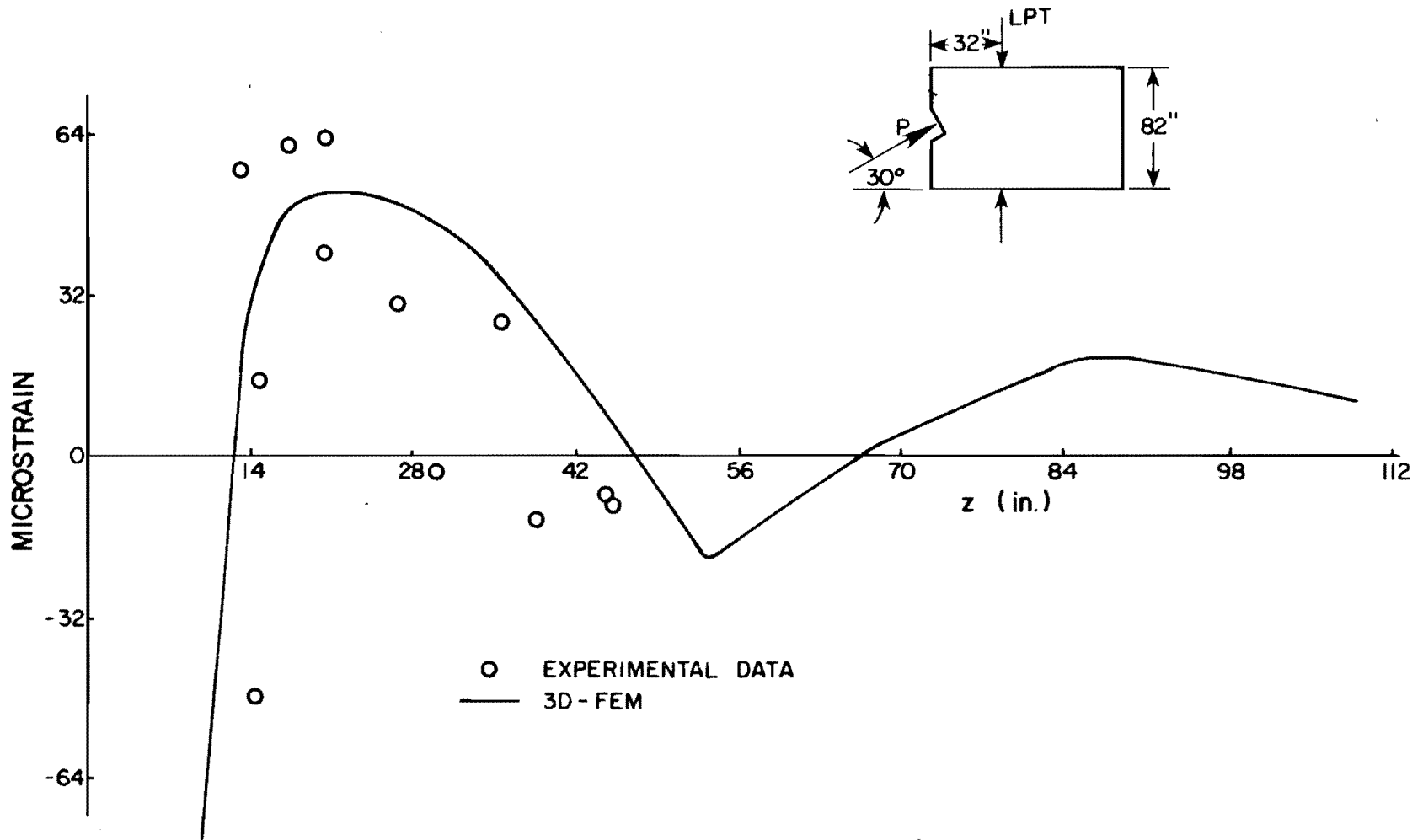


Fig. 3.37 FS5A 3D-FEM vs experimental bursting strain distribution

	<u>Gage No.</u>	$\frac{\epsilon_p}{\epsilon_a}$	<u>x</u>	
Fig. 3.23	1	1.14	.7a	
M3-2 Data	2	1.06	a	$\bar{X} = 1.03$
	3	.92	1.3a	S.D. = .093
	4	1.0	1.6a	
Fig. 3.22	1	1.10	.7a	
M2-2 Data	2	1.12	a	$\bar{X} = 1.038$
	3	1.13	1.3a	S.D. = .23
	4	.66	1.6a	
	5	1.0	1.9a	
Fig. 3.28	1	.825	.7a	
M1-3 Data	2	1.14	a	$\bar{X} = 1.12$
	3	1.23	1.3a	S.D. = .20
	4	1.3	1.6a	
Fig. 3.33	1	.11	.36a	
FS1A Data	2	.89	.51a	
	3	1.11	.66a	$\bar{X} = 1.12$
	4	1.25	.80a	S.D. = .52
	5	1.42	.95a	
	6	1.28	1.1a	
	7	1.8	1.24a	
Fig. 3.35	1	1.0	.31a	
FS5A Data	2	1.0	.34a	
	3	.6	.34a	
	4	.87	.39a	$\bar{X} = 1.03$
	5	.89	.44a	S.D. = .26
	6	1.28	.44a	
	7	1.56	.61a	
	8	1.06	.88a	

Notes:  $\epsilon_p$  = FEM predicted strain       $\epsilon_a$  = Actual gage strain

$\bar{X}$  = Mean value of  $\frac{\epsilon_p}{\epsilon_a}$       S.D. = Standard deviation

Fig. 3.38 Statistical comparison of FEM predicted strain vs experimental gage data for various tests

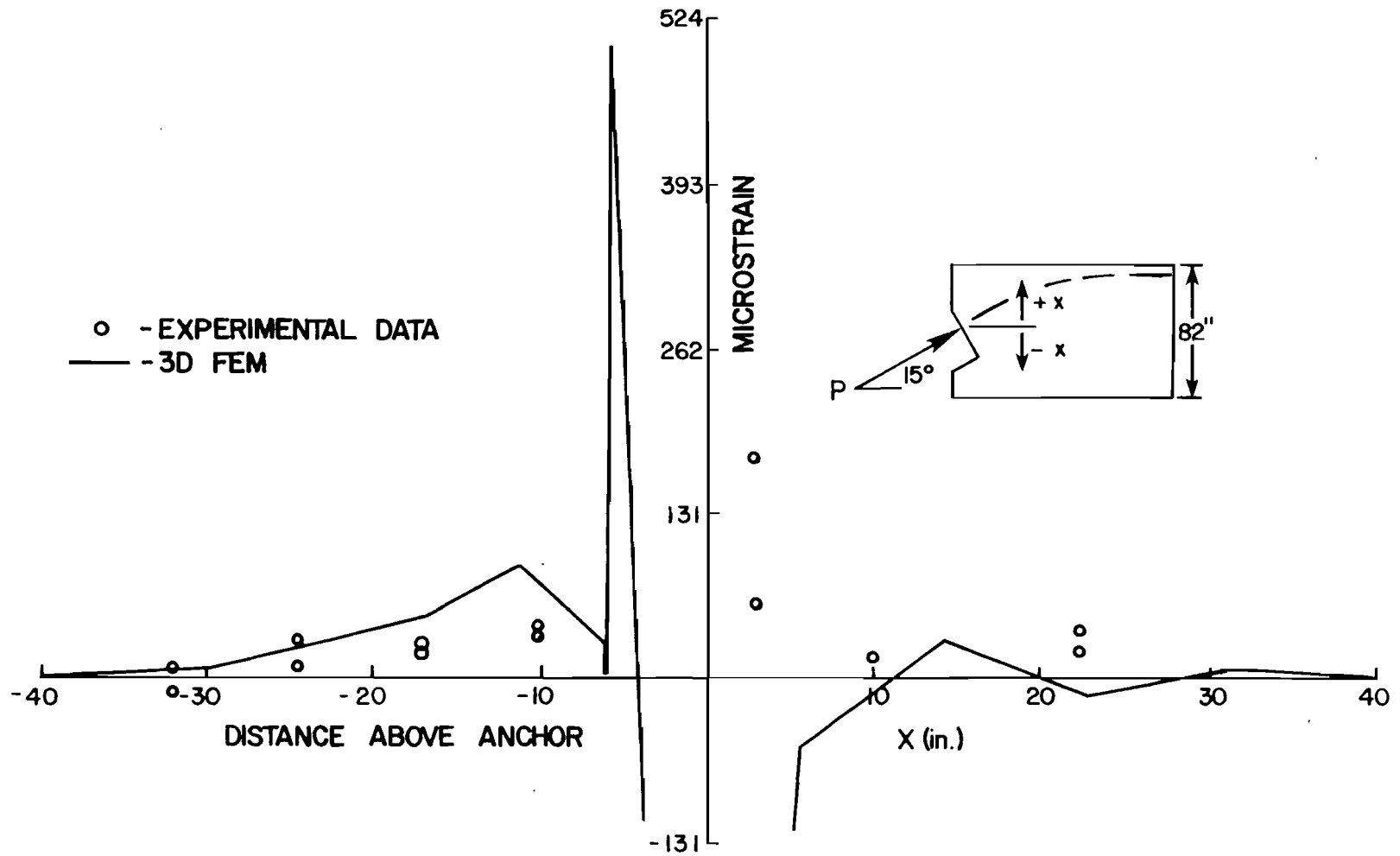


Fig. 3.39 FS2A spalling strain distribution: 3D-FEM vs experimental

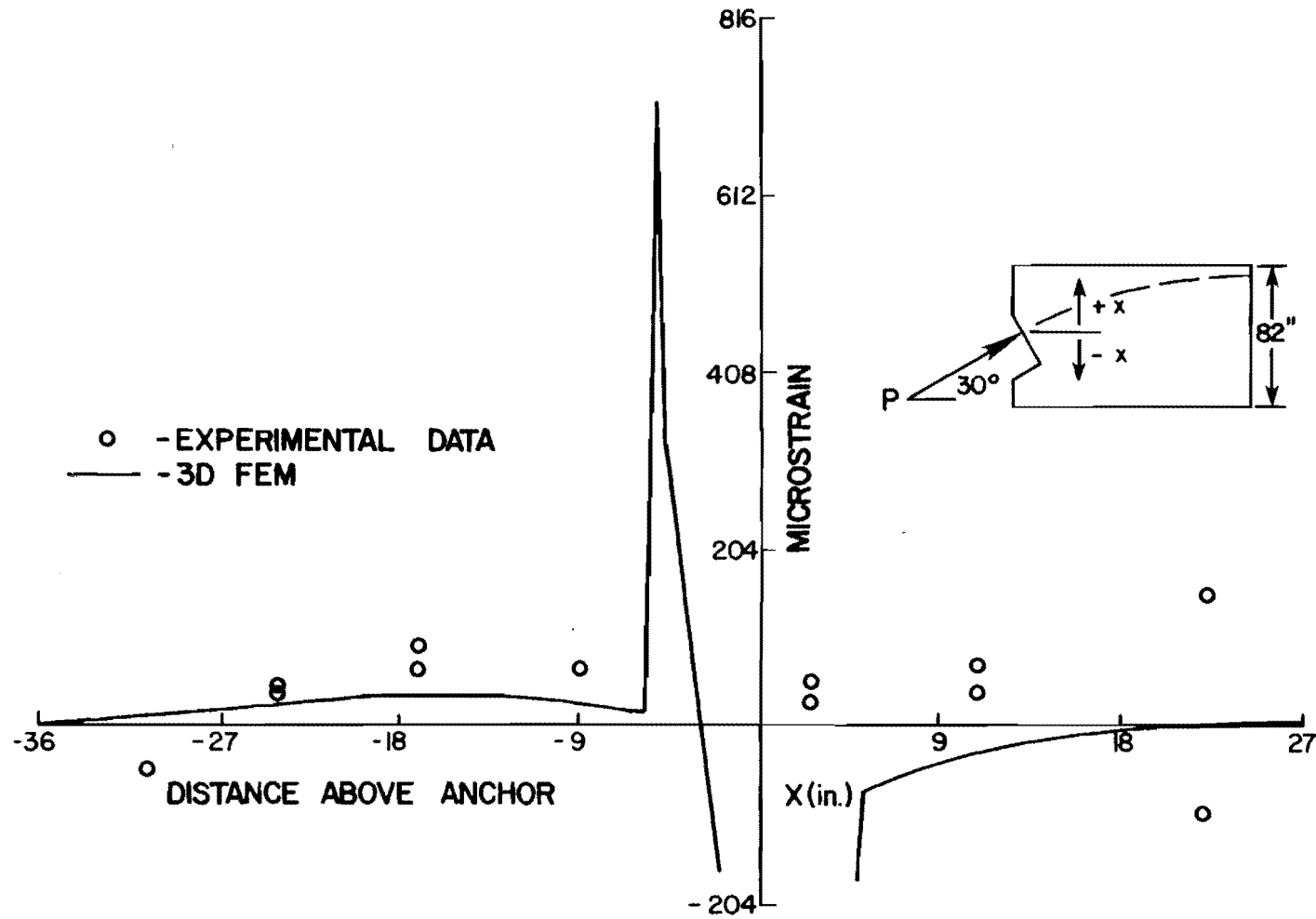


Fig. 3.40 FS2B spalling strain distribution: 3D-FEM vs experimental

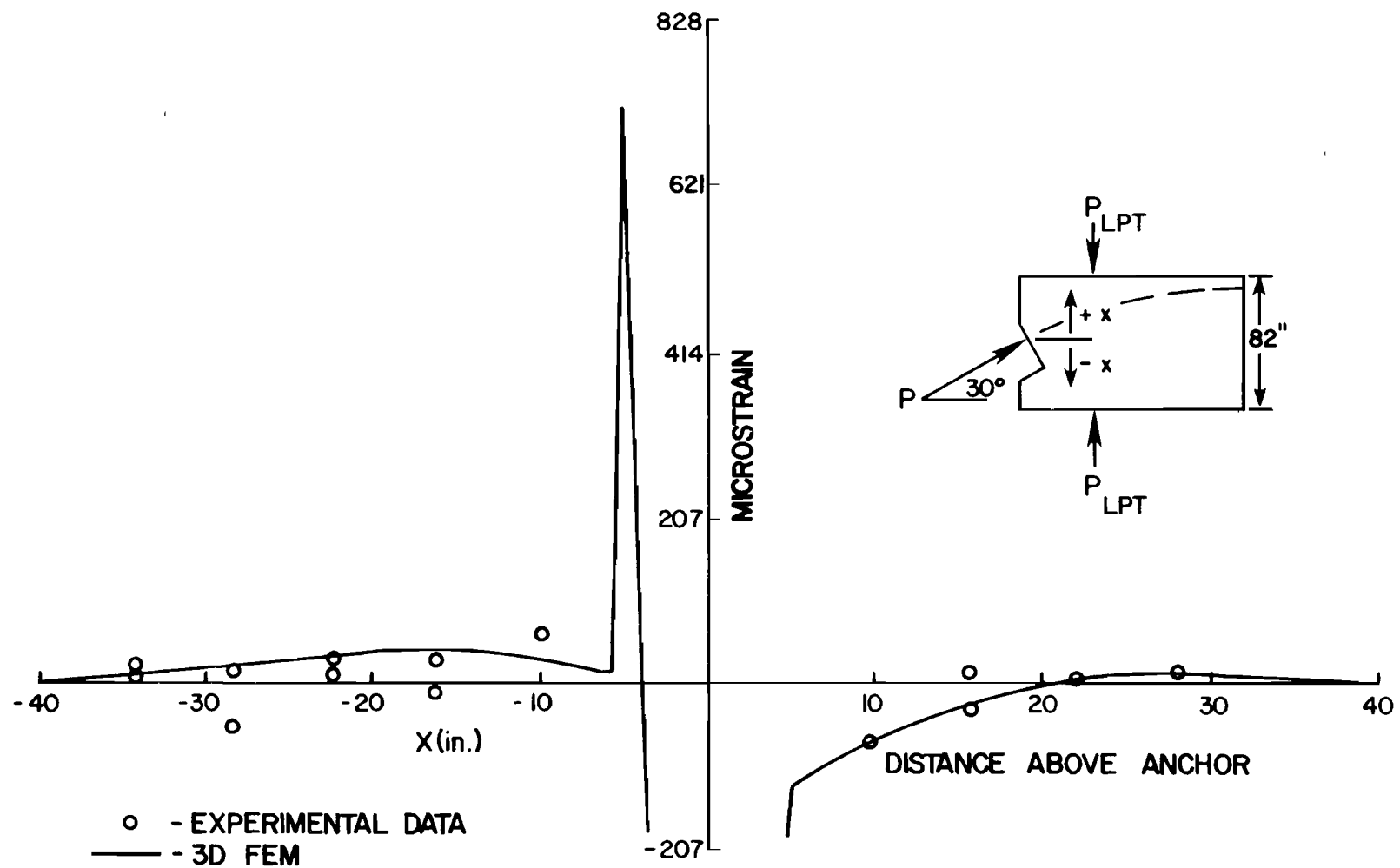


Fig. 3.41 FS5A spalling strain distribution: 3D-FEM vs experimental

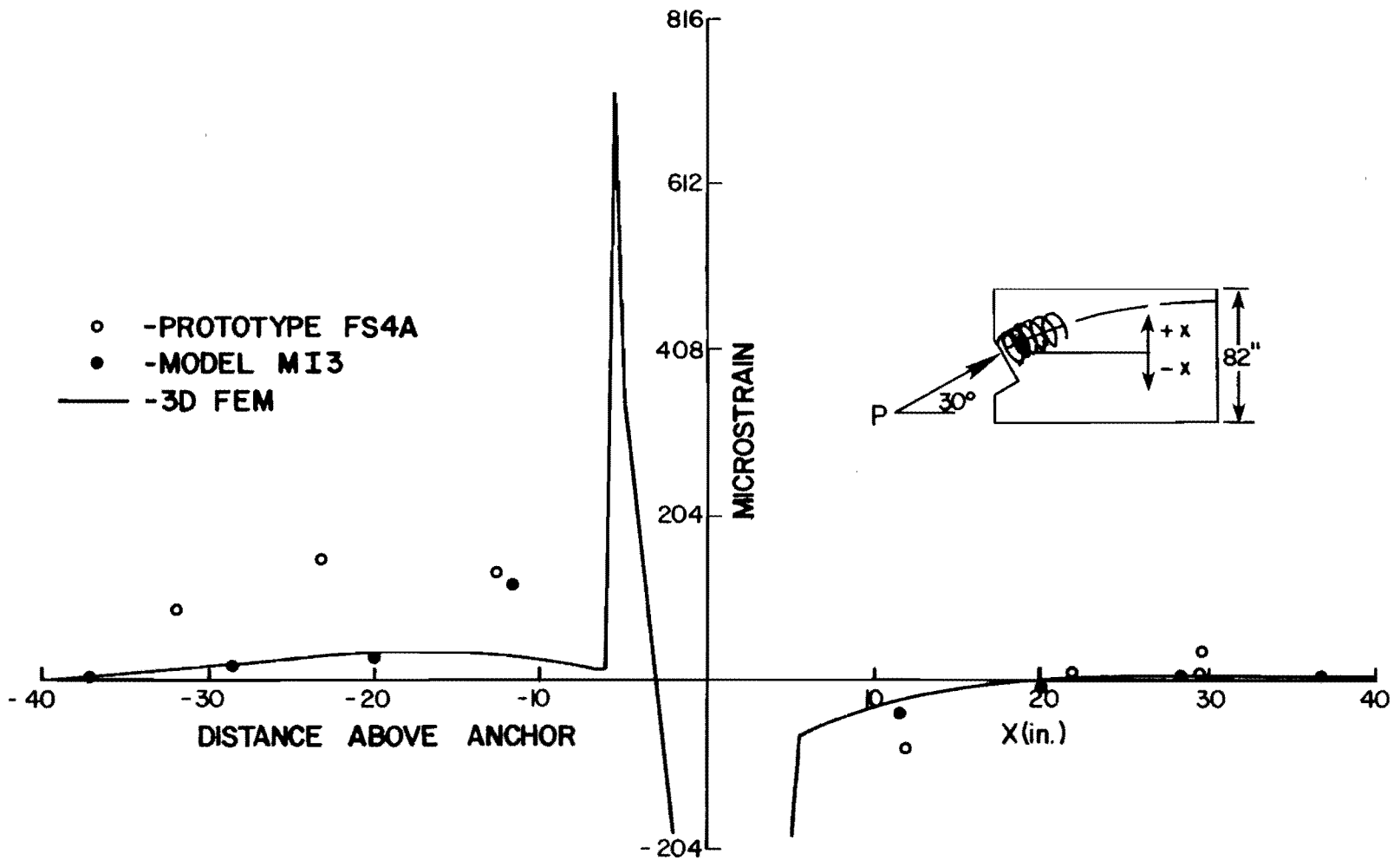


Fig. 3.42 FS4A spalling strain distribution: 3D-FEM vs experimental

occurs near the anchor plate. In modeling the inclined tendon specimens a right angle block out was provided to achieve the desired angle, as was done in the physical specimen. The introduction of this idealized right angle, or reentrant corner, gives rise to a stress concentration (approximately = 6) in the vicinity of the corner. As will be shown in a later report, the calculated spalling tensile strain near the anchor plate edge appears to be a critical indicator of the load at which the tendon path crack forms. Thus, the accurate assessment of the strain between the blockout corner and the plate edge takes on great significance. Experimentally, direct measurement of the tensile strain at the blockout corner was not possible due to space limitations. However, since the program generally yielded a spalling distribution with similar shape and strain magnitude at points along the end face away from the anchor where measurements were made, it was assumed that the analytical results, although high due to the idealized corner, gave a reasonable indication of the relative magnitude of the peak spalling strain for specimens with varying degrees of inclination achieved through tendon blockouts. The highly localized concentration of these spalling stresses could not be verified directly in the experiments but the cracking loads correlated well with the magnitude of the predicted strains. Rather than try to isolate a precise stress concentration factor due to the idealized corner, different "trigger" strains were developed for inclined tendons and straight tendons for the prediction of formation of the tendon path crack. These are outlined in the next report of this series.



## C H A P T E R 4

### CONCLUSIONS

#### 4.1 General

At the inception of this study in 1975 the state-of-the-art in American practice for anchorage reinforcement design was for the structural designer to choose a post-tensioning system and rely on the hardware supplier to furnish detailed advice on the use of the system. Often the suppliers' knowledge was based on limited tests, on practical experience, generally with enlarged cast-in-place end blocks, and on the published work of such investigators as Zielinski and Rowe, who relied on the classical bursting stress approach to supplementary anchorage reinforcement design.

Although these designs might work well for straight tendon applications with little eccentricity in enlarged anchor zones, they were insufficient to control cracking in some thin member applications such as in precast segmental box girder bridge web sections. In these applications, the tendons were often not only eccentric, but also highly inclined in order to pick up a portion of the dead load shear. Because of the highly proprietary nature of the industry those companies which did have experience with such problems were often reticent to show this knowledge in the public literature. American specifications such as AASHTO and the ACI Building Code were framed in very limited terms of allowable bearing stresses, and did not reflect the effects of section aspect ratio, of tendon eccentricity, curvature and section aspect ratio, of tendon eccentricity, curvature and inclination, nor of the effect of supplementary reinforcement.

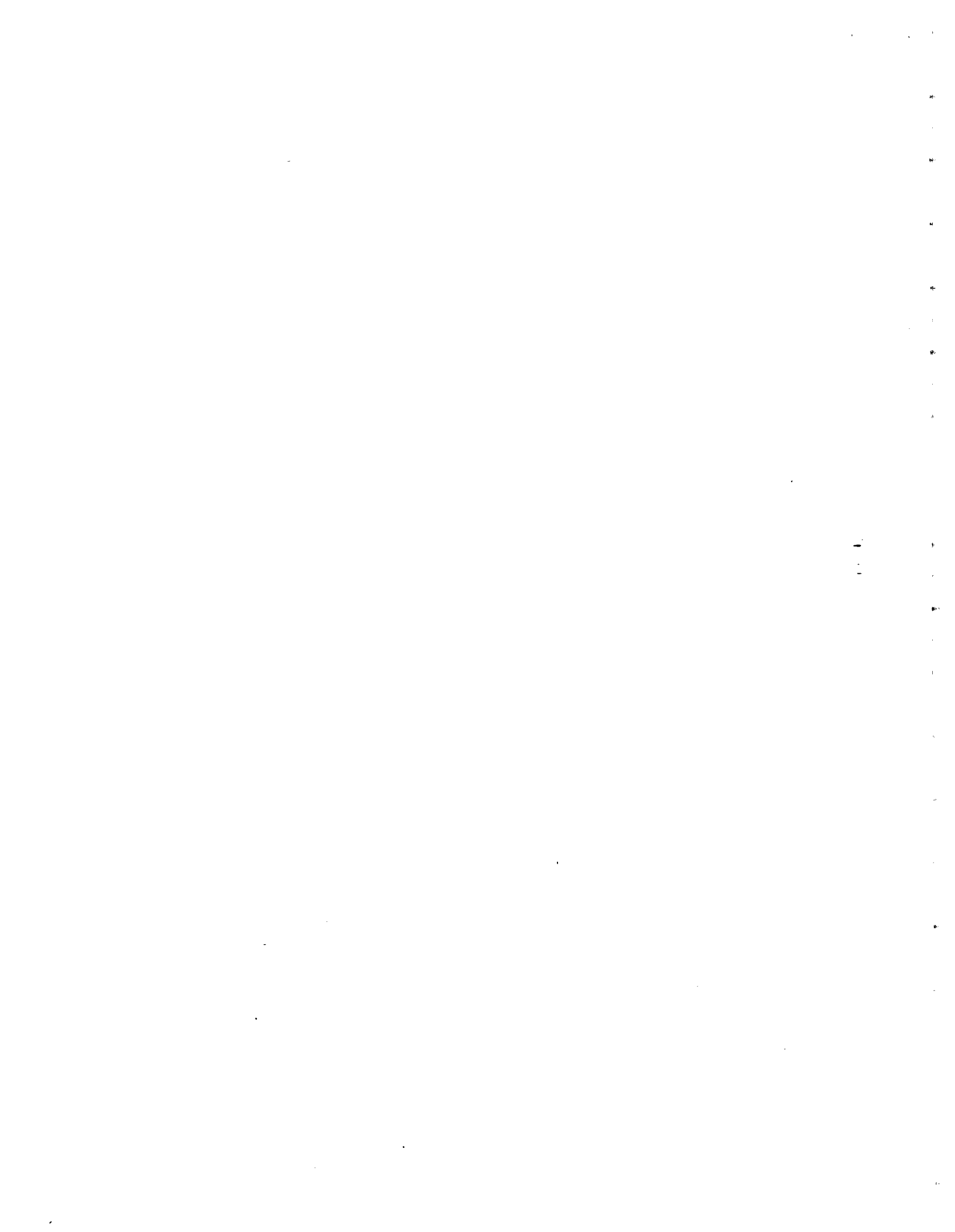
This report summarized an extensive literature study of all published analytical, experimental, and design-related papers and reports concerning anchorage zone stresses for post-tensioned applications. Many proprietary documents exist which were not available to the investigators. Most of the published analyses and test data are for concentric, straight tendons. Extension to eccentric, inclined, and curved tendons is limited and questionable. American design codes and specifications are limited to conservative bearing stress formulae and performance language warning the designer to resist bursting, splitting, and spalling stresses. Little guidance or direction is given on how such resistance should be provided. It was shown that one widely used design method which was based exclusively on straight tendon tests was insufficient to prevent anchorage zone cracking when applied to a major bridge structure with inclined, eccentric tendons.

The report introduced two- and three-dimensional finite element programs which have greater solution capabilities than programs heretofore used. The results predicted with the 2D FEM programs were in close agreement with results of other elastic analyses and photoelastic tests. They do indicate major effects when variables such as tendon inclination and eccentricity are examined. The 3D FEM tests showed very good agreement with bursting stress data obtained in 30 concrete model tests. Comparison of test data obtained in full-scale members showed greater scatter but was still classed as good. General agreement with spalling stress distributions was also good except in high peak regions immediately adjacent to the anchorage blockout corner where no experimental data could be obtained.

The programs are a useful tool for examination of the effect of variables such as cover, inclination, tendon duct curvature, and eccentricity.

These static, linear elastic, three-dimensional finite element analyses can be used to predict the state of stress of the anchorage zone with reasonable accuracy up to the cracking load. They are not valid once cracking begins and thus do not give ultimate load information except that the cracking load is a lower bound.

Experimental verification of the effect of variables and design recommendations are summarized in the other two reports in this series.



## B I B L I O G R A P H Y

1. Breen, J. E., Cooper, R. L., and Gallaway, T. M., "Minimizing Construction Problems in Segmentally Precast Box Girder Bridges," Research Report No. 121-6F, Center for Highway Research, The University of Texas at Austin, August 1975.
2. Dilger, W. H., and Ghali, A., "Remedial Measures for Cracked Webs of Prestressed Concrete Bridges," Journal of the Prestressed Concrete Institute, Vol. 19, No. 4, July-August 1974.
3. Gergely, P., "Anchorage Systems in Prestressed Concrete Pressure Vessels; Anchorage Zone Problems," Report to Oak Ridge National Laboratory, Contract No. W-7405-eng-26, subcontract No. 2852.
4. Guyon, Y., Prestressed Concrete, John Wiley and Sons, Inc., New York, 1953.
5. Guyon, Y., The Limit State Design of Prestressed Concrete, Vol. II; The Design of the Member, Translated by F. H. Turner, John Wiley & Sons, New York, 1974.
6. Rhodes, B., and Turner, F. H., "Design of End Blocks for Post-Tensioned Cables," Concrete, December 1967.
7. Comité Euro-International Du Béton (CEB) and the Fédération Internationale de La Précontrainte (FIP), Model Code for Concrete Structures, English Translation, 1978.
8. Tesar, M. International Association for Bridge and Structural Engineering, 1932, from Ref. 4.
9. Zielinski, T., and Rowe, R. E., "The Stress Distribution Associated with Groups of Anchorages in Post-Tensioned Concrete Members," Cement and Concrete Association, Research Report No. 13, London, October 1962; No. 9, London, September 1960.
10. Zielinski, T., and Rowe, R. E., "An Investigation of the Stress Distribution in the Anchorage Zones of Post-Tensioned Concrete Members," Cement and Concrete Association, London, Research Report No. 9, September 1960.

11. Douglas, D. J., and Trahair, N. S., "An Examination of the Stresses in the Anchorage Zone of a Post-Tensioned Prestressed Concrete Beam," Magazine of Concrete Research, Vol. 12, No. 34, March 1960, pp. 9-18.
12. Iyengar, K. T. S. R., "Two-Dimensional Theories of Anchorage Zone Stresses in Post-Tensioned Prestressed Beams," Journal of the American Concrete Institute, Vol. 59, No. 10, October 1962, pp. 1443-1446.
13. Bleich, F., "Der gerade stab mit rechteckquerschnitt als ebenes problem," Der Bauingenieur (Berlin), No. 9, 1923, pp. 255-259; No. 10, 1923, pp. 304-307.
14. Sievers, H. "Uber den spannungszustand im bereich der ankerplatten von spanngliedern vorgespannter stahlbetonkonstruktionen," Der Bauingenieur (Berlin), Vol. 31, 1956, pp. 134-135.
15. Iyengar, K. T. S. R., and Prabhakara, M. K., "Anchor Zone Stresses in Prestressed Concrete Beams," Journal of the Structural Division, ASCE, Vol. 97, No. ST3, March 1971, pp. 807-824.
16. Gergely, P., and Sozen, M. A., and Siess, C. P., "The Effect of Reinforcement on Anchorage Zone Cracks in Prestressed Concrete Members," University of Illinois, Civil Engineering Structural Research Series, No. 271, July 1963.
17. Magnel, G., Prestressed Concrete, McGraw-Hill Co. Inc., New York, 3rd ed. 1954, p. 345.
18. Morsch, E. "Uber die berechnung der gelenkquader," Beton und eisen, No. 12, 1924, pp. 156-161.
19. Schlee, W., "The Stress Pattern at the Support of a Prestressed Concrete Beam," Beton-und stahlbetonbau (Berlin), Vol. 58, No. 7, July 1963, pp. 157-171.
20. Gergely, P., and Sozen, M. A., "Design of Anchorage Zone Reinforcement in Prestressed Concrete Beams," Journal of the Prestressed Concrete Institute, Vol. 12, No. 2, April 1967, pp. 63-75.
21. Lenschow, R., and Sozen, M., "Practical Analysis of the Anchorage Zone Problem in Prestressed Beams," Journal of the American Concrete Institute, Nov. 1965, pp. 1421-1437.
22. Yettram, A. L., and Robbins, K., "Anchorage Zone Stresses in Post-Tensioned Uniform Members with Eccentric and Multiple Anchorage," Magazine of Concrete Research, Vol. 22, No. 73, December 1970, pp. 209-218.
23. Hawkins, N. M., "The Behavior and Design of End Blocks for Prestressed Concrete Beams," Civil Engineering Transactions, Institution of Engineers of Australia, October 1966.

24. Christodoulides, S. P., "Three-Dimensional Investigation of the Stresses in the End Anchorage Blocks of a Prestress Concrete Gantry Beam," The Structural Engineer, Vol. 35, No. 9, September 1957.
25. Sargious, M., "Beitrag zur ermittlung der hauptzugspannungen am endauflager vorgespannter betonbalken," Ph.D. dissertation, Technische Hochschule, Stuttgart, July 1960.
26. Leonhardt, F., Prestressed Concrete--Design and Construction, Wilhelm Ernest and Son, Berlin, 1964.
27. Vaughn, S. D., "An Exploratory Photoelastic Investigation of Post-Tensioned Concrete Anchorage Zone Bursting Stresses," unpublished M.S. thesis, The University of Texas at Austin, August 1977.
28. Rydzewski and Whitbread, "Short End Blocks for Prestressed Beams," The Structural Engineer, Vol. 41, No. 2, Feb. 1963.
29. Mahajan, K. D., "Analysis of Stresses in a Prestressed Beam Using Araldite Models," Indian Concrete News, Aug. 1958, pp. 112-117.
30. Hiltcher, R. and Florin, G., "Die Spaltzugkraft in einseitig eingespannten am gegenueberliegenden runde belasteten rechteckigen scheiben," Bautechnik, Vol. 39, No. 10, Oct. 1962, pp. 325-328.
31. Taylor, S. J., "Anchorage Bearing Stresses," Conference on PCPV, Group H., paper 49, March 13-17, 1967 (London); The Institution of Civil Engineers, London, 1968.
32. Billig, K., A Proposal for a Draft Code of Practice for Prestressed Concrete, Cement and Concrete Association, London, 1948.
33. Komendant, A. E., Prestressed Concrete Structures, McGraw-Hill Book Company, Inc., 1952, pp. 172-173.
34. Middendorf, K. H., "Practical Aspects of End Zone Bearing of Post-Tensioning Tendons," Prestressed Concrete Institute Journal, Vol. 8, No. 4, August 1963.
35. Hawkins, N. M., "The Bearing Strength of Concrete Loaded through Rigid Plates," Magazine of Concrete Research, Vol. 20, No. 62, March 1968.
36. Hawkins, N. M., "The Bearing Strength of Concrete for Strip Loadings," Magazine of Concrete Research, Vol. 22, No. 71, June 1971.
37. Niyogi, S. K., "Bearing Strength of Reinforced Concrete Blocks," Journal of the Structural Division, ASCE, Vol. 101, No. ST5, May 1975.
38. American Concrete Institute, Building Code Requirements for Reinforced Concrete and Commentary (ACI 318-77), Detroit, Michigan, 1977.

39. American Association of State Highway and Transportation Officials, Standard Specifications for Highway Bridges, 12th Edition, 1977.
40. Post-Tensioning Institute, PTI Post-Tensioning Manual, Illinois, 1976.
41. Stone, W. C., "Design Criteria for Post-Tensioned Anchorage Zone Tensile Stresses," Ph.D. Dissertation, The University of Texas at Austin, May 1980.
42. Zienkiewicz, O. C., The Finite Element Method in Engineering Science, McGraw-Hill, London, 2nd edition, 1971.
43. TEXGAP-3D Users Manual, TICOM, Dept. of Aerospace and Engineering Mechanics, University of Texas at Austin, 78712.
44. Irons, B. M., "A Frontal Solution Program for Finite Element Analysis," International Journal of Numerical Methods in Engineering, Vol. 2, 1970, pp. 5.32.
45. Johnson, C. P., "Frontal-based Solver with Multi Level Substructuring," Advances in Civil Engineering Through Engineering Mechanics, Proceedings May 23-25, 1977, ASCE.